

**PETROGENESIS OF HORNBLENDE-BEARING
LAVAS (RHÖN, GERMANY)**

Dissertation

zur Erlangung des Doktorgrades
der Naturwissenschaften im Fachbereich
Geowissenschaften
der Universität Hamburg

vorgelegt von:
Bernhard Mayer

aus
Eichstätt

Hamburg

2013

Als Dissertation angenommen vom Fachbereich Geowissenschaften der
Universität Hamburg

auf Grund der Gutachten von Prof. Dr. Stefan Jung

und Prof. Dr. Rolf L. Romer

Tag der mündlichen Prüfung 21.01.2013

Hamburg, den 12. Dezember 2012

Prof. Dr. Dir Gajewski
Vorsitzender des Fach-Promotionsausschusses

Abstract

Hornblende-bearing basanites and alkali basalts from the Rhön area of Germany (part of the Cenozoic Central European volcanic province (CEVP)) have high TiO_2 (3–4 wt. %), moderate high Mg# (mostly > 0.50) and some variation in Cr (400–30 ppm) and Ni (160–20 ppm) abundances together with enrichment in incompatible trace elements and REE. In primitive mantle-normalized multi-element diagrams a strong depletion in Ba, Rb, and K relative to trace elements of similar incompatibility can be seen. Some alkali basalts and more differentiated rocks have lower Mg# and lower abundances of Ni and Cr and have undergone fractionation of olivine, clinopyroxene, Fe-Ti oxide and amphibole. Trace element constraints (i.e., low Nb/U and Ce/Pb ratios) and the Sr-Nd-Pb isotope compositions of some basalts indicate that assimilation of lower crustal material has modified the composition of few primary mantle-derived magmas. Most of the basanites and alkali basalts approach the Sr-Nd-Pb isotope compositions inferred for the European Asthenospheric Reservoir (EAR) component. Variations in Rare Earth Element (REE) abundances and correlations between REE ratios suggest partial melting of amphibole-bearing spinel peridotite containing a significant portion of non peridotitic material e.g. pyroxenite. The presence of residual amphibole indicated by depletion of K and Rb relative to Ba and Nb requires melting close to the lithosphere-asthenosphere boundary (LAB) or within the lithospheric mantle most likely from a veined mantle source.

The hornblende in the studied basalts are comagmatic kaersutite and pargasite and may have affiliations to amphibole from magmatic veins. Different isotope signatures in these phenocrysts may report different domains of the subcontinental lithospheric mantle (SCLM) in contrast to the host rocks which are close to the composition inferred for the EAR component. One group approaches the Sr-Nd-Pb isotope composition of the inferred EAR but have slightly more radiogenic $^{207}\text{Pb}/^{204}\text{Pb}$ and $^{208}\text{Pb}/^{204}\text{Pb}$ ratios which could indicate involvement of subducted crustal materials. Unradiogenic Pb and Nd isotope composition for other kaersutite may be associated with an involvement of ancient crustal material.

Thermobarometric calculations support the inferred source of partial melting being close to the LAB or within the lithospheric mantle based on geochemical observations. Temperature and pressure estimates using whole-rock compositions indicate a depth of melting for the most primitive lavas at ~ 80 km at temperatures of ~ 1290 °C. Based on

their composition temperatures for crystallization of kaersutite are estimated at about 1150 °C which are consistent with the stability field of amphibole.

Based on Sr-Nd isotope and trace element constraints it is proposed that asthenospheric melts, similar in composition to EAR melts observed elsewhere in the CEVP, precipitated at the asthenosphere-lithosphere thermal boundary as hornblende-bearing veins in the lithospheric mantle. These veins were remelted after only short storage times by ascending asthenospheric melts imposing the prominent amphibole signature upon the basalts. Confirmed by new $^{40}\text{Ar}/^{39}\text{Ar}$ ages which are older than other volcanic lavas in the Rhön area the hornblende-bearing basalts seem to be the early volcanic products of "wet melting" of a metasomatized SCLM. The fairly radiogenic Pb isotope signatures are expected to originate from melting of enriched, low melting temperature portions incorporated in the depleted upper (asthenospheric) mantle and therefore does not require upwelling of deep-seated mantle sources for the Rhön or many other continental alkaline lavas with similar Pb isotope signatures.

Contents

| | |
|--|-----------|
| Glossary | VII |
| List of Figures | IX |
| List of Tables | X |
| 1 Introduction | 1 |
| 1.1 Alkaline basalts | 1 |
| 1.2 Phenocrysts | 1 |
| 1.3 Central European Volcanic Province | 2 |
| 1.4 Rhön | 3 |
| 2 Objectives | 4 |
| 3 Geological setting | 5 |
| 4 Analytical techniques | 8 |
| 4.1 Whole-rock geochemistry | 8 |
| 4.2 Mineral geochemistry | 8 |
| 4.3 Whole-rock isotope chemistry | 10 |
| 4.4 Mineral isotope chemistry | 11 |
| 5 Results | 14 |
| 5.1 Petrography | 14 |
| 5.2 Whole-rock geochemistry | 15 |
| 5.2.1 Major element compositions | 15 |
| 5.2.2 Trace element compositions | 15 |
| 5.2.3 Isotope compositions | 20 |
| 5.3 Mineral chemistry | 22 |
| 5.3.1 Major and trace element compositions | 22 |
| 5.3.2 Isotope compositions | 28 |
| 5.4 Geochronology | 31 |
| 6 Discussion | 33 |
| 6.1 Fractional crystallization | 33 |
| 6.2 Crustal contamination | 34 |
| 6.3 Partial melting | 37 |
| 6.4 Nature of the source | 41 |

PETROGENESIS OF HORNBLLENDE-BEARING LAVAS (RHÖN, GERMANY)

Contents

| | | |
|----------|---|-----------|
| 6.5 | Origin of hornblende in basaltic lavas | 43 |
| 6.6 | Implications from isotope compositions | 46 |
| 6.7 | Hornblende implications for petrogenetic settings | 49 |
| 7 | Conclusion | 52 |
| | Bibliography | 56 |
| A | Appendix | 73 |
| 8 | Acknowledgement | 87 |

Glossary

Glossary

- AFC assimilation-fractional crystallization
- apfu atoms per formula unit
- BSE Bulk Silicate Earth
- CEVP Cenocoic Central European volcanic province
- EAR European Asthenospheric Reservoir
- EC-AFC energy-constrained assimilation-fractional crystallization
- EMPA electron microprobe analyses
- HFSE High Field Strength Element
- HREE Heavy Rare Earth Element
- ICP-MS inductively coupled plasma mass spectrometry
- LA-ICP-MS laser ablation inductively coupled plasma mass spectrometry
- LAB lithosphere-asthenosphere boundary
- LILE Large Ion Lithophile Element
- LOI loss on ignition
- LREE Light Rare Earth Element
- LVC low-velocity component
- Moho Mohorovičić-discontinuity
- MORB Mid Ocean Ridge Basalt
- NHRL northern hemispheric reference line
- OIB Ocean Island Basalt

Glossary

- REE Rare Earth Element
- RSD relative standard deviation
- SCLM subcontinental lithospheric mantle
- SIMS secondary ion mass spectrometry
- TIMS thermal ionization mass spectrometer
- XRF X-ray fluorescence

List of Figures

| | | |
|------|--|----|
| 3.1 | Map of CEVP; lithosphere thickness; and Rhön area | 7 |
| 5.1 | Thin section phtotography of kaersutite in Rh10/09 | 14 |
| 5.2 | Major element variations in lavas from the Rhön area | 16 |
| 5.3 | Trace element variations in lavas from the Rhön area | 17 |
| 5.4 | Trace element ratios in lavas from the Rhön area | 18 |
| 5.5 | REE distributions of lavas from the Rhön area; C1-normalized | 19 |
| 5.6 | Incompatible trace element compositions of lavas from the Rhön area; primitive mantle normalized | 19 |
| 5.7 | $^{87}\text{Sr}/^{86}\text{Sr}$ vs. $^{143}\text{Nd}/^{144}\text{Nd}$ isotope diagram for lavas from the Rhön area . . | 20 |
| 5.8 | Lead isotope compositions of lavas from the Rhön area | 21 |
| 5.9 | Major element compositions of hornblende from the Rhön area | 23 |
| 5.10 | BSE image of kaersutite Hbl-Rh10/09 | 24 |
| 5.11 | REE distributions of hornblende from the Rhön area; C1-normalized . . . | 25 |
| 5.12 | Incompatible trace element compositions of hornblende from the Rhön area; primitive mantle normalized | 26 |
| 5.13 | Nb/Th vs. Lu/Hf covariations of hornblende from the Rhön area | 27 |
| 5.14 | $^{87}\text{Sr}/^{86}\text{Sr}$ vs. $^{143}\text{Nd}/^{144}\text{Nd}$ isotope diagram for hornblende from the Rhön area | 28 |
| 5.15 | Lead isotope compositions of hornblende from the Rhön area | 29 |
| 5.16 | Oxygen and Sr isotope compositions of hornblende from the Rhön area . | 30 |
| 5.17 | Ar-Ar results of hornblende from the Rhön area | 32 |
| 6.1 | Fractional crystallization calculation using Cr and Sc concentrations . . . | 34 |
| 6.2 | EC-AFC calculations using $^{87}\text{Sr}/^{86}\text{Sr}$ and $^{206}\text{Pb}/^{204}\text{Pb}$ isotope ratios | 36 |
| 6.3 | Partial melting calculations using REE covariation | 38 |
| 6.4 | Pressure-temperature diagram using whole-rock compositions | 40 |
| 6.5 | Calculated incompatible trace element concentrations of amphibole . . . | 45 |
| 6.6 | Temperature estimates using hornblende compositions | 51 |
| 7.1 | Petrogenetic model of the hornblende-bearing lavas | 55 |
| A.1 | Raman spectra of hornblende from the Rhön area | 73 |

List of Tables

| | | |
|-----|--|----|
| A.1 | Chemical compositions of Rhön lavas | 74 |
| A.2 | Sr, Nd, and Pb isotope compositions of Rhön lavas | 79 |
| A.3 | EC-AFC parameters | 80 |
| A.4 | Major element compositions of hornblende from the Rhön area | 81 |
| A.5 | Trace element compositions of hornblende from the Rhön area measured by SIMS | 83 |
| A.6 | Trace element compositions of hornblende from the Rhön area measured by LA-ICP-MS | 85 |
| A.7 | Isotope compositions of hornblende from the Rhön area | 86 |
| A.8 | Summary of results from Ar-Ar dating of hornblende from the Rhön area | 86 |

1 Introduction

1.1 Alkaline basalts

Primitive alkaline mafic volcanic rocks found in oceanic or intra-continental settings provide important information about the chemical composition of the Earth's mantle (Hofmann *et al.*, 1986; Zindler & Hart, 1986; Hofmann, 1997; Stracke *et al.*, 2005). The subcontinental lithospheric mantle (SCLM) has been isolated from the convective mantle and is connected with an influx of fluids and/or melts of variable composition (Foley, 1992; Pilet *et al.*, 2008, 2010, 2011). In intra-continental settings the generation of common alkali basalts is thought to be related either to plume activity or to melting of updoming asthenospheric material (Hawkesworth & Vollmer, 1979; Wörner *et al.*, 1986; McKenzie & Bickle, 1988; Hawkesworth *et al.*, 1990; Bradshaw *et al.*, 1993; Bogaard & Wörner, 2003; Haase *et al.*, 2004; Jung *et al.*, 2005, 2006; Lustrino & Wilson, 2007). In both cases, uprising partial melts may tap lithospheric metasomatized mantle material which can contain abundant hydrous minerals (amphibole, phlogopite) (Foley, 1992; Peccerillo, 1999; Wilson & Downes, 2006; Pilet *et al.*, 2008; Niu *et al.*, 2011). Metasomatic enrichment processes either by CO₂ flux from the deeper mantle or by devolatilization of subducting slabs lead to the formation of secondary minerals (clinopyroxene, amphibole, phlogopite) in veins and batches within the ambient upper mantle.

1.2 Phenocrysts

Secondary minerals associated with metasomatic enrichment processes have indicative Large Ion Lithophile Element (LILE), Light Rare Earth Element (LREE), and High Field Strength Element (HFSE) concentrations (Francis & Ludden, 1995; Ionov & Hofmann, 1995). Previous studies have shown that the composition of uncommon minerals observed in upper mantle-derived volcanic rocks reveal important additional information on the petrogenesis of these rocks (Simonetti & Bell, 1993; Francis & Ludden, 1995; Harmon & Hoefs, 1995; Hegner *et al.*, 1995). It is probable that hydrous minerals carry information on the nature of the inferred metasomatic event (Ben Othman *et al.*, 1990; Rosenbaum, 1993; Powell *et al.*, 2004). Geochemical and isotope composition of minerals (even if comagmatic) are not necessarily similar to the host rock isotope composition

1 Introduction

due to an unsystematic distribution of incompatible trace elements between the host lava and the hydrous phases (Wilkinson & Hensel, 1991; Simonetti & Bell, 1993, 1994; Hegner *et al.*, 1995; Molina *et al.*, 2009). The presence of such hydrous phenocrysts limits the melting region of the alkaline basalts due to the stability field of hydrous minerals. Therefore, partial melting of upper mantle rocks to generate alkali basalts carrying these phenocrysts implies "wet melting" at specific lower temperature. In this context, studies on the stability of TiO₂ rich hornblende is constrained to 1.5–2.5 GPa at 1050–1250 °C (Huckenholz & Gilbert, 1984). In contrast, Green *et al.* (2010) have shown that the stability of pargasite extends to 3 GPa at lower temperatures of ca. 1100 °C.

1.3 Central European Volcanic Province

Primitive alkaline rocks from the Cenozoic Central European volcanic province (CEVP) are geochemically similar to enriched Mid Ocean Ridge Basalts (MORBs) and some Ocean Island Basalts (OIBs) (Wörner *et al.*, 1986; Blusztajn & Hart, 1989; Wilson & Downes, 1991; Hegner *et al.*, 1995; Wilson *et al.*, 1995; Jung & Masberg, 1998; Wedepohl & Baumann, 1999; Jung & Hoernes, 2000; Bogaard & Wörner, 2003; Haase *et al.*, 2004; Jung *et al.*, 2005, 2006, 2011, 2012). On the basis of their geochemical and isotope composition three models have been proposed for the generation of alkaline lavas from the CEVP: (i) The lavas originate from partial melting of a deep mantle plume. This view was substantiated by high resolution seismic mantle tomography that identified low velocity domains in the mantle at various depths beneath the CEVP (Hoernle *et al.*, 1995; Goes *et al.*, 1999; Ritter *et al.*, 2001), (ii) the lavas are partial melts from a metasomatically enriched asthenospheric mantle (Wedepohl *et al.*, 1994) with some further evolution within the lithospheric mantle (Hegner *et al.*, 1995; Jung *et al.*, 2005), (iii) the lavas represent partial melts from the lithosphere-asthenosphere boundary (LAB) (Wilson *et al.*, 1995). The geochemical diversity of mantle xenoliths (Witt-Eickschen & Kramm, 1997), observed in alkaline rocks from the CEVP, show that enrichment processes produced substantial chemical heterogeneity in the lithospheric mantle beneath central Europe as a result of mantle metasomatism. This inferred metasomatic event is considered to be associated with the Variscan orogeny where several subduction zones were active and different material had been subducted (Kroner *et al.*, 2010). These inferred processes lead to an enrichment of incompatible elements by percolation of hydrous fluids and melts causing the appearance of hydrous mineral phases (amphibole/phlogopite) in the mantle (Wörner *et al.*, 1986; Wilson & Downes, 1991; Wedepohl *et al.*, 1994). The

1 Introduction

subducted oceanic crust now preserved as eclogite or pyroxenite with additional CO₂ is thought to be the major prerequisite to mafic alkaline basalts in intracontinental settings (Foley, 1991, 1992; Dasgupta *et al.*, 2006, 2007; Pilet *et al.*, 2008, 2010, 2011). Melting of metasomatized lithospheric mantle therefore appears to be also a geologically plausible scenario for the origin of at least some of the CEVP lavas.

1.4 Rhön

In the Rhön area as a part of the CEVP, an unusual suite of alkali basalts occur carrying cm-sized hornblende. Available geochemical data from these hornblende (Freerk-Parpatt, 1990; Jung & Hoernes, 2000) show that these unzoned amphibole are high-TiO₂/high-MgO hornblende suggesting igneous crystallization from TiO₂-rich alkali basaltic lavas. The stability of such high TiO₂ amphibole limits the melting region of such hornblende-bearing alkaline rocks to 1.5–2.5 GPa at 1050–1250 °C (Huckenholz & Gilbert, 1984). These temperature estimates are broadly similar to experimental results for the stability of hornblende in upper mantle rocks (Wallace & Green, 1991; Green *et al.*, 2010). Hydrous megacrysts (amphibole; phlogopite) have been observed only in some mafic volcanic rocks of the CEVP (Rhön: Jung *et al.*, 2005; Urach/Hegau: Hegner *et al.*, 1995; Eifel: Shaw & Eyzaguirre, 2000; North Hessian Depression: Vinx & Jung, 1977). Amphibole and phlogopite are also very common in pyroxenitic veins in upper mantle peridotites from the CEVP (Witt-Eickschen *et al.*, 1998). In this case, the site of melting must be within the lithospheric part of the mantle because it has been shown experimentally (Green *et al.*, 2010) that amphibole is not stable at depths greater than 90 km; a view that was previously constrained by geochemical arguments (Class & Goldstein, 1997). However, distinguishing the primary geochemical signatures of asthenosphere-derived or lithosphere-derived melts from those of subsequent interaction of these melts with other lithospheric or crustal domains is challenging because both crust and metasomatically enriched subcontinental mantle may have similar isotope characteristics. This is particularly important for the Rhön lavas because it has been shown that contamination of alkaline lavas with crustal material has obscured the primary chemical and isotope signatures of lavas in some areas of the CEVP (Jung & Masberg, 1998; Bogaard & Wörner, 2003; Haase *et al.*, 2004; Jung *et al.*, 2005, 2011, 2012).

2 Objectives

If you're not part of the solution...

... then you're part of the precipitate

(Stephen Wright)

The CEVP represent a well-studied volcanic area where different types of volcanic rocks are present. The SCLM is thought to be inhomogeneous and underwent metasomatic processes. The studied rocks (hornblende-bearing basalts in the Rhön area) are unique in their geochemical and mineralogical composition within the CEVP. The high TiO_2 concentrations of the basalts are similar to some other mafic rocks occurring within the CEVP. In addition, the basalts contain large amphibole which are collectively referred to as "megacrysts". In previous studies of these hornblende-bearing basalts only few samples have been investigated or only major-, trace-element concentrations and Sr isotope ratios have been analysed. Amphibole as a nominally hydrous mineral can potentially obtain more information on the nature of the inferred metasomatic event than nominally anhydrous minerals.

In this study we will evaluate the role of amphibole during petrogenesis of intra-plate alkaline rocks and the isotope relationships between phenocrysts and the host rock. In addition, these TiO_2 -rich mafic basalts together with the hydrous phenocrysts can reveal important information about (i) different parts in the SCLM, (ii) metasomatic processes in the mantle, (iii) clarify the origin of these rocks within the upper mantle, and (iv) elucidating processes near the LAB. In this study we will clarify if these hydrous minerals in the Rhön may represent (i) products of interaction of the lava with peridotitic wall rocks, (ii) residual minerals from the ambient mantle, or (iii) igneous megacrysts that crystallized directly from the alkaline melt.

3 Geological setting

After the alpine orogeny especially the collapse and subduction of the Mediterranean and Pannonian basins in Central Europe caused the Neogene rift system related with volcanism in CEVP (Ziegler, 1992). The CEVP consist of different volcanic rocks with several petrogenetic implications. Seismic data (Granet *et al.*, 1995; Goes *et al.*, 1999; Ritter *et al.*, 2001) suggest the existence of deep-mantle rooted volcanic systems beneath the CEVP. This is suggested e.g. for the Eifel magmatic lavas, Germany (Goes *et al.*, 1999). Griffiths & Campbell (1990) suggested that mantle plumes originating from the core-mantle boundary can have diameters of up to 600 km, which is appropriate for the observed spatial distribution of volcanic centres within the CEVP (Wilson & Downes, 1991). A single upper mantle reservoir in the asthenosphere (Hoernle *et al.*, 1995; Granet *et al.*, 1995) is e.g. proposed for Urach melilitetes which represent low-temperature melting heterogeneities of that upwelling asthenosphere (Hegner *et al.*, 1995). In central Germany, the CEVP encompasses the following regions from west to east: Eifel, Siebengebirge, Westerwald, Vogelsberg, Hessian Depression, Rhön, Heldburger dyke swarm, and the Oberpfalz area (Fig. 3.1 a). These volcanic provinces run perpendicular to the main NNE-SSW trending rift system of the Upper Rhine valley which formed as a result of post-alpine extension (Ziegler, 1992). Alone in the German part of the CEVP, several thousand cubic kilometers of mafic lavas erupted during the Miocene. In Germany and Central Europe, the development of Tertiary (mainly Miocene to Pliocene) basins provides evidence for continental rifting. Alternatively, it has been speculated that the large masses of basaltic rocks in the Vogelsberg area (approximately 500 km³) and the Cantal area (Massif Central, France) cannot be attributed to continental extension alone (Wilson & Downes, 2006). Detailed age analyses have shown that basement uplift accompanied by plume activity is not coeval with the rift development and uplift started 20–40 Ma after the beginning of rifting (Ziegler, 1992). Since the whole volume is probably too large to have been produced entirely within the lithosphere it has been suggested that the isolated volcanic parts of the CEVP were fed from upwelling asthenospheric material, probably in the form of small, isolated "plumelets" or "hot fingers" (Wilson & Downes, 1991; Granet *et al.*, 1995).

The Cenozoic volcanism of the CEVP is either located on Variscan fault-bounded blocks (e.g., Eifel, Westerwald, Heldburg) or associated with rift structures (Rhine graben, Hessian Depression) (Fig. 3.1 a). These faults and rifts are associated with a marked uplift

3 Geological setting

of the Mohorovičić-discontinuity (Moho) and crustal thinning. The maximum of crustal thinning coincides with the trace of the northern Rhine graben (Ziegler, 1990). The crustal thickness has been estimated to be less than 30 km (Prodehl, 1981; Prodehl *et al.*, 1992). Babuška & Plomerová (1988) estimated a lithosphere thickness of 100–140 km prior to the Cenozoic rifting and suggested a present-day depth of less than 60 km for the LAB beneath the Rhenish Massif. Recent estimates (Babuška & Plomerová, 2006), however, indicate a somewhat deeper level for the LAB of about 90 km (Fig. 3.1 b).

The Rhön area in central Germany has an extent of ca. 1500 km³ and is located at the southeastern margin of the Hessian Depression which has been interpreted to be the northern extension of the Rhine graben. As typical for continental rift zones, this extensional region is characterized by variable, but high heat flow and thin crust and lithospheric mantle. The Tertiary volcanic activity in the Rhön area is restricted to graben-like structures that transect the Variscan fault-bound block. The rift structure is not associated with basement uplift but strike-slip movement in the upper crust that probably allowed passive mantle upwelling. Volcanism in the Rhön area lasted from the late Oligocene to the mid Miocene (26–11 Ma; Lippolt, 1982).

The volcanic activity culminated between 22 and 18 Ma in the voluminous eruption of alkali basalts and volcanic breccias followed by less voluminous phonolites, tephrites, basanites, and nephelinites. The Mesozoic and Cenozoic sedimentary sequences into which the alkaline volcanic rocks intruded consist of sandstones, carbonates, and claystones. The underlying Variscan to Pre-Variscan basement is part of the Mid German Crystalline Zone and consists of greenschist to granulite-facies metapelites as well as metabasites and orthogneisses (Mengel *et al.*, 1991). The main occurrences of hornblende-bearing basalts are located on the "Kuppen"-Rhön and therefore most of the samples are from this region (Fig. 3.1 c) in which the distribution of the hornblende-bearing basalts occurs in an area of c. 400 km³.

3 Geological setting

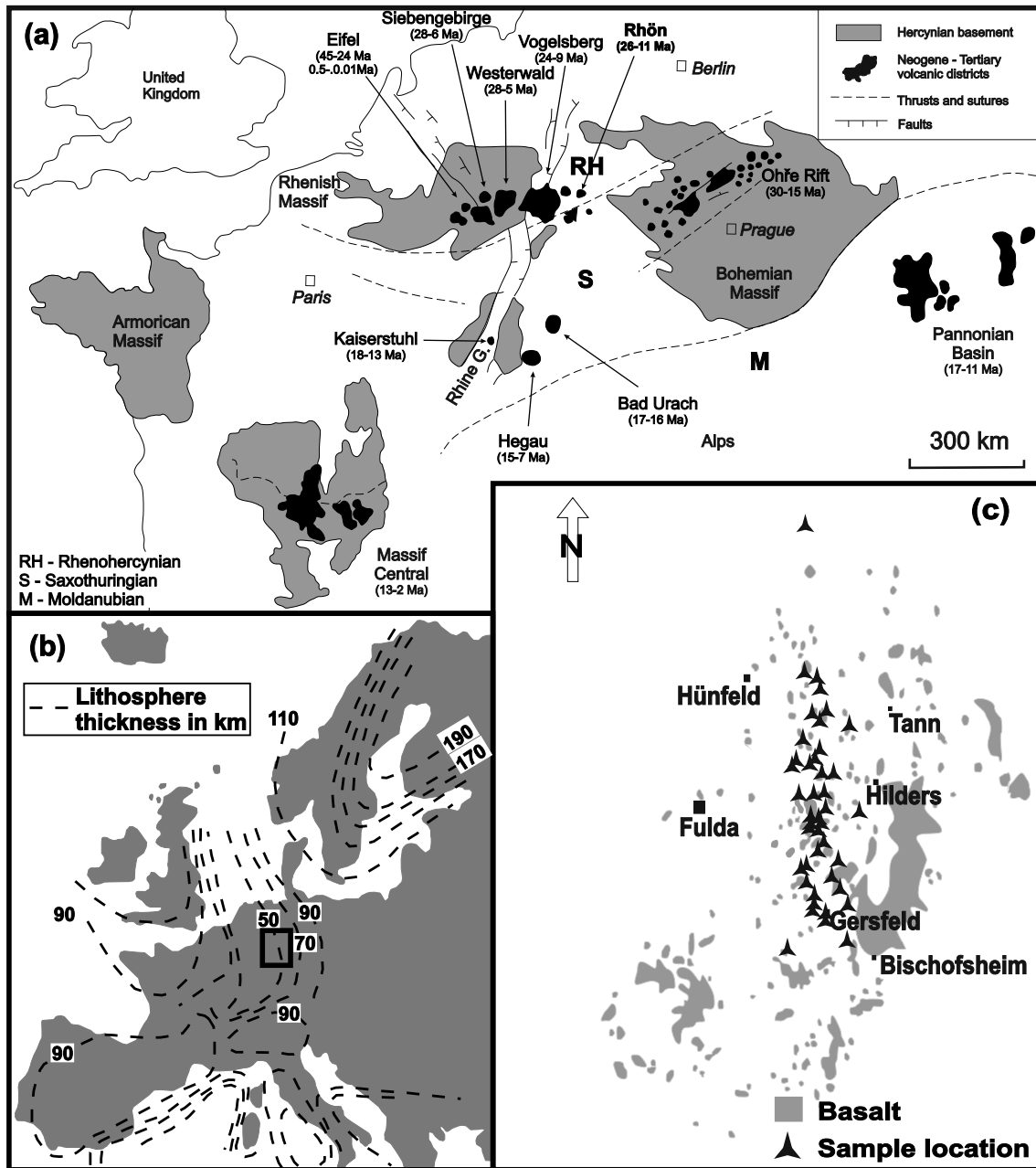


Figure 3.1: (a) Distribution of Cenozoic volcanism in Central Europe (adopted and modified from Blusztajn & Hegner, 2002) with K-Ar ages after Lippolt (1982); Lustrino & Wilson (2007); (b) Contour map of lithosphere thickness in Europe after Wedepohl *et al.* (1994); Babuška & Plomerová (2006); (c) Sample locations of the basaltic lavas (Rhön area).

4 Analytical techniques

4.1 Whole-rock geochemistry

Samples were taken from several volcanic necks and plugs, with a focus on samples carrying mm- to cm-sized hornblende. Thin sections were prepared for all samples. For geochemical analyses, the samples were crushed in an agate shatterbox. Aliquots were analysed for major elements and Sc by fused lithium-tetraborate glass beads using standard X-ray fluorescence (XRF) techniques at the Mineralogisch-Petrographisches Institut at Universität Hamburg (Vogel & Kuipers, 1987). The international rock standard (JGB-1) was run together with the samples and the measured values are in good agreement with the recommended values (Table A.1). Loss on ignition (LOI) was determined gravimetrically at 1050 °C (Lechler & Desilets, 1987). The samples were analysed for trace elements by inductively coupled plasma mass spectrometry (ICP-MS) either at Activation Laboratories, Canada or Institute of Geosciences, Universität Kiel. Analytical precision as estimated from duplicate sample digestions was typically better than 1–3 % relative standard deviation (RSD) for most elements except for elements Tl, being < 5 % RSD. For samples analysed at Activation Laboratories, Canada rock powders were mixed with a flux of lithium metaborate and lithium tetraborate and fused in an induction furnace. The melt was immediately poured into a solution of 5 % nitric acid containing an internal standard, and mixed continuously until completely dissolved. Samples were diluted and analysed by a Perkin Elmer Sciex ELAN ICP-MS. The international rock standard (BIR-1) was run together with the samples and the measured values are also in good agreement with the recommended values (Table A.1). At Universität Kiel, the samples were dissolved following a table-top, multistep, mixed-acid digestion procedure. Sub-sequent analyses were accomplished with an Agilent 7500cs. Repeated measurements of the standard BHVO-2 was in good agreement with recommended values (Table A.1). Additional information can be found in Garbe-Schönberg (1993).

4.2 Mineral geochemistry

Electron microprobe analyses (EMPA) were performed for hornblende in thin sections with a Cameca microprobe SX100 (WDS system) at Mineralogisch-Petrographisches

4 Analytical techniques

Institut, Universität Hamburg. Operating conditions were 15 keV and 20 nA, with a counting time of 20 seconds for most elements. Fluor was counted with a peak time of 60 seconds. Sodium, Sr and Ba were counted for 30 seconds. The ZAF correction procedure was applied.

Additional trace elements were analyzed with a secondary ion mass spectrometry (SIMS) on an upgraded Cameca IMS-3f at Max-Planck Institute in Mainz. Spots were selected for ion microprobe analysis after detailed petrographic and electron microprobe studies. Only optically clear domains that showed no signs of alteration or cpx exsolution were analyzed. Negative oxygen ions were used as primary ions (accelerating potential of 12.5 kV and 20 nA beam current). The spot size for these operating conditions was 15–20 μm . Positive secondary ions were extracted using an accelerating potential of 4.5 kV with a 25 eV energy window, a high-energy offset of -80 V, and fully open entrance and exit slits. Each measurement consisted of a six-cycle routine, where in each cycle the species ^{16}O , ^{23}Na , ^{39}K , ^{30}Si , ^{44}Ca , ^{45}Sc , ^{47}Ti , ^{51}V , ^{52}Cr , ^{88}Sr , ^{89}Y , ^{90}Zr , ^{138}Ba , ^{139}La , ^{140}Ce , ^{145}Pr , ^{146}Nd , ^{147}Sm , ^{153}Eu , ^{157}Gd , ^{163}Dy , ^{167}Er and ^{174}Yb were analysed, in that order. In each cycle, most REE and Ba were measured for 30 s, Ce for 20 s, Y for 5 s, Zr for 2 s and the other elements for 1 s. At the beginning of each analysis, peak centers were determined for ^{30}Si , ^{47}Ti , ^{89}Y and ^{140}Ce by scanning the peak in 20 steps across a 1.5 wide B-field. The neighboring masses (Na, K, and Ca on Si, Sc, V, and on Ti, Sr and Zr on Y, and Ba and all REE on Ce) were then adjusted to these new peak centers. From one measurement to the next, however, the peak shift was rarely significant (< 50 ppm). For all silicates, ^{30}Si (3.1% isotopic abundance) is used as a reference mass, as the SiO_2 concentration of standards and samples is known from electron microprobe analysis. For each cycle, mass to ^{30}Si ratios were determined after correction for time-dependence of count rates, detector deadtime (20 ms) and background [10^{-3} c.p.s. (counts per second)]. The average of these ratios was used to calculate the element concentration, multiplying the measured ratios by a constant factor. These so-called sensitivity factors were determined for each element on the well studied standard glass KL2-G (Jochum *et al.*, 2000). For this purpose, a different measurement routine that determines the mass spectrum between 133 and 191 was adopted (Zinner & Crozaz, 1986). This approach is necessary to obtain accurate sensitivity factors for the REE. Although the applied energy filtering technique (Shimizu *et al.*, 1978) eliminates the effect of most molecular interferences, it is well known that element monoxides can produce significant interferences, particularly on REE (e.g. PrO on Gd). A detailed description of this iterative data reduction procedure was presented by Zinner & Crozaz (1986). Furthermore, six oxides were found to produce

4 Analytical techniques

significant interferences: $^{137}\text{BaO}^+$ interferes with $^{153}\text{Eu}^+$, $^{141}\text{PrO}^+$ with $^{157}\text{Gd}^+$, $^{147}\text{SmO}^+$ with $^{163}\text{Dy}^+$, $^{151}\text{EuO}^+$ with $^{167}\text{Er}^+$, and both $^{158}\text{GdO}^+$ and $^{158}\text{DyO}^+$ with $^{174}\text{Yb}^+$ $^{174}\text{Yb}^+$, and their MO^+ to M^+ ratios used for the corrections are 0.038, 0.125, 0.058, 0.049, 0.08 and 0.07, respectively (with errors <10%). As all elements of these oxides are free of interferences, they were measured directly. For the concentrations of Eu, Gd, Dy and Er these corrections were always <2% of the measured element/Si ratio. For Yb, the correction was 11%. The well-studied glass KL2-G (Jochum *et al.*, 2000) was used as an external standard. The overall accuracy is between 7% and 19% for the REE and better than 11% for all other elements (95% confidence level). To distinguish "real" counts from background noise at extremely low counting rates, separate background measurements with long counting times of between 10 and 30 minutes were carried out. All reported analyses are corrected for the background.

Additional trace element spot analyses were carried out by laser ablation inductively coupled plasma mass spectrometry (LA-ICP-MS) at Institute of Geosciences, University of Bremen, using a NewWave UP193ss solid-state laser coupled to a ThermoFinnigan Element2™. Analytical conditions included a laser pulse rate of 10 Hz, irradiance of ca. 1 GW/cm², a spot size of 75–100 μm, and a plasma power of 1200 W. Helium (0.6 l/min) was used as sample gas, and Argon (0.9 l/min) was subsequently added as make-up gas. Formation of oxides in the plasma was low (ThO/Th < 0.2 %) so that no interference correction for the REE was necessary. All isotopes were analyzed at low resolution with five samples in a 20% mass window and a total dwell time of 25 ms per isotope. Blanks were measured for 20 s prior to ablation. NIST612 glass was analyzed as external calibration standard for every 10 samples using the values of Pearce *et al.* (1997). For data quantification the Cetac GeoPro™ software was used with ^{43}Ca as internal standard. Data quality was assessed by repeated analyses of USGS glass reference material BHVO-2G along with the samples; the mean deviation from the reference values (GeoReM data base, MPI Mainz) is <10% for all elements except Cu, Y, Zr, Nb and Tb (<15%). External precision as determined by repeated analyses of standards is better than 5% for most elements at concentrations above 0.3 μg/g.

4.3 Whole-rock isotope chemistry

Strontium and Nd isotope analyses were carried out at Westfälische Wilhelms Universität Münster using a Finnigan Triton thermal ionization mass spectrometer (TIMS)

4 Analytical techniques

operating in static collection mode. Whole-rock chips were leached in 6N HCl for at least 1 h at 100 °C on a hotplate. The samples were washed three times with ultra-pure H₂O. Subsequently, the samples were dissolved in a mixture of 5HF:1HNO₃ and after evaporation redissolved in 6N HCl. Strontium and Rare Earth Elements (REEs) were separated by standard cation exchange chromatography with a DOWEX® AG 50 -X 12 resin using 2.5N HCl for Sr and 6N HCl for the REE. Neodymium was separated from the other REE by using 0.17N HCl in HDEHP-coated Teflon columns. Neodymium isotopes were normalized to $^{146}\text{Nd}/^{144}\text{Nd} = 0.7219$ and are reported relative to the standard LaJolla with $^{143}\text{Nd}/^{144}\text{Nd} = 0.511850$. Repeated measurements of the LaJolla standard gave $^{143}\text{Nd}/^{144}\text{Nd} = 0.511843 \pm 0.000005$ and a longterm reproducibility of 0.511863 ± 0.000003 . The long-term reproducibility of the Sr standard (NBS 987) is 0.710203 ± 0.000023 (2σ ; $n = 64$). During the course of this study, NBS 987 yielded $^{87}\text{Sr}/^{86}\text{Sr} = 0.710212 \pm 0.000008$. Fractionation was normalized to $^{86}\text{Sr}/^{88}\text{Sr} = 0.1194$. The Pb isotope composition was determined on a Finnigan MAT262 multicollector mass spectrometer using static multicollection, performed at Deutsches GeoForschungsZentrum (GFZ), Germany. Lead was separated using anion exchange resin Bio Rad AG1-X8 (100–200 mesh) in Teflon columns by HCl-HBr ion exchange chemistry adapted from Romer *et al.* (2005). The resin was cleaned with 6N HCl and conditioned with 2N HCl. Samples were loaded in 2N HCl, rinsed with 2N HCl, 0.8N HBr, and 2N HCl. Pb was eluted in 6N HCl and purified by a second pass over the column. Pb was loaded together with H₃PO₄ and silica gel on single Re-filaments (Gerstenberger & Haase, 1997). Instrumental fractionation was corrected with 0.1%/a.m.u. as determined from repeated measurement of lead reference material NBS 981. Accuracy and precision of reported Pb ratios are better than 0.1 % at the 2-sigma level. Total procedural blanks for whole-rock samples are better than 15–30 pg Pb and are therefore considered negligible.

4.4 Mineral isotope chemistry

The Sr and Nd isotope composition of hornblende was measured at GFZ (Potsdam) on a Thermo TRITON multi-collector mass-spectrometer using dynamic multi-collection for Sr- and Nd- and static multi-collection for Pb isotope composition. For the isotope study, mineral separates were leached in 6N HCl for at least 6 hours. The leachate was decanted. The residues were rinsed three times thoroughly with Millipore® water to remove unrelated Sr. Samples used to determine the Pb isotope composition were dissolved with concentrated HF for four days at 160 °C on the hot plate. The digested samples

4 Analytical techniques

were taken up in 2N HNO₃ to convert fluorides into nitrated and dried slowly at low temperature overnight. Thereafter, the samples were taken up in 6N HCl. Strontium, Nd, and Pb were separated and purified using the ion-exchange chromatography procedures described in Romer *et al.* (2005). Strontium and REE were separated using standard cation exchange columns with a DOWEX® AG 50 W-X 8 (100-200 mesh) resin and 2.5N HCl for Sr. Ba was removed using 2.5N HNO₃ before the REE were eluted using 6N HCl. Neodymium was separated from the other REE using HDEHP coated Teflon® columns and 0.12 N HCl. Neodymium isotopes were normalized to $^{146}\text{Nd}/^{144}\text{Nd} = 0.7219$. Repeated measurements of the La Jolla Nd reference material gave $^{143}\text{Nd}/^{144}\text{Nd} = 0.511858 \pm 0.000006$ (2σ ; $n = 6$). The reproducibility of Sr reference material NBS 987 is $^{87}\text{Sr}/^{86}\text{Sr} = 0.710252 \pm 0.000006$ (2σ ; $n = 24$). Sr isotope ratios were normalized to $^{86}\text{Sr}/^{88}\text{Sr} = 0.1194$. Lead isotope data corrected for mass discrimination with 0.06% / A.M.U. as estimated from the repeated measurement of lead reference material NBS 981. Reproducibility at 2σ level is better than 0.1%.

For oxygen isotopes determination hornblende separates were analyzed at Universität Göttingen. Here, O-isotope analyses were conducted by infrared (IR) laser fluorination in combination with gas chromatography isotope ratio monitoring gas mass spectrometry (GC-irmMS) (Sharp, 1990; Jones *et al.*, 1999). The gas extraction technique is described, e.g. in Gehler *et al.* (in press). In brief, 1.0–1.3 mg of sample material was loaded along with MORB glass and NBS-28 quartz into a 18-pit nickel sample holder. After evacuation overnight and pre-fluorination, samples were reacted in a ~ 20 mbar atmosphere of purified F₂ gas (Asprey, 1976) by means of heating with a SYNRAD 50 W CO₂-laser. Liberated O₂ was cleaned from excess F₂ by reacting with NaCl (110 °C). The purified sample O₂ was expanded into a stainless steel capillary and transported with He carrier gas through a second trap, where O₂ was cryofocused at -196 °C on a molecular sieve. Sample O₂ was then released at 92 °C back into the He carrier gas stream and transported through a 5 Å molecular sieve GC column of a Thermo Gasbench-II. Sample O₂ was injected via an open split valve of the GasBench-II into the source of a THERMO MAT 253 gas mass spectrometer. The signals of $^{16}\text{O}^{16}\text{O}$ and $^{18}\text{O}^{16}\text{O}$ were simultaneously monitored on Faraday cups. Sample peaks ($m/z = 32$) had an amplitude of 20 - 30 V and a full width at half maximum of ~ 20 s. Reference O₂ was injected before the sample through a second open split valve of the GasBench-II. The external error of a single analysis was ± 0.25 ‰.

Hornblende separates from four samples have been dated using the $^{40}\text{Ar}/^{39}\text{Ar}$ method (see Table A.8 and Fig. 5.17). $^{40}\text{Ar}/^{39}\text{Ar}$ analyses were carried out at Argonlabor Freiberg

4 Analytical techniques

(ALF) at TU Bergakademie Freiberg, Germany. The sample packets were loaded in wells on Al discs (33 mm diameter) for irradiation, which was done for 2.5 hours at the LVR-15 research reactor of the Nuclear Research Institute in Řež, Czech Republic. The thermal neutron fluence was $\sim 5 \times 10^{13}$ n/cm²s at a thermal to fast neutron ratio of ~ 2 . Irradiated samples were unwrapped and loaded into small Mo-crucibles for furnace step heating experiments. Step heating was performed using a Createc® high-temperature cell (HTC) controlled by a Eurotherm 3504 controller. Gas purification was achieved by two AP10N getter pumps one at room temperature and one at 400 °C. Heating time was 7 minutes, cleaning time was 10 minutes per step. Ar isotope compositions were measured in static mode on a GV Instruments ARGUS noble gas mass spectrometer equipped with five faraday cups and 1012 Ω resistors on mass positions 36–39 and a 1011 Ω resistor on mass position 40. Typical blank levels are 2.5×10^{-16} mol ⁴⁰Ar and 8.1×10^{-18} mol ³⁶Ar. Measurement time was 7.5 minutes per temperature step acquiring 45 scans at 10 seconds integration time each. Mass bias was corrected assuming linear mass dependent fractionation and using an atmospheric ⁴⁰Ar/³⁶Ar ratio of 295.5. For raw data reduction and time-zero intercept calculation an in-house developed Matlab® toolbox was used, isochron, inverse isochron and plateau ages have been calculated using ISOPLOT 3.7 (Ludwig, 2008). All ages were calculated against Fish Canyon sanidine as flux monitor (28.305 ± 0.036 Ma; Renne *et al.*, 2010), errors on ages are 1σ . Corrections for interfering Ar isotopes have been done using $(^{36}\text{Ar}/^{37}\text{Ar})_{\text{Ca}} = 0.000245 \pm 0.000012$, $(^{39}\text{Ar}/^{37}\text{Ar})_{\text{Ca}} = 0.000932 \pm 0.000035$, $(^{38}\text{Ar}/^{39}\text{Ar})_{\text{K}} = 0.01211 \pm 0.00061$, $(^{40}\text{Ar}/^{39}\text{Ar})_{\text{K}} = 0.00183 \pm 0.00009$.

5 Results

5.1 Petrography

The hornblende-bearing basalts from the Rhön area are porphyritic and contain partly altered olivine and clinopyroxene. Commonly, the majority of olivine and clinopyroxene have grain sizes of ca. 0.5–2.0 and 0.2–5.0 mm. The olivine of the hornblende-bearing basalts dominantly appears as euhedral phenocrysts with sharply defined crystal edges. Rarely, olivine are more skeletal, which is indicative of fast cooling. Some olivine show evidence of marginal resorption, re-entrants and internal cavities, which can be interpreted as a disequilibrium feature. Clinopyroxene is zoned and generally composed of a subhedral to anhedral colorless to pale brown core and a darker brown, slightly pleochroic rim. In some samples, clinopyroxene with an olive-green to light-green core, a colorless to pale brown mantle and a dark brown rim occurs in addition to the clinopyroxene described above (e.g. Duda & Schmincke, 1985; Jung *et al.*, 2006). The majority of the samples contain optically homogeneous, unzoned brown amphibole with a grain size between 0.5 cm and 2.0 cm (e.g. Fig. 5.1) Some of these hornblende are surrounded by an opacitized rim of variable thickness or are completely altered. Other amphibole

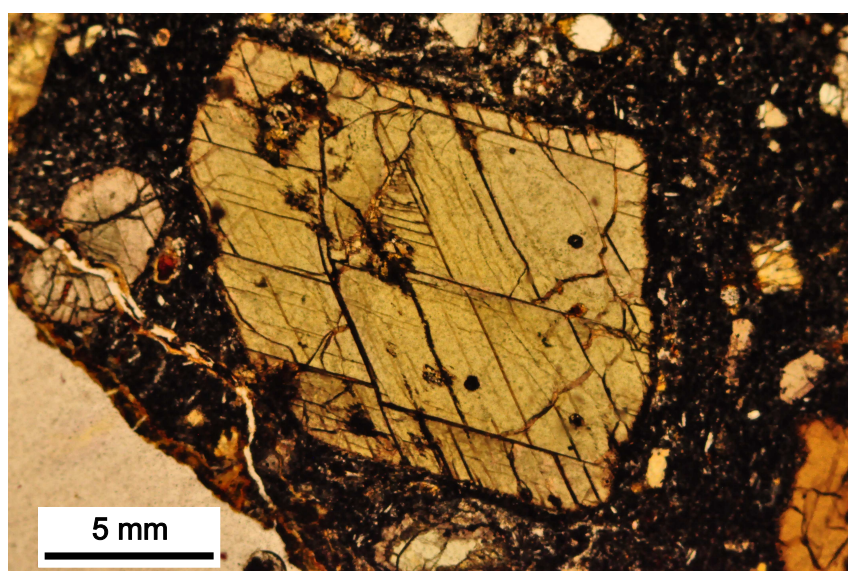


Figure 5.1: Brown kaersutite (Hbl-Rh10/09) with typical cleavage of 124° . Thin section (25 μm) photography under polarized light.

5 Results

grains show replacement by clinopyroxene. Plagioclase is common only in some alkali basalts and in the more differentiated rocks. It is generally unzoned.

5.2 Whole-rock geochemistry

5.2.1 Major element compositions

The hornblende-free and hornblende-bearing basalts from the Rhön area are basanites (SiO_2 : 42–45 wt.%; MgO : 4.0–12.0 wt.%) and alkali basalts (SiO_2 : 45–47 wt.%; MgO : 5.7–8.2 wt.%). More differentiated rocks are rare and include hornblende-bearing trachybasalts and phonotephrites (Fig. 5.2 a). The basalts have high TiO_2 concentrations (3.1–3.9 wt.%) except for the more differentiated lavas with lower TiO_2 contents of about 2.0 wt.%. Many hornblende-free lavas tend to have TiO_2 contents below 3.0 wt.%. In general, TiO_2 increases first until c. 10 wt.% MgO and then decrease with decreasing MgO (Fig. 5.2 b). The SiO_2 contents increase with decreasing MgO (Fig. 5.2 c). Some hornblende-free basanites show relatively high MgO concentrations up to 18 wt.%. A compilation of data from the literature from the Rhön shows that most hornblende-free lavas have higher MgO and lower TiO_2 than hornblende-bearing lavas (Fig. 5.2 b). High MgO samples show increasing CaO with decreasing MgO whereas most samples with lower MgO (< 10 wt.%) show decreasing CaO with decreasing MgO (Fig. 5.2 d). In general, Al_2O_3 abundances increase with decreasing MgO (Fig. 5.2 f). The $\text{CaO}/\text{Al}_2\text{O}_3$ ratio is low (0.6–1.0) and decrease with decreasing MgO whereas the $\text{Al}_2\text{O}_3/\text{TiO}_2$ ratio is comparatively low (3.6–4.9) and increase with decreasing MgO (Fig. 5.2 g-h).

5.2.2 Trace element compositions

Compatible elements such as Cr (30–400 ppm), Ni (20–160 ppm), Sc (13–42 ppm), and V (200–400 ppm) decrease with decreasing MgO (Fig. 5.3 a-b). Abundances of incompatible trace elements, i.e. Sr, Y, Zr and Nb are similar in hornblende-bearing and hornblende-free lavas and increase with decreasing MgO (Fig. 5.3 c-f). Consequently, ratios of LILE/LREE (Ba/La: 10–18; Fig. 5.4 a), LILE/HFSE (Ba/Nb: 7.3–11.4), LREE/HFSE (La/Nb: 0.66–0.73 0.66-0.73), and HFSE/HFSE (Zr/Nb: 2.8–5.1) of the hornblende-bearing lavas are broadly similar to other lavas in the CEVP. In general, hornblende-free

5 Results

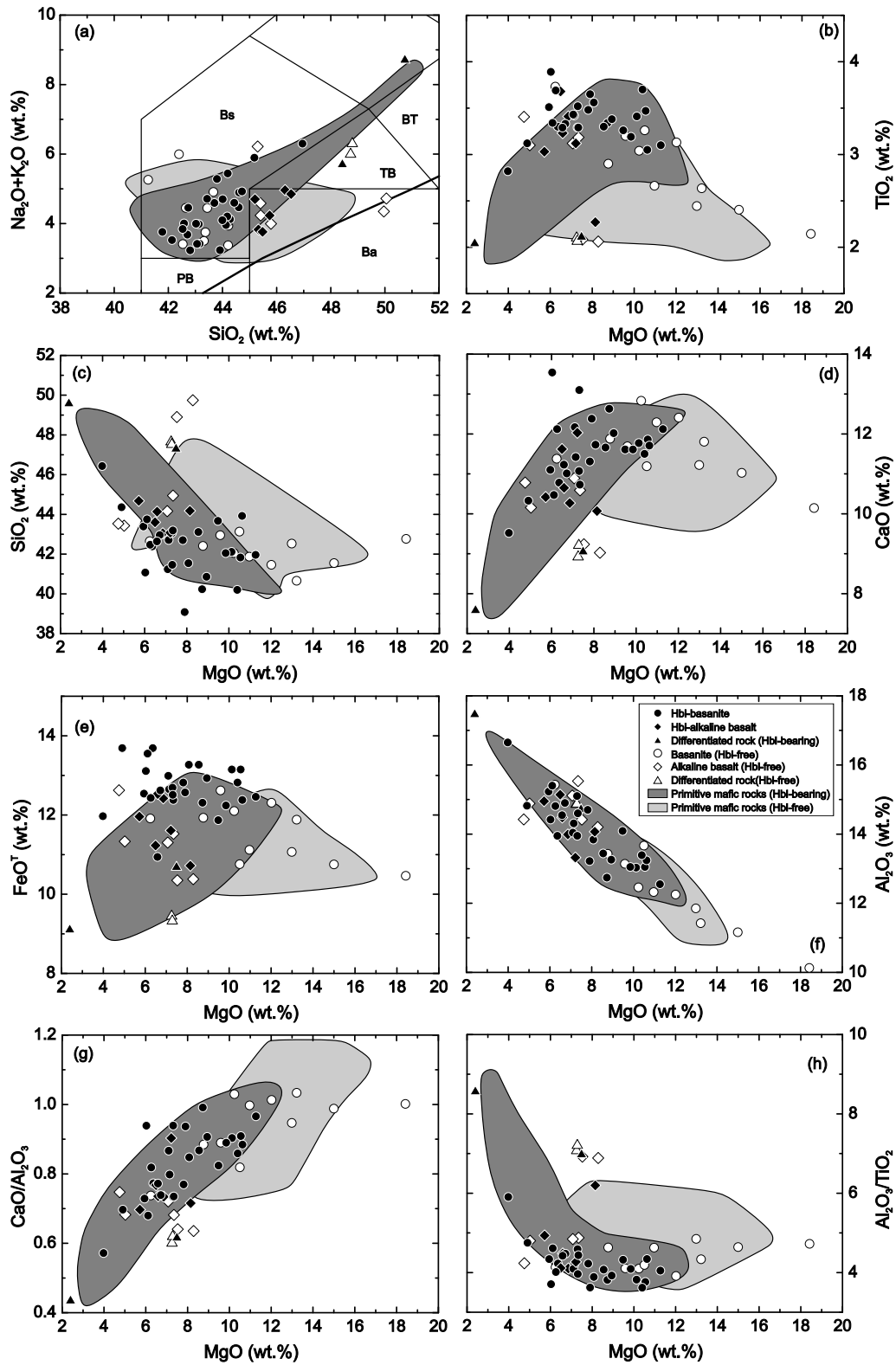


Figure 5.2: Major element compositions of lavas from the Rhön area: (a) Total alkali silica diagram (LeBas *et al.*, 1986) (b) TiO₂ vs. MgO (c) SiO₂ vs. MgO, (d) CaO vs. MgO, (e) FeO^T vs. MgO, (f) Al₂O₃ vs. MgO, (g) CaO/Al₂O₃ vs. MgO, (h) Al₂O₃/TiO₂ vs. MgO. Dark grey field: hornblende-bearing lavas (Rhön area), light grey field: hornblende-free lavas (Rhön area). Data are from Freerk-Parpatt (1990); Jung (1995); Jung & Hoernes (2000).

5 Results

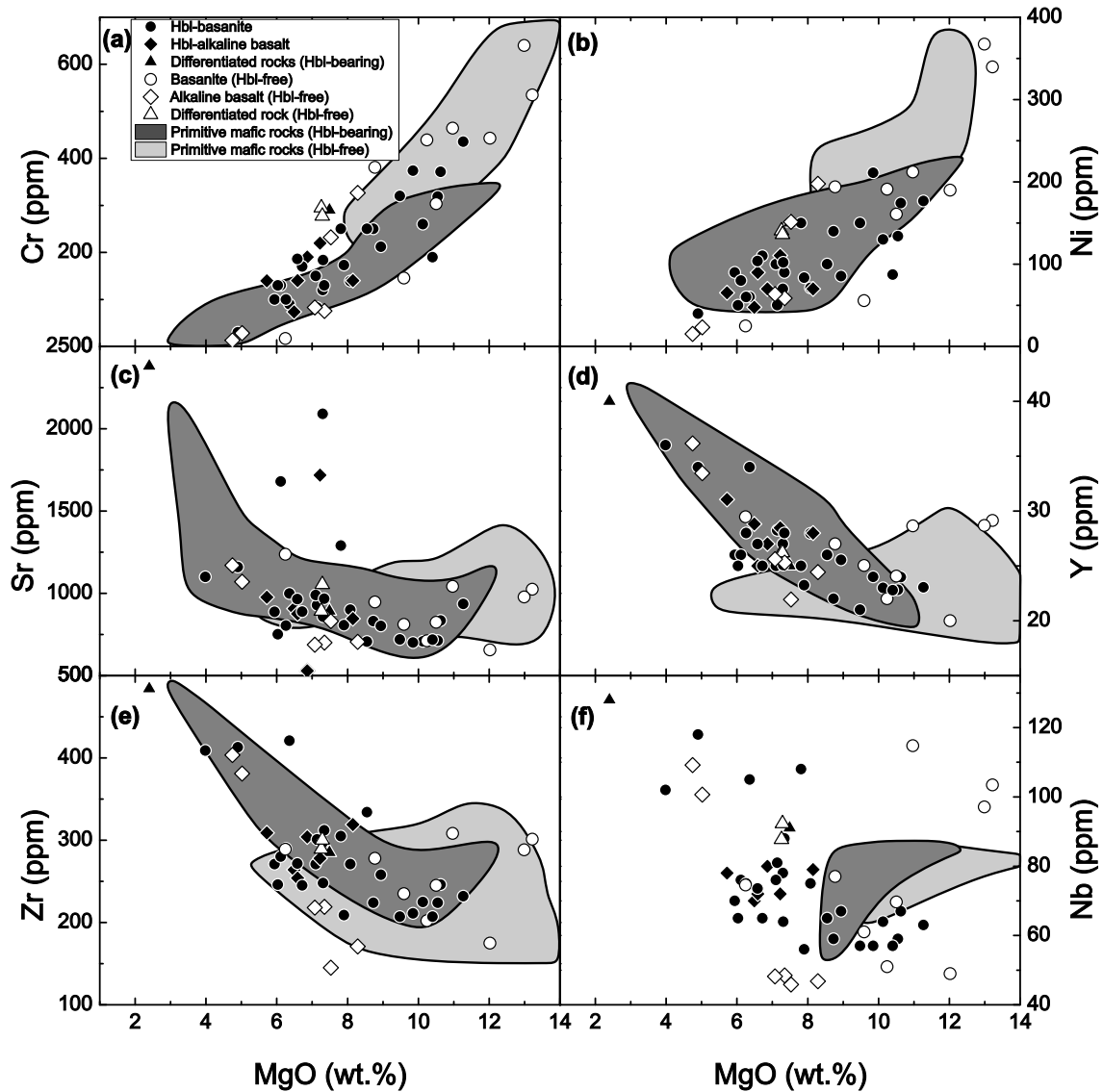


Figure 5.3: Trace element compositions of lavas from the Rhön area: (a) Cr vs. MgO, (b) Ni vs. MgO, (c) Sr vs. MgO (d) Y vs. MgO, (e) Zr vs. MgO, (f) Nb vs. MgO. Dark grey field: hornblende-bearing lavas (Rhön area), light grey field: hornblende-free lavas (Rhön area). Data are from Freerk-Parpatt (1990); Jung (1995); Jung & Hoernes (2000).

and hornblende-bearing basanites and alkaline basalts have similar Nb/U and Ce/Pb ratios in which a significant number of samples have Ce/Pb ratios above 30 (Fig. 5.4 b).

Rare Earth element patterns show LREE enrichment (Fig. 5.5) with no significant Eu anomalies similar to other alkaline volcanic rocks from the CEVP in which hornblende-free and hornblende-bearing samples have similar $(La/Yb)_N$ ratios ranging from 15–25.

5 Results

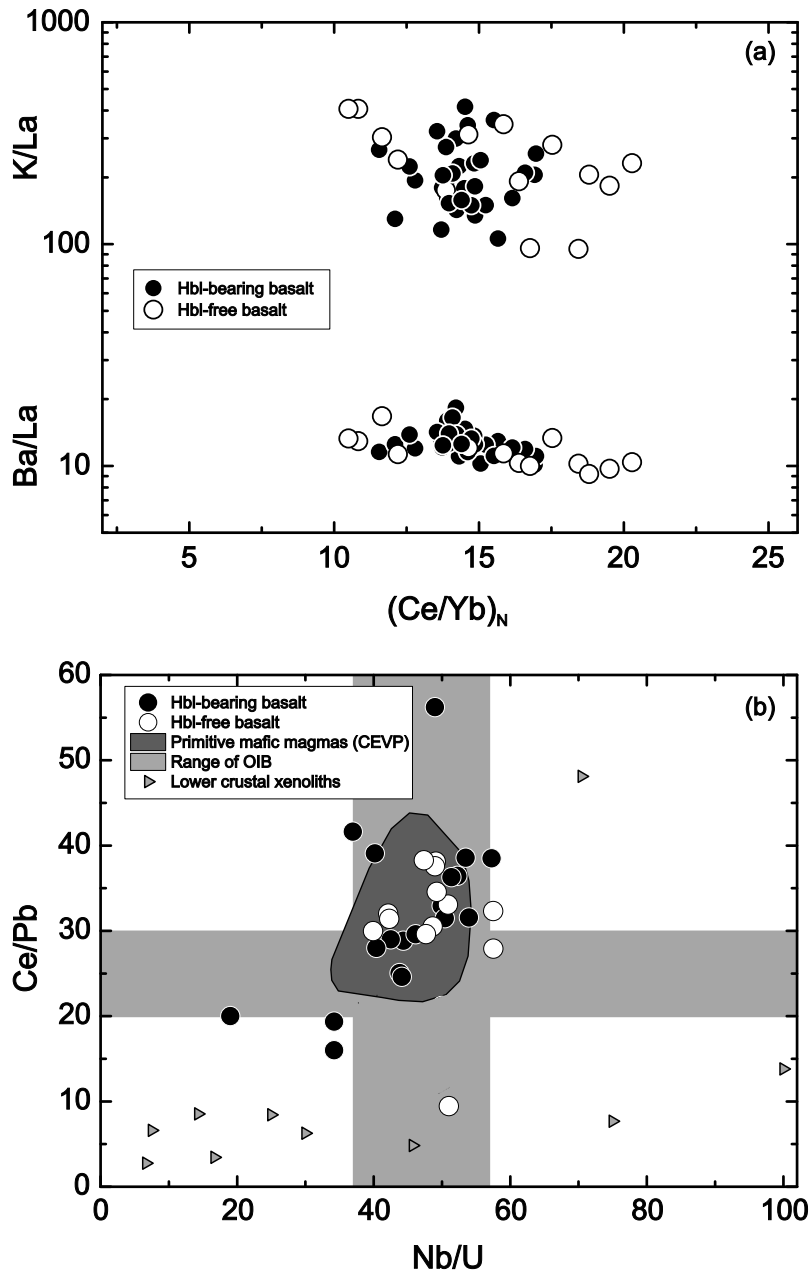


Figure 5.4: (a) K/La and Ba/La ratios versus chondrite-normalized Ce/Yb ratio of lavas from the Rhön area. (b) Covariation of Ce/Pb vs Nb/U for the Rhön lavas. Data for CEVP lavas from Jung & Hoernes (2000); Bogaard & Wörner (2003); Haase *et al.* (2004); Jung *et al.* (2006); Grey bars denote the range of typical OIB magma (Hofmann *et al.*, 1986); composition of lower crustal granulites from the Eifel from Sachs & Hansteen (2000).

The hornblende-bearing and hornblende-free lavas of the Rhön show strong enrichment in highly incompatible and moderately incompatible elements in primitive mantle-normalized element plots (Fig. 5.6). With increasing incompatibility, the normalized

5 Results

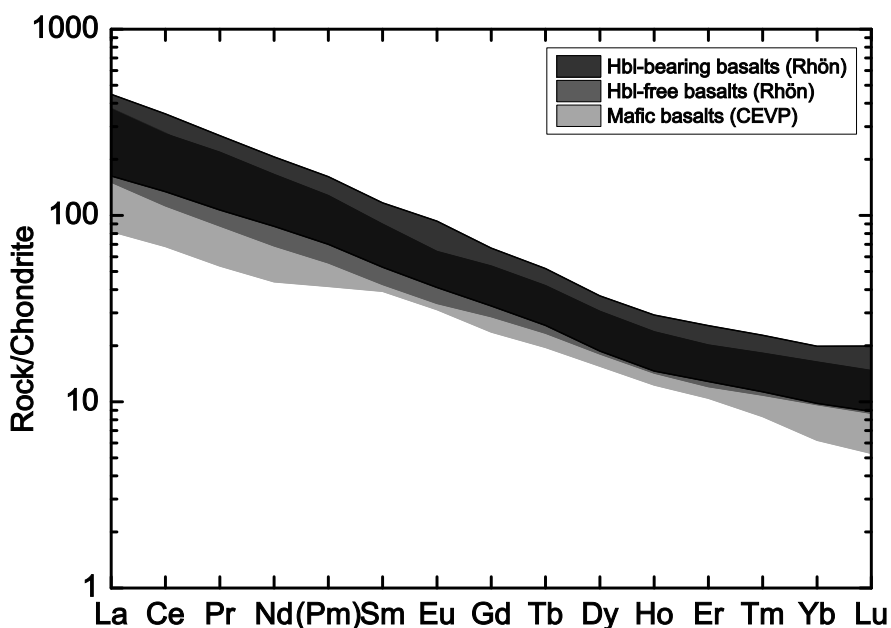


Figure 5.5: Chondrite-normalized Rare Earth Element diagram of hornblende-bearing and hornblende-free basalts from the Rhön area. Normalization values from McDonough & Sun (1995). Compositions for CEVP mafic lavas from Jung & Hoernes (2000); Bogaard & Wörner (2003); Haase *et al.* (2004); Jung *et al.* (2006).

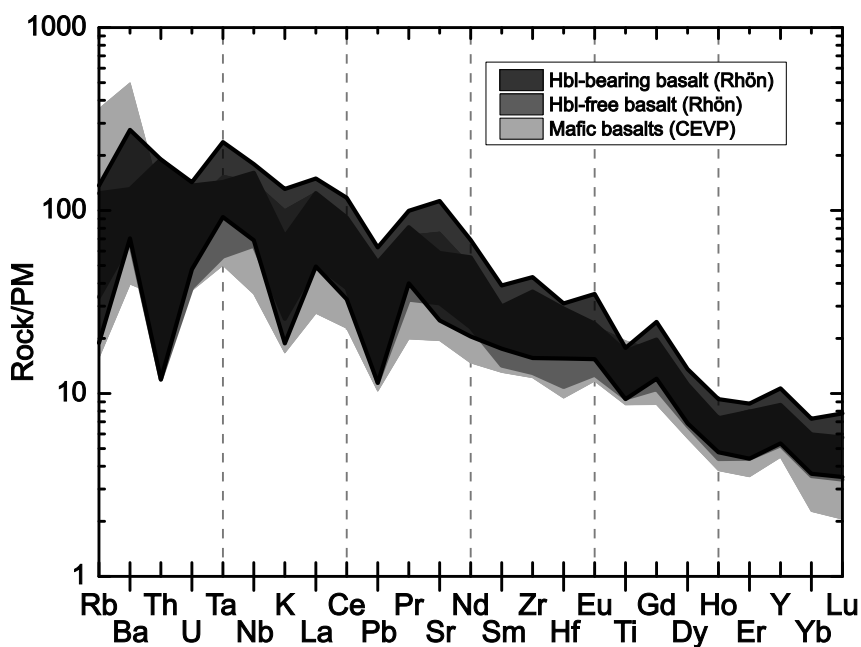


Figure 5.6: Primitive mantle normalized incompatible trace element diagram of hornblende-bearing and hornblende-free basalts from the Rhön area. Normalization values from McDonough *et al.* (1992). Compositions for CEVP mafic lavas from Jung & Hoernes (2000); Bogaard & Wörner (2003); Haase *et al.* (2004); Jung *et al.* (2006).

5 Results

concentrations increase and are similar to the pattern of many alkaline basalts from rift-related settings. Rubidium, Th, K, and Pb are strongly depleted compared to elements with similar compatibility. In comparison with basalts from the CEVP (Bogaard & Wörner, 2003; Haase *et al.*, 2004; Jung *et al.*, 2006, 2011) some hornblende-bearing lavas are enriched in Ba relative to similar incompatible elements. In addition, the hornblende-bearing basalts from the Rhön area show a weak positive Zr enrichment relative to similarly incompatible elements.

5.2.3 Isotope compositions

The hornblende-bearing basalts from the Rhön area are very similar in their $^{143}\text{Nd}/^{144}\text{Nd}$ isotope composition that range from 0.51279 to 0.51284. On the other hand, they show some variation in initial $^{87}\text{Sr}/^{86}\text{Sr}$ ratios ranging from 0.7034 to 0.7041 (Table A.2). In

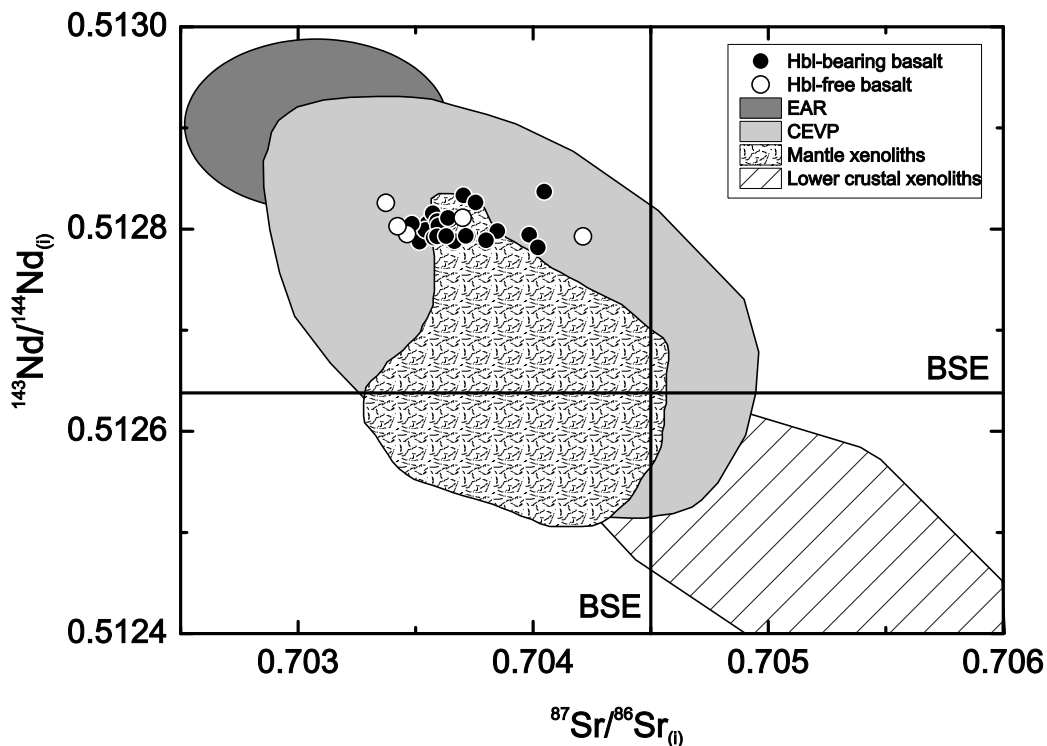


Figure 5.7: $^{143}\text{Nd}/^{144}\text{Nd}$ vs. $^{87}\text{Sr}/^{86}\text{Sr}$ isotope diagram for the Rhön lavas. Light grey area represents data for the CEVP (Jung & Masberg, 1998; Jung & Hoernes, 2000; Bogaard & Wörner, 2003; Haase *et al.*, 2004; Jung *et al.*, 2006, 2011). EAR denotes the European Asthenospheric Reservoir (Cebriá & Wilson, 1995); mantle xenolith isotope composition data from Witt-Eickschen *et al.* (2003) and isotope composition of lower crustal xenoliths data from Stosch & Lugmair (1984); Loock *et al.* (1990).

5 Results

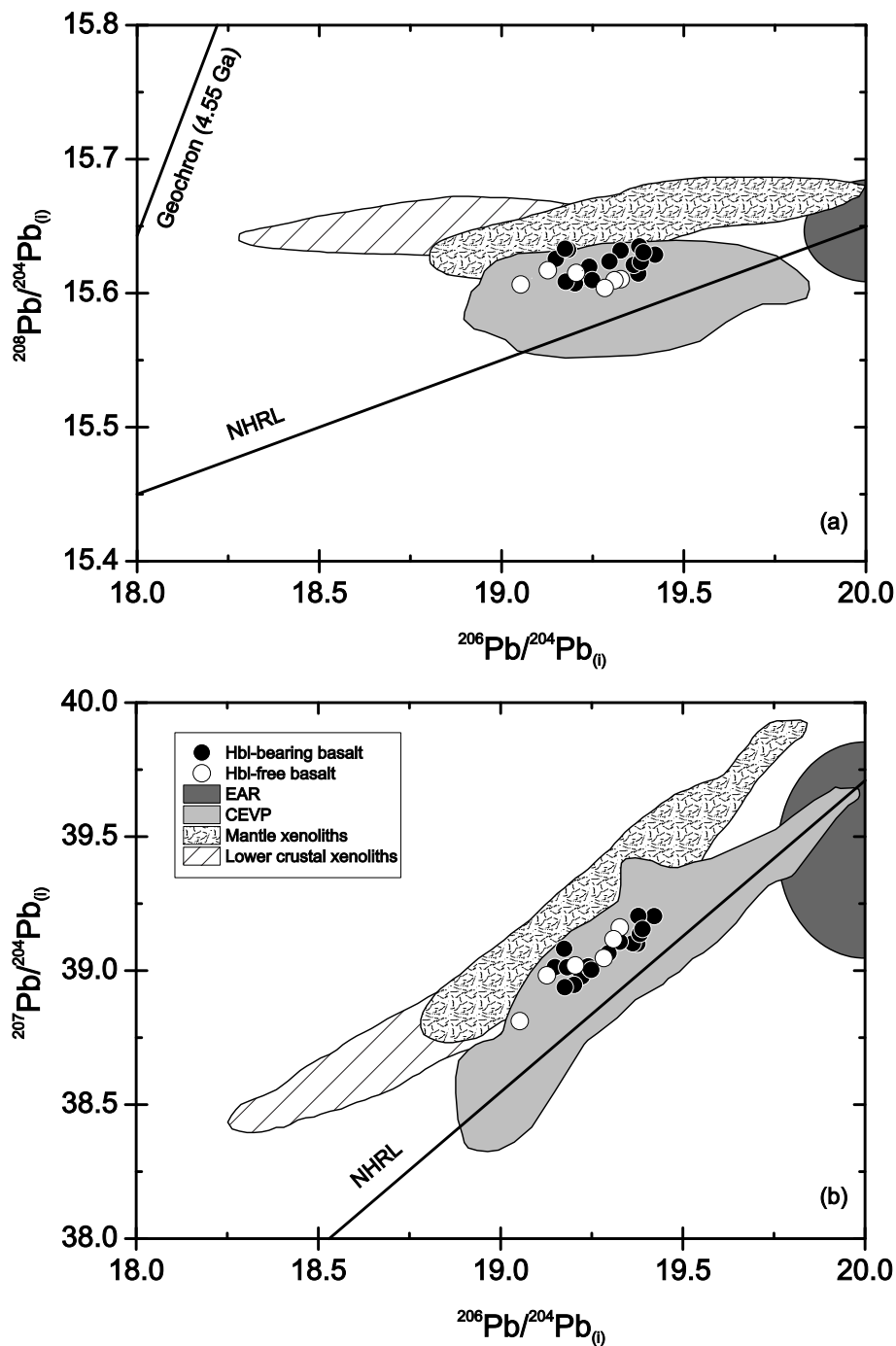


Figure 5.8: (a) $^{207}\text{Pb}/^{204}\text{Pb}$ vs. $^{206}\text{Pb}/^{204}\text{Pb}$ and (b): $^{208}\text{Pb}/^{204}\text{Pb}$ vs. $^{206}\text{Pb}/^{204}\text{Pb}$ diagram for lavas from the Rhön area. Light grey area represents data for the CEVP (Bogaard & Wörner, 2003; Haase *et al.*, 2004; Jung *et al.*, 2005, 2011). EAR denotes the European Asthenospheric Reservoir (Cebriá & Wilson, 1995); mantle xenolith isotope composition data from Witt-Eickschen *et al.* (2003) and isotope composition of lower crustal xenoliths data from Rudnick & Goldstein (1990). NHRL, Northern Hemisphere Reference Line (Hart, 1984).

5 Results

the $^{143}\text{Nd}/^{144}\text{Nd}$ vs. $^{87}\text{Sr}/^{86}\text{Sr}$ diagram (Fig. 5.7), the samples plot in the "depleted field" relative to Bulk Silicate Earth (BSE) close to the inferred position of EAR (Cebriá & Wilson, 1995). Similar ranges of Sr and Nd isotopes are represented by other Cenozoic mafic alkaline rocks from elsewhere in Germany (Wörner *et al.*, 1986; Wedepohl *et al.*, 1994; Hegner *et al.*, 1995; Jung & Masberg, 1998; Jung & Hoernes, 2000; Bogaard & Wörner, 2003; Haase *et al.*, 2004; Jung *et al.*, 2006, 2012), and in other CEVP complexes; for example, the Massif Central, Poland, the Pannonian basin and the Eger Graben (Downes, 1984; Alibert *et al.*, 1987; Blusztajn & Hart, 1989; Wilson & Downes, 1991; Downes *et al.*, 1995; Haase & Renno, 2008). In Pb isotope composition, the samples define an array parallel above the northern hemispheric reference line (NHRL) (Hart, 1984), i.e., have higher $^{207}\text{Pb}/^{204}\text{Pb}$ and $^{208}\text{Pb}/^{204}\text{Pb}$ ratios at given $^{206}\text{Pb}/^{204}\text{Pb}$ ratios (< 19.5) (Fig. 5.8) (Table A.2). In comparison to other lavas from the eastern part of CEVP (Haase *et al.*, 2004; Jung *et al.*, 2005) the hornblende-bearing basalts from the Rhön have similar $^{206}\text{Pb}/^{204}\text{Pb}$ (19.10–19.43) and $^{208}\text{Pb}/^{204}\text{Pb}$ ratios (38.94–39.22) but tend to have higher $^{207}\text{Pb}/^{204}\text{Pb}$ ratios (> 15.61).

5.3 Mineral chemistry

5.3.1 Major and trace element compositions

Chemical analysis indicate that amphibole from the Rhön lavas is rich in CaO (11–12 wt.%), MgO (12–15 wt.%; Fig. 5.9 a; Mg#:0.5–0.6), TiO_2 (4–7 wt.%, Fig. 5.9 a), FeO^{T} (9–12 wt.%), and Al_2O_3 (12–14 wt.%) with minor amounts of Na_2O and K_2O (Table A.4). All analyzed amphibole have Mg/(Mg+Fe) ratios above 0.5 and most analyses have Ti abundances of close to or higher than 0.5 Ti atoms per formula unit (apfu) which leads to classification as kaersutite ($\text{Ti} \geq 0.5$) or pargasite ($\text{Ti} < 0.5$) after Leake *et al.* (1997) (Fig. 5.9 b). In this amphibole classification kaersutite as well as pargasite consists predominantly of OH-groups at the W-position. However, a recent work of Hawthorne *et al.* (2012) consider kaersutite no longer as a $^{\text{W}}(\text{OH}, \text{F}, \text{Cl})$ -dominant calcium-bearing amphibole and classify this mineral as an oxo-amphibole with dominant O^{2-} at the W-position. Preliminary measurements of the amphibole in the hornblende-bearing lavas from the Rhön area with Raman spectroscopy reveal a certain amount of OH (Raman shift $\sim 3400 \text{ cm}^{-1}$; Fig. A.1) and analyses with EMPA indicate fluorine concentrations around 0.5 apfu. For simplicity, the amphibole in the hornblende-bearing lavas from

5 Results

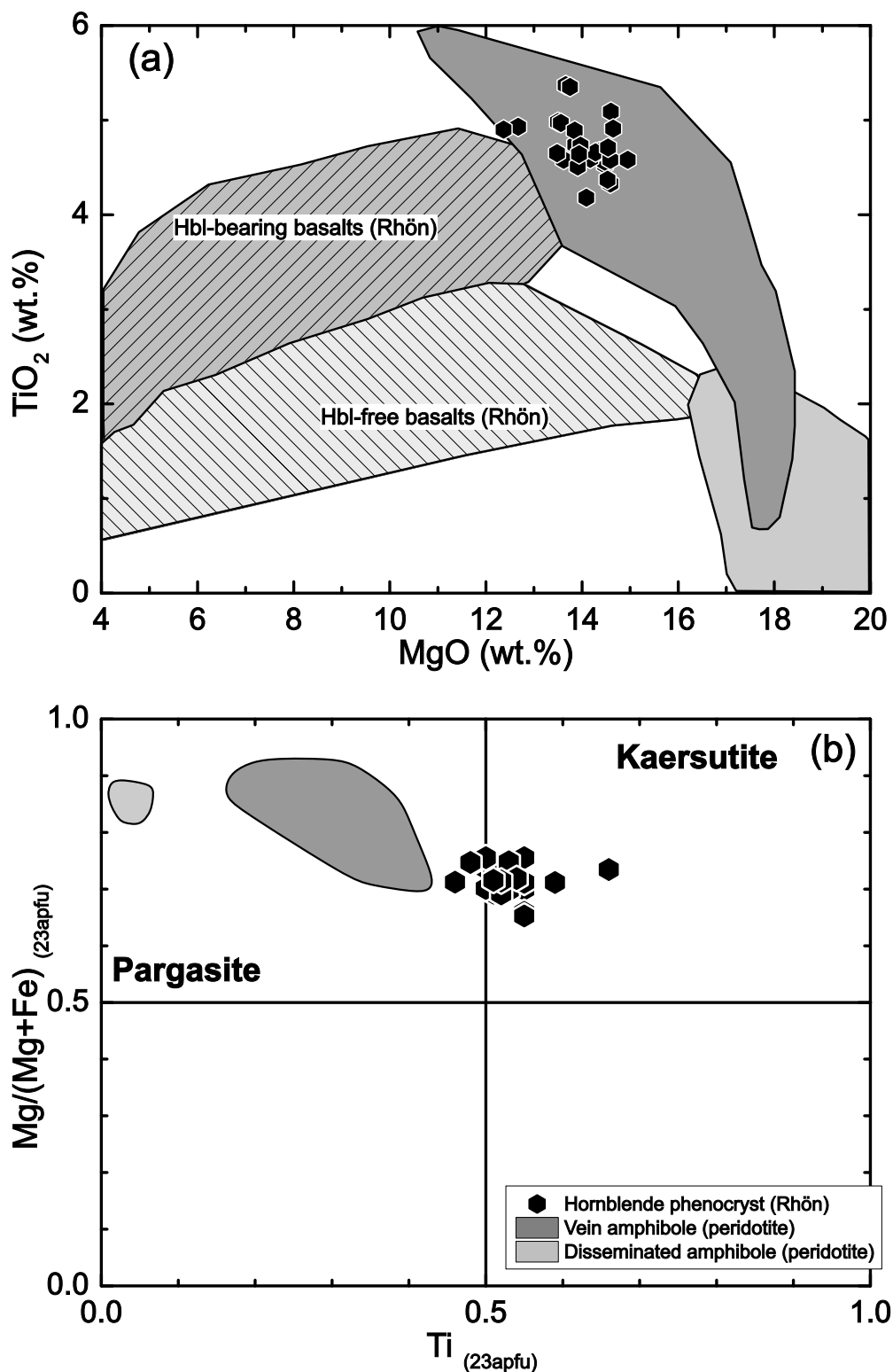


Figure 5.9: (a) MgO vs. TiO₂ and (b) Mg/(Mg/Fe) vs. Ti variations of hornblende from the Rhön area; for comparison representative vein amphibole and disseminated amphibole compositions (Bedard, 1988; Colville & Novak, 1991; Ionov & Hofmann, 1995; Witt-Eickschen *et al.*, 2003; Powell *et al.*, 2004) and whole-rock composition of hornblende-bearing and hornblende-free basalts of this study are also shown.

5 Results

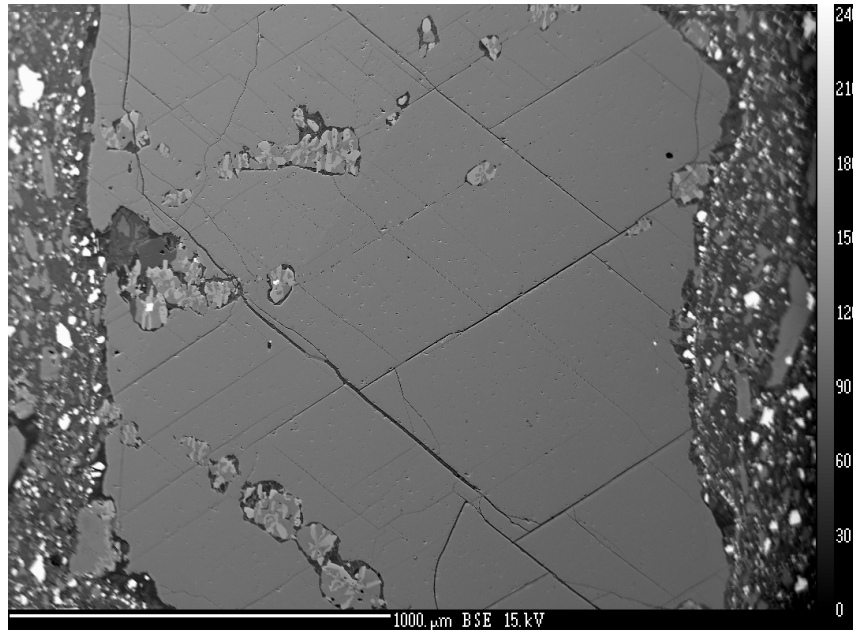


Figure 5.10: Backscattered electron image of kaersutite (Hbl-Rh10/09).

the Rhön area are hereafter referred to kaersutite with the chemical formula (23 oxygen per formula): $K_{0.3}Na_{0.6}Ca_{1.7-1.9}Ti_{0.5-0.6}Mg_{2.9-3.2}Fe_{1.1-1.3}Al_{2.4}Si_{5.8}O_{23}(F_{0.1-0.5}OH)$.

In comparison to amphibole found in peridotite xenoliths from the CEVP (Witt-Eickschen *et al.*, 2003) and from other provinces (Ionov & Hofmann, 1995; Powell *et al.*, 2004) the kaersutite have, in general, higher TiO_2 and FeO^T and slightly higher K_2O concentrations, but lower MgO , Na_2O , and SiO_2 concentrations. Rare examples from a magmatic vein (Witt-Eickschen *et al.*, 2003) have broadly similar geochemical compositions than the kaersutite found in the alkalic lavas from the Rhön. Detailed backscattered secondary electron images (BSE) from electron microprobe studies (e.g. Fig. 5.10) and major element distributions obtained by EMPA analyses and trace element concentrations measured with SIMS reveal no significant variation from core to rim (Table A.4 and A.5). Differences in core-rim compositions of the kaersutite can be only observed in their F content. Although there are some differences (e.g. TiO_2 , MgO) between some phenocrysts, these differences are small and are correlated with the TiO_2 and MgO concentrations of the corresponding lavas. CaO , on the other side, show only a small variation but is not correlated with the variation to concentrations in the host rock. Rare Earth Element analyses show enrichment of LREE relative to Heavy Rare Earth Element (HREE) and a general convex REE pattern with a maximum concentration at Nd. LREE concentrations are enriched (20 to 50 times chondritic) and concentrations of the HREE are around 5-10 times chondrite. The absolute concentrations of the REE in amphibole

5 Results

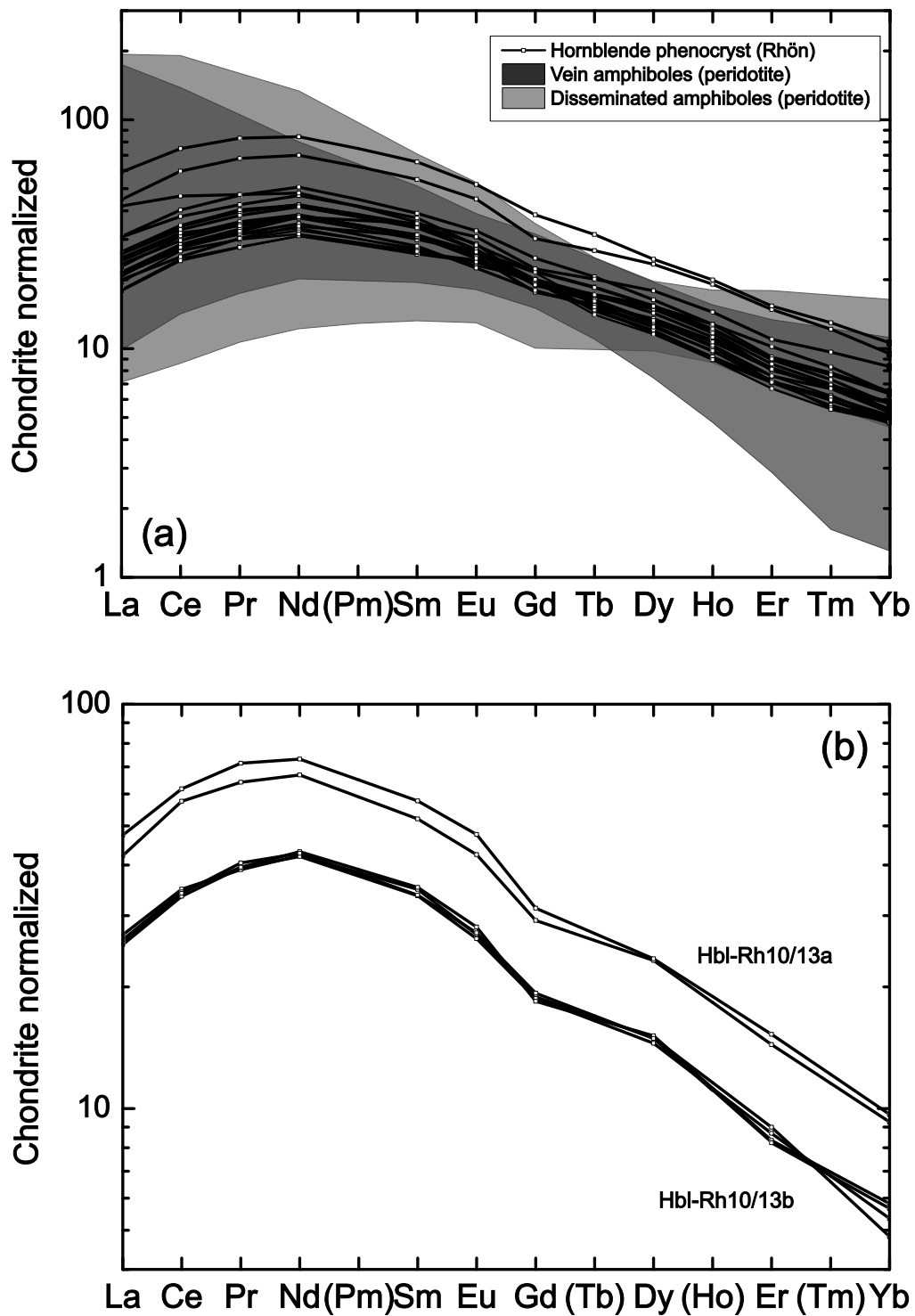


Figure 5.11: (a) Hornblende REE-pattern normalized to C1-Chondrite (McDonough & Sun, 1995); dark grey field represent vein amphibole and bright grey field disseminated amphibole (Ionov & Hofmann, 1995; Witt-Eickschen *et al.*, 2003; Powell *et al.*, 2004); (b) REE of Hbl-Rh10/13a and Hbl-Rh10/13b normalized to C1-chondrite.

5 Results

differ between the different host rocks (Fig. 5.11 a) and even between minerals in the same lava (Fig. 5.11 b). In general, amphibole related to veins in peridotite xenoliths show REE pattern similar to those described here. In contrast, disseminated amphibole from peridotite xenoliths show a flat REE pattern and are more enriched in HREE (Ionov & Hofmann, 1995; Witt-Eickschen *et al.*, 2003; Powell *et al.*, 2004).

Relative to the primitive mantle, the kaersutite from this study are enriched in almost all elements except Th and U. In a primitive mantle normalized diagram Ba, Sr, and Ti are enriched and show positive anomalies relative to elements with similar chemical incompatibility; Th, U, Pb, and Zr are depleted compared to similarly incompatible elements and show negative anomalies (Fig. 5.12). Most kaersutite show $(\text{Nb}/\text{Ta})_N$ and $(\text{Zr}/\text{Hf})_N$ ratios < 1 . Vein amphibole from other localities have similar $(\text{Nb}/\text{Ta})_N$ and $(\text{Zr}/\text{Hf})_N$ ratios at lower HFSE concentrations (Ionov & Hofmann, 1995; Witt-Eickschen *et al.*, 2003; Powell *et al.*, 2004). Though the LILE concentrations of the studied kaersutite are

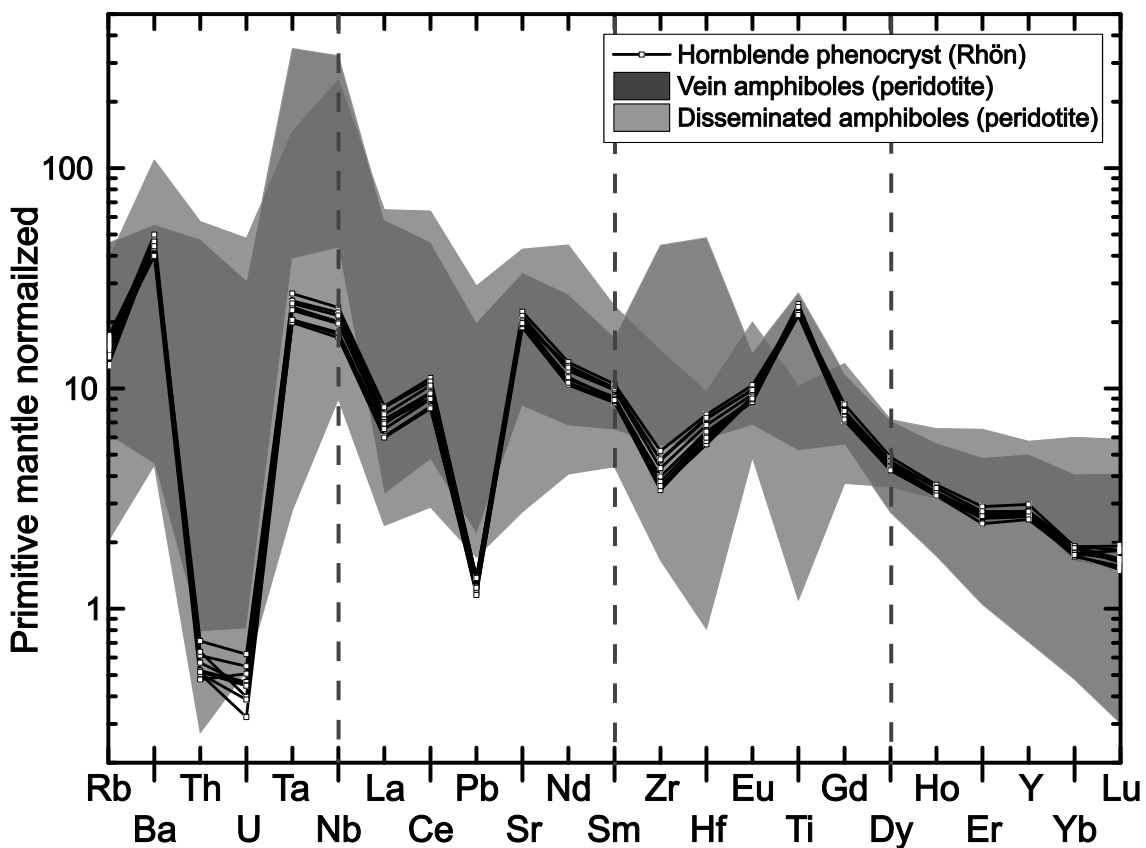


Figure 5.12: Incompatible trace element patterns of hornblende normalized to primitive mantle (McDonough *et al.*, 1992); dark grey field represent vein amphibole and bright grey field disseminated amphibole (Ionov & Hofmann, 1995; Witt-Eickschen *et al.*, 2003; Powell *et al.*, 2004).

5 Results

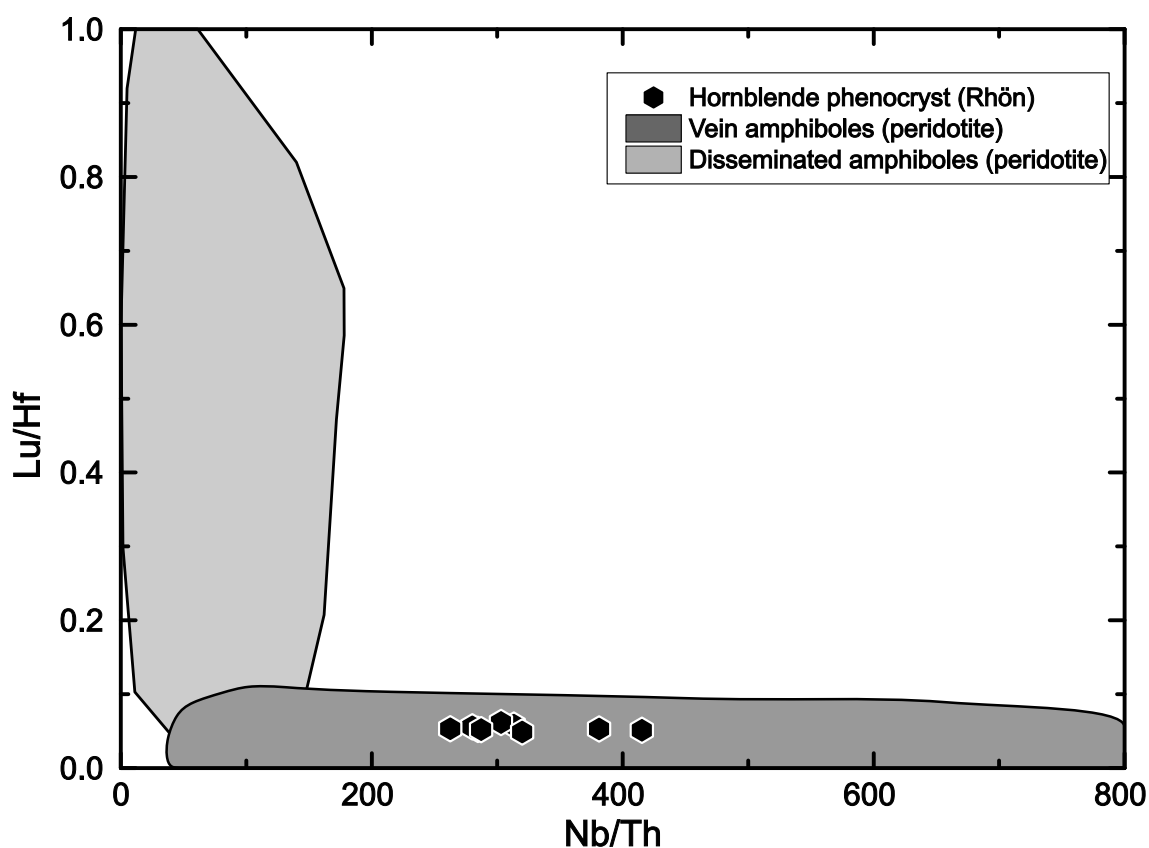


Figure 5.13: Nb/Th vs. Lu/Hf covariations of hornblende from the Rhön area and representative vein amphibole and disseminated amphibole compositions (Ionov & Hofmann, 1995; Witt-Eickschen *et al.*, 2003; Powell *et al.*, 2004).

similar to disseminated amphibole from peridotitic xenoliths, the HFSE concentrations and resulting pattern are different. In detail the Hf concentrations tend to be lower and Nb, Y, and HREE are higher in disseminated amphibole than in vein amphibole. The Rb/Sr ratios of kaersutite (~ 0.025) are broadly similar to other vein amphibole (0.03–0.043) but tend to be higher than in disseminated amphibole from peridotite xenoliths (< 0.02) (Ionov & Hofmann, 1995; Ionov *et al.*, 1997; Witt-Eickschen *et al.*, 2003; Powell *et al.*, 2004). Comparing vein amphibole and disseminated amphibole from peridotite xenoliths, the amphibole from the Rhön lavas plot into the field of vein amphibole with low Lu/Hf ratios and variable but high Nb/Th ratios (Fig. 5.13).

5.3.2 Isotope compositions

Hornblende from different samples show a wide range in their Sr, Nd, and Pb isotope composition (Table A.7). Three kaersutite (Hbl-Rh10/01; Hbl-Rh10/13; Hbl-Rh10/33) comprise a group which has similar Pb, Sr, and Nd isotope composition (Fig. 5.14). These phenocrysts have $^{206}\text{Pb}/^{204}\text{Pb}$ (19.3–19.4), $^{207}\text{Pb}/^{204}\text{Pb}$ (15.63–15.67) and $^{208}\text{Pb}/^{204}\text{Pb}$ (39.1–39.3) ratios that are comparable to the isotope composition of the host lava, although the $^{208}\text{Pb}/^{204}\text{Pb}$ (Fig. 5.15 a) and the $^{207}\text{Pb}/^{204}\text{Pb}$ (Fig. 5.15 b) ratio is slightly higher in the minerals than in the lava. Strontium (initial $^{87}\text{Sr}/^{86}\text{Sr}$: 0.7035–0.7036) and Nd isotope compositions (ϵNd : +3.8 to +4.0) of these phenocrysts plot in the "depleted field" relative to bulk silicate earth close to the inferred position of the European Asthenospheric Reservoir (EAR; Cebriá & Wilson, 1995). The hornblende from sample Rh10/25 is similar in its Pb and Nd isotope ratios, but tend to be slightly more radiogenic in the initial Sr isotope composition ($^{87}\text{Sr}/^{86}\text{Sr}$: 0.7037) than the other phenocrysts. Two

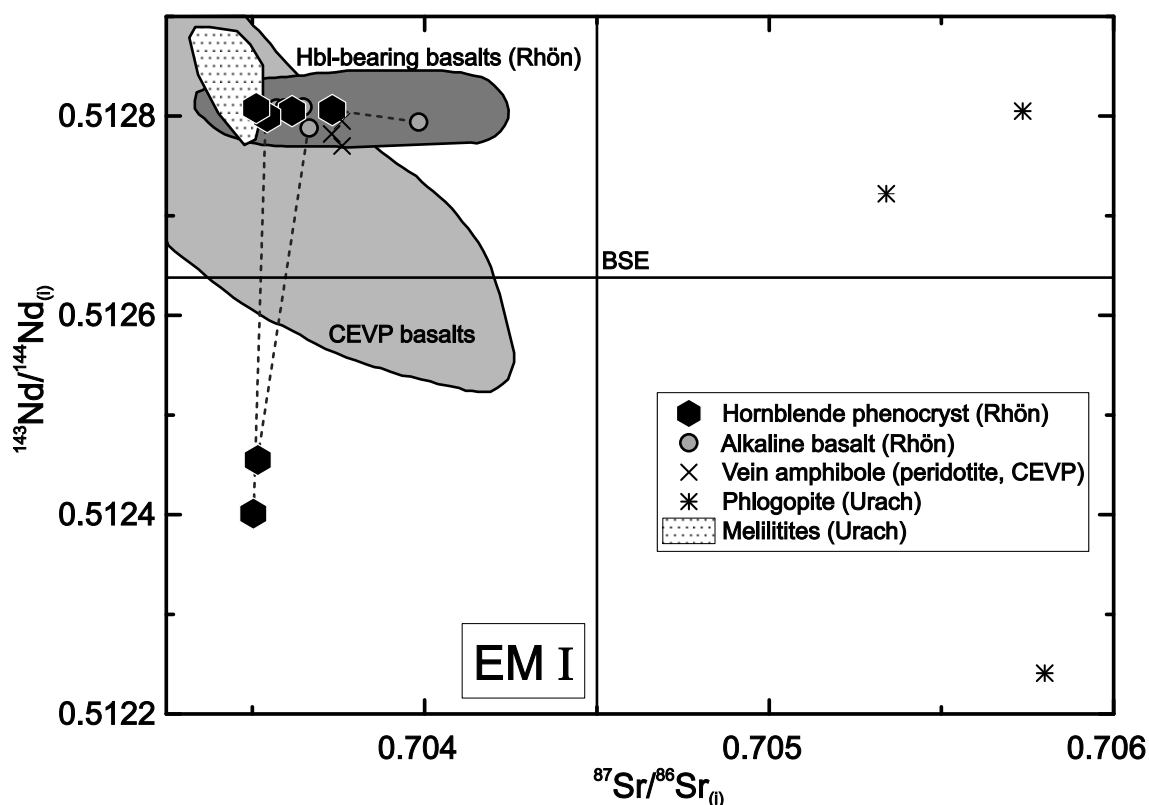


Figure 5.14: $^{87}\text{Sr}/^{86}\text{Sr}$ vs. $^{143}\text{Nd}/^{144}\text{Nd}$ isotope diagram for hornblende from the Rhön area. Hornblende-bearing basalt isotope compositions are shown for comparison. Vein amphibole (CEVP) compositions from Witt-Eickschen *et al.* (2003); phlogopite and melilitite isotope compositions from Urach for comparison (Hegner *et al.*, 1995).

5 Results

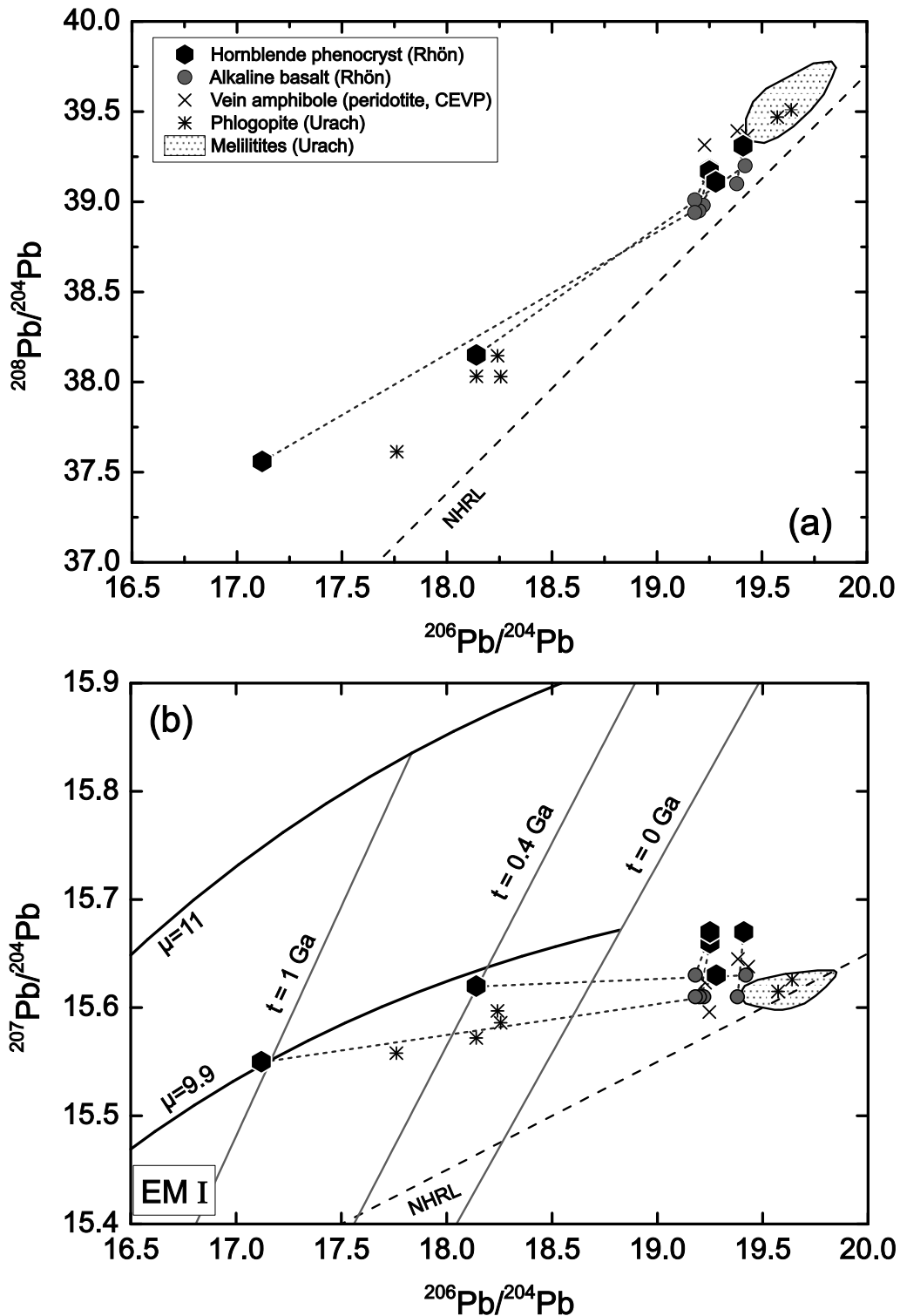


Figure 5.15: (a) $^{208}\text{Pb}/^{204}\text{Pb}$ vs. $^{206}\text{Pb}/^{204}\text{Pb}$ and (b): $^{207}\text{Pb}/^{204}\text{Pb}$ vs. $^{206}\text{Pb}/^{204}\text{Pb}$ diagram for hornblende from the Rhön area. Hornblende-bearing basalt isotope compositions for comparison. Vein amphibole (CEVP) compositions from Witt-Eickschen *et al.* (2003); phlogopite and melilitite isotope compositions from Urach for comparison (Hegner *et al.*, 1995); two stage Pb evolution curve according to Stacey & Kramers (1975) with higher μ is plotted; EMI endmember from Zindler & Hart (1986).

5 Results

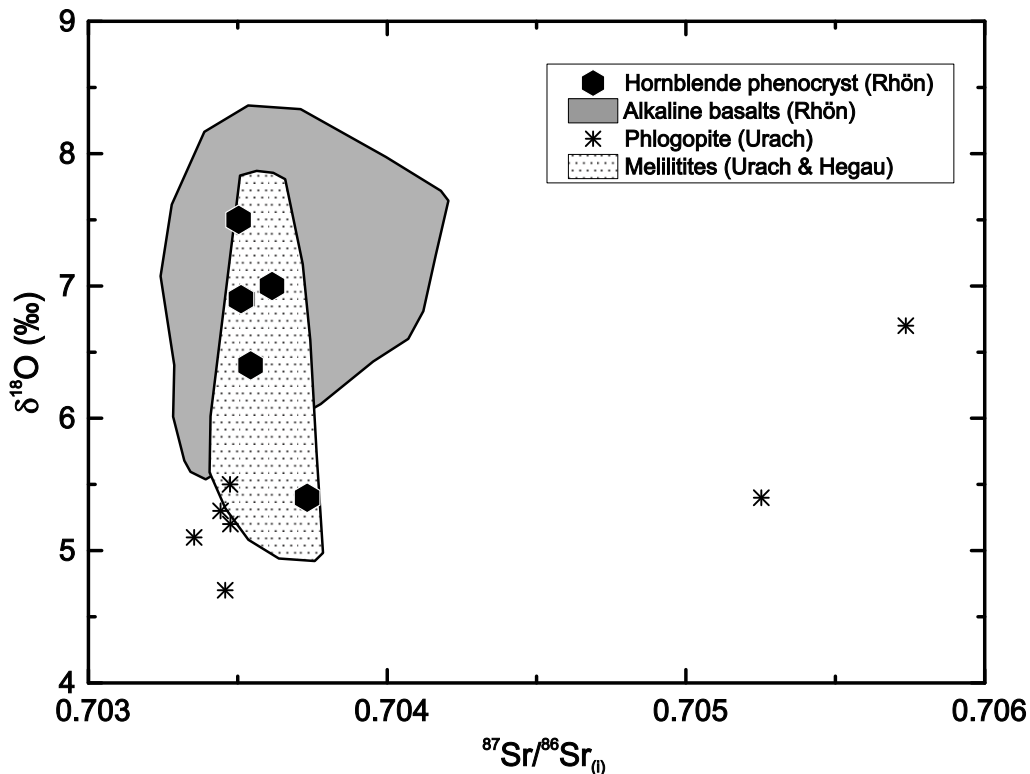


Figure 5.16: $^{87}\text{Sr}/^{86}\text{Sr}$ vs $\delta^{18}\text{O}$ isotope compositions of hornblende from the Rhön area. Whole rock O isotope compositions corrected for 0.5 LOI (data from Freerk-Parpatt (1990); Jung & Hoernes (2000)). Phlogopite and melilitite data (Urach/Hegau) from Hegner *et al.* (1995); Hegner & Vennemann (1997).

phenocrysts (Hbl-Rh10/07 and Hbl-Rh10/09) show Sr isotope ratios similar to their host lava and the other phenocrysts in this study but different Pb and Nd isotope compositions with less radiogenic Pb isotope ratios and negative ϵNd values ($^{206}\text{Pb}/^{204}\text{Pb}$: 17.1 and 18.2; $^{207}\text{Pb}/^{204}\text{Pb}$: 15.55 and 15.62; $^{208}\text{Pb}/^{204}\text{Pb}$: 37.6 and 38.2 ; ϵNd : -4.0 and -2.9).

The kaersutite show variable $\delta^{18}\text{O}$ values ranging from 5.4 ‰ for kaersutite of sample Rh10/25 to 7.5 ‰ for the other minerals (Fig. 5.16; Table A.7). The lower $\delta^{18}\text{O}$ value of sample Hbl-Rh10/25 is correlated with a higher Sr isotope ratio, whereas the $\delta^{18}\text{O}$ ratios of the other phenocrysts are not correlated with the Sr isotope ratio. Alteration-corrected $\delta^{18}\text{O}$ values of whole-rock analyses of samples from the Rhön area are between 6 ‰ and 8 ‰ (Freerk-Parpatt, 1990; Jung & Hoernes, 2000). Phlogopite and hornblende minerals of the nearby Urach volcanic field have in general lower $\delta^{18}\text{O}$ values (4.5–5.5 ‰) and similar or higher $^{87}\text{Sr}/^{86}\text{Sr}$ isotope ratios (0.7035–0.7057) (Hegner & Vennemann, 1997).

5.4 Geochronology

Hornblende separates from four samples have been dated using the $^{40}\text{Ar}/^{39}\text{Ar}$ method (see Table A.7 and Fig. 5.17). All four samples yield perfect plateau ages of 24.0 ± 0.2 and 24.1 ± 0.2 Ma, respectively, in very good agreement with the inverse isochron ages derived from all measured temperature steps (Fig. 5.17). For two of the samples (Hbl-Rh10/01 and Hbl-Rh10/07), the correction for initial $^{40}\text{Ar}/^{36}\text{Ar}$ to calculate the age spectrum has been done using $^{40}\text{Ar}/^{36}\text{Ar} = 331$ and 307 , respectively, as the inverse isochron plots of the plateau steps of these samples suggest the presence of an excess argon component (see insets in Fig. 5.17 b, d). Due to the low abundance of initial argon in all samples, however, the adopted initial $^{40}\text{Ar}/^{36}\text{Ar}$ influenced the final ages by less than 0.2 Ma.

5 Results

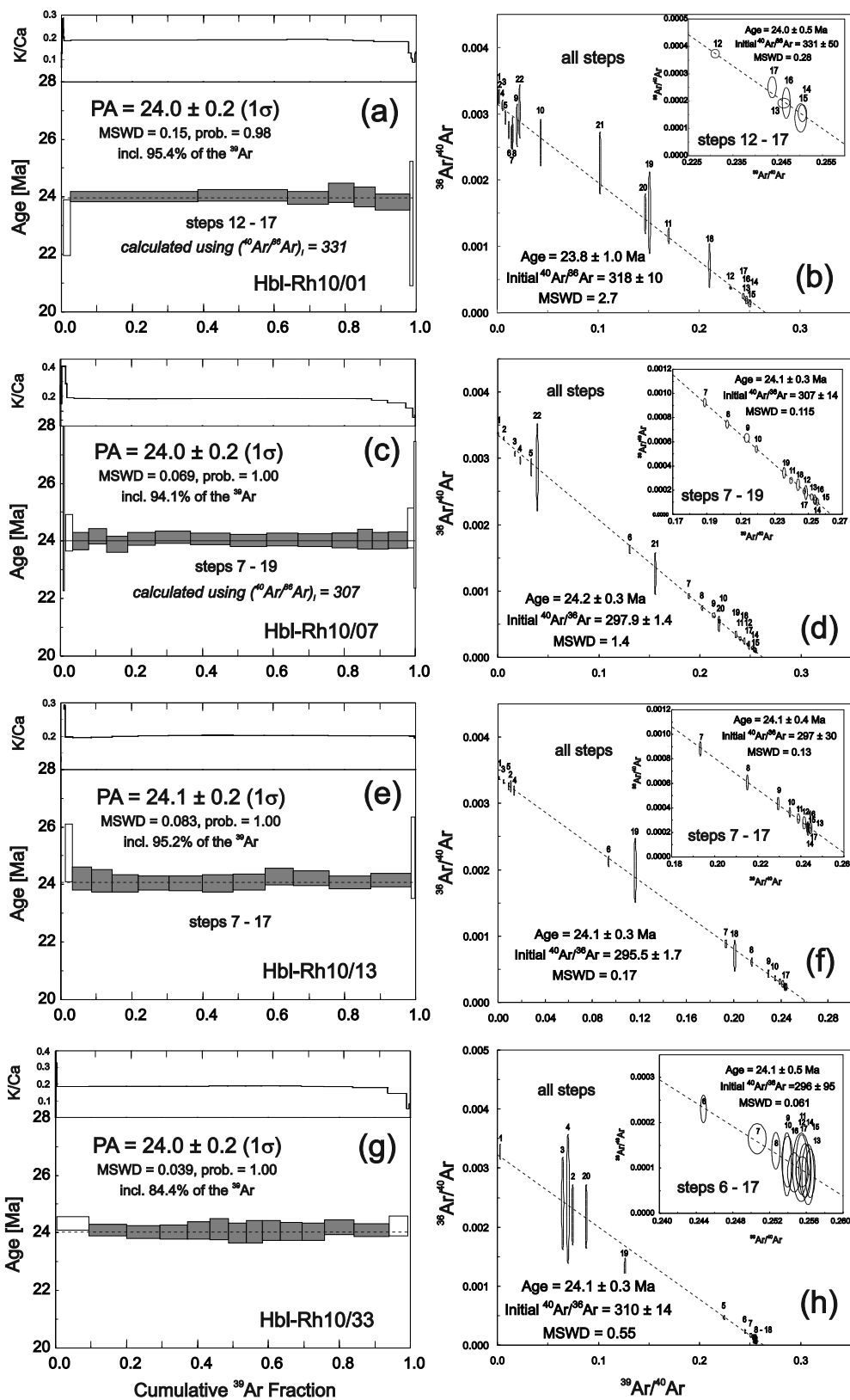


Figure 5.17: Ar-Ar plateau for (a) Hbl-Rh10/01, (c) Hbl-Rh10/07, (e) Hbl-Rh10/13, (g) Hbl-Rh10/33 with inverse isochron of all steps and used steps as inlet of (b) Hbl-Rh10/01, (d) Hbl-Rh10/07, (f) Hbl-Rh10/13, (h) Hbl-Rh10/33.

6 Discussion

6.1 Fractional crystallization

The chemical variation in all studied lavas from the Rhön area indicates that fractional crystallization significantly affected the magma composition. The most primitive basanites have MgO and highly compatible element (Ni, Cr, Sc) abundances that are higher than the concentrations usually assumed for primitive basaltic melts (Frey *et al.*, 1978; Hart & Davis, 1978). Some primitive basanites with MgO abundances from 8 wt.% to 12 wt.% appear to be near-primary melts with moderately high Ni (> 100 ppm), high Cr (> 200 ppm), and high Sc (> 30 ppm) concentrations. The CaO/Al₂O₃ ratio decreases with decreasing MgO abundances for lavas with less than 12 wt.% MgO indicating that clinopyroxene is a major mineral phase during fractionation. Decreasing concentrations of Ni with decreasing MgO suggests that olivine was also a major fractionating mineral phase. TiO₂, V, and Sc decrease with decreasing MgO indicating that, beside Ti-augite, amphibole was a fractionating mineral phase ($K_{d_{Ti}}: 1.35; K_{d_V}: 5.7; K_{d_{Sc}}: 4.2$; Adam & Green, 2006) especially for some lavas with MgO < 6 wt.%. In primitive mantle-normalized trace element patterns (Fig. 5.6), a few lavas are enriched in Sr relative to elements with similar incompatibility. The lack of negative Eu anomalies and increasing Al₂O₃ with decreasing MgO implies that plagioclase was not a major mineral phase during fractionation.

The degree of fractional crystallization can be estimated using equations from Neumann *et al.* (1954) utilizing the high sensitivity of compatible elements upon fractional crystallization with distribution coefficients from Villemant *et al.* (1981); Adam & Green (2006). The elements Cr and Sc are used for this calculation because of their compatible behavior in basaltic liquids and their high but distinct partition coefficients for minerals such as olivine, clinopyroxene, and amphibole. Based on the Cr vs Sc distribution several distinct fractionation paths are possible (Fig. 6.1). Path A is characterised by fractionation of only olivine whereas path B uses olivine plus clinopyroxene as fractionating mineral phases. Path C involves fractionation of olivine, clinopyroxene plus amphibole to explain some samples with low Sc and Cr abundances.

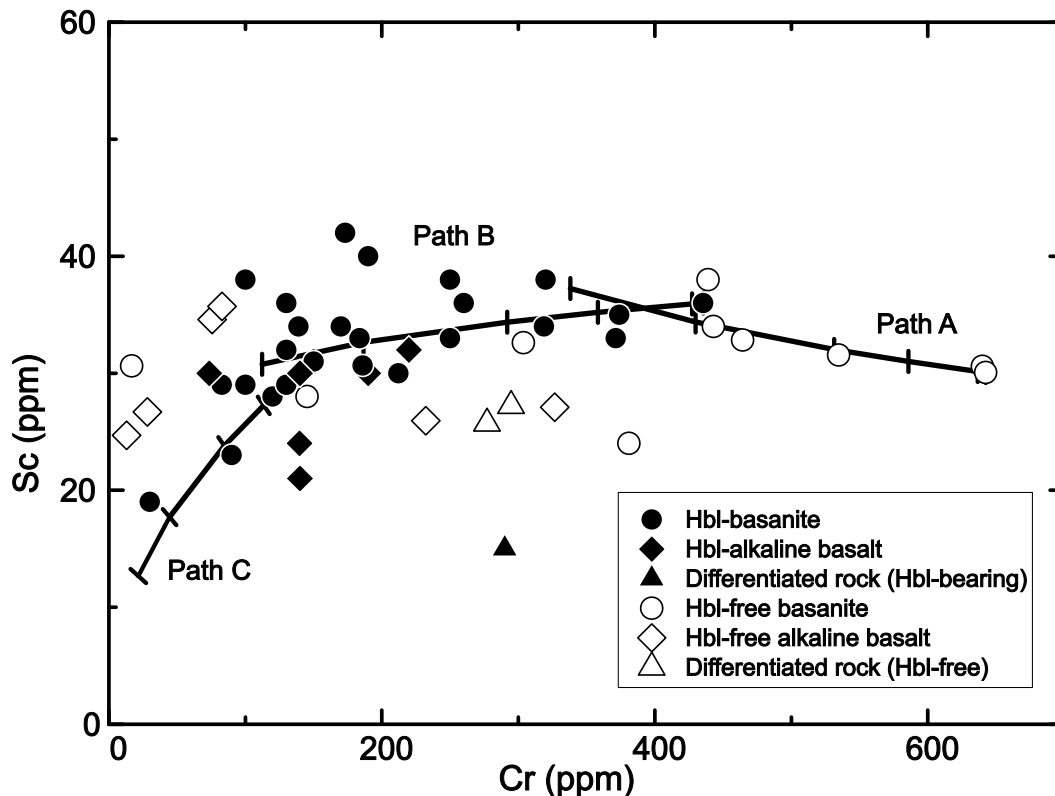


Figure 6.1: Cr vs. Sc variations for the Rhön lavas. Path (A) shows a possible fractionation path comprising olivine only for lavas with > 10 wt.% MgO assuming sample 27557 as the primary melt. For lavas with < 10 wt.% MgO fractionation of 20 % olivine and 80 % clinopyroxene is indicated (path B) with sample Rh10/11 as the starting melt. For some lavas with less than 6 wt.% MgO, a mixture of 5 % olivine, 20 % clinopyroxene and 75 % amphibole (path C) and a primary starting melt (sample Rh10/13) is shown. Tick marks on curves represent 10 % fractional crystallisation.

6.2 Crustal contamination

Most of the variation in major and trace element concentrations can be explained by fractional crystallization of the lavas during ascent. Previous studies have shown that common alkali basalts carrying green-core clinopyroxene stagnated in the lower crust at pressures of ~ 0.65 GPa corresponding to depths of ~ 20 km (Duda & Schmincke, 1985; Sachs & Hansteen, 2000). The Rhön lavas investigated in this study also contain clinopyroxene with green-cores which have low Ti/Al ratios and high Al_2O_3 concentrations (Jung & Hoernes, 2000) similar to some green-core-clinopyroxene found in volcanic rocks from the Eifel area (Duda & Schmincke, 1985; Jung *et al.*, 2006). Therefore it can be suggested that the hornblende-bearing basalts from the Rhön stagnated at comparable depths. It is therefore possible that these alkaline lavas have also undergone

6 Discussion

crustal contamination. The lower crust beneath the Rhenish Massif consists of mafic to felsic granulites (Mengel *et al.*, 1991). Detailed geochemical studies with trace element and isotope data exist only for the lower crustal xenoliths from the Eifel area (Stosch & Lugmair, 1984; Stosch *et al.*, 1986; Loock *et al.*, 1990; Rudnick & Goldstein, 1990; Stosch *et al.*, 1992) and these data can be used to constrain the influence of assimilation of crustal rocks upon the composition of the hornblende-bearing lavas. Lower crustal granulite xenoliths have Sr and Nd isotope compositions that extend from Bulk Earth values towards more unradiogenic $^{143}\text{Nd}/^{144}\text{Nd}$ but more radiogenic $^{87}\text{Sr}/^{86}\text{Sr}$ isotope compositions (Fig. 5.7). Felsic granulites tend to have more radiogenic $^{87}\text{Sr}/^{86}\text{Sr}$ isotope compositions, although some mafic granulites are also fairly radiogenic. Lead isotope compositions of these granulites are also fairly radiogenic plotting above NHRL in $^{206}\text{Pb}/^{204}\text{Pb}$ - $^{207}\text{Pb}/^{204}\text{Pb}$ - $^{208}\text{Pb}/^{204}\text{Pb}$ space (Fig. 5.8).

It is generally assumed that assimilation of crustal rocks by ascending basaltic magmas and fractional crystallization would have occurred simultaneously. The heat required for partial melting of crustal wall rocks is released by the fractional crystallization process. Recent models indicate that common assimilation-fractional crystallization processes (AFC) can be described as energy-constrained assimilation-fractional crystallization processes (EC-AFC) (Spera & Bohron, 2001). Therefore, the EC-AFC model of Spera & Bohron (2001) is used to test the influence of concurrent crustal assimilation and fractional crystallization upon the composition of the basalts using the parameters given in Table A.3. In contrast to the standard crustal model parameters given by Spera & Bohron (2001) we used a higher initial temperature (900 °C) for the lower crust. This higher temperature is in agreement with recent estimated lower crustal temperatures from the Eifel (> 800 °C; Sachs & Hansteen, 2000), and probably mirrors more closely the effects of rifting, uplift of the LAB, and continuing magmatism in Tertiary-Quaternary times.

In our model, we used sample Rh10/07 to represent the parental melt; this is a basanite with high MgO (9 wt.%), high Cr and Ni abundances (250 and 140 ppm, respectively), and has unradiogenic $^{87}\text{Sr}/^{86}\text{Sr}$, and highest Pb isotope ratios (Table A.1 and A.2). As the assimilant we used sample S 35 (Stosch & Lugmair, 1984; Loock *et al.*, 1990; Rudnick & Goldstein, 1990) which is a granulite xenolith with elevated $^{87}\text{Sr}/^{86}\text{Sr}$, low $^{143}\text{Nd}/^{144}\text{Nd}$, and fairly radiogenic Pb isotope ratios (Table A.3). Due to heterogeneity of crustal composition and the presence of some lavas with more radiogenic Sr composition an alternative crustal contamination model uses another primitive hornblende-free sample (26199 with MgO: 11 wt.%; Cr: 464 ppm; Ni: 212 ppm) and a crustal contaminant

6 Discussion

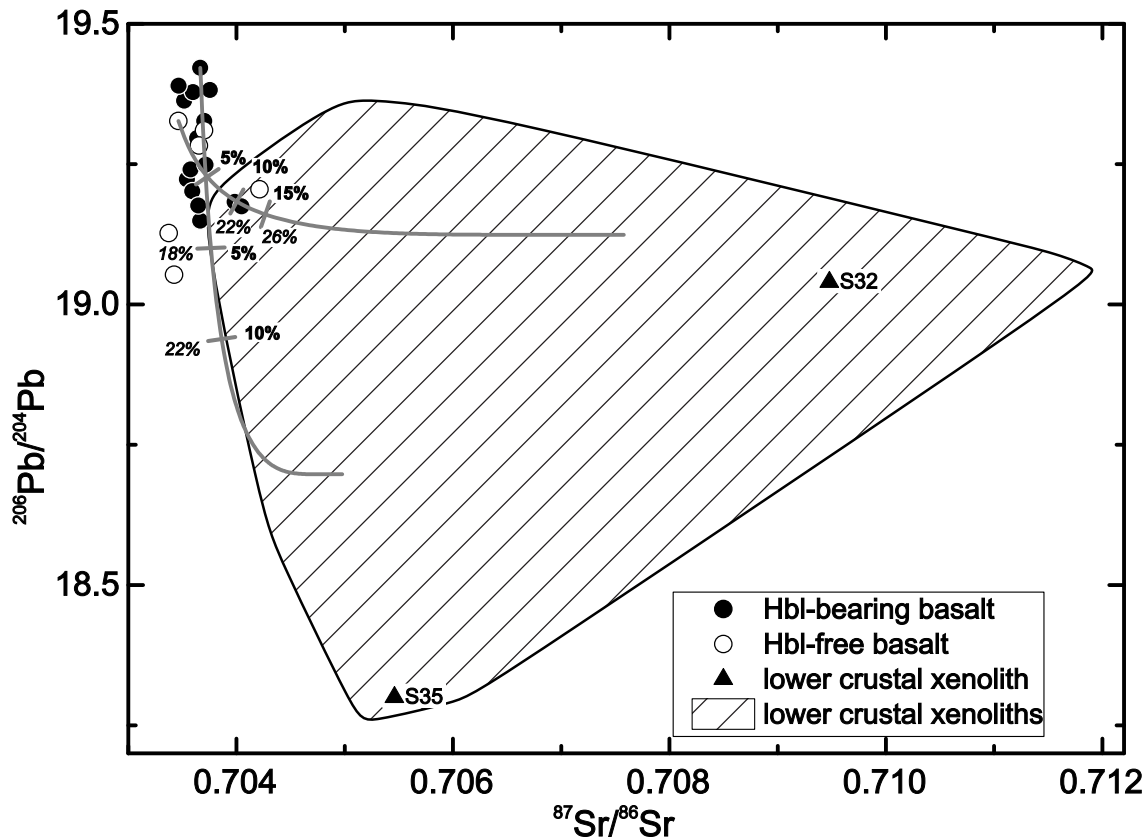


Figure 6.2: $^{206}\text{Pb}/^{204}\text{Pb}$ vs $^{87}\text{Sr}/^{86}\text{Sr}$ isotope composition diagram for the Rhön lavas. Lines showing the result of EC-AFC calculations with model parameters and endmember compositions from Table A.3.

(sample S 32 from Stosch & Lugmair (1984); Loock *et al.* (1990)). It can be seen that the range in $^{87}\text{Sr}/^{86}\text{Sr}$ and $^{206}\text{Pb}/^{204}\text{Pb}$ isotope composition of the lavas can be reproduced by EC-AFC models (Fig. 6.2), implying that energy-constrained assimilation-fractional crystallization processes played an important role in the evolution of these Rhön lavas. Based on this model, the isotope composition of the lavas with more radiogenic Sr isotope compositions can be explained by ca. 22–26 % fractional crystallization and ca. 5–15 % assimilation of a granulite facies lower crust with an isotope composition similar to that of S 32 or S 35 (Fig. 6.2).

Some trace element constraints are also compatible with assimilation of crustal material. Crustal rocks in general (Rudnick & Fountain, 1995) and the lower crustal xenoliths from the Rhenish Shield have Ce/Pb ratios < 20 and Nb/U ratios between ca. 10 and 50 (Sachs & Hansteen, 2000) (Fig. 5.4 b). In contrast, oceanic basalts have high Ce/Pb (25 ± 5) and Nb/U ratios (47 ± 10) that are commonly not fractionated during mantle melting and therefore reflect the composition of the Earth's mantle (Hofmann *et al.*, 1986). Low

6 Discussion

Ce/Pb (< 20) and low Nb/U (< 37) ratios of two samples from the hornblende-bearing lavas (Fig. 5.4 b) may suggest contamination of these alkaline lavas with crustal material similar in composition than the xenoliths investigated by Sachs & Hansteen (2000).

6.3 Partial melting

The trace element and Sr, Nd, and Pb isotope composition of the hornblende-bearing basalts is similar to lavas from elsewhere in the CEVP (Wilson & Downes, 1991; Jung & Masberg, 1998; Jung & Hoernes, 2000; Bogaard & Wörner, 2003; Haase *et al.*, 2004; Jung *et al.*, 2006, 2011). Isotope compositions are close to the inferred isotope composition of the European Asthenospheric Reservoir (EAR) which is assumed to be located at the lithosphere-asthenosphere boundary (LAB) (Wilson *et al.*, 1995). It was previously suggested that magma generation of other lavas from the CEVP occurred in the garnet peridotite stability field (Haase *et al.*, 2004) or at the garnet-spinel transition zone (Jung & Masberg, 1998; Jung & Hoernes, 2000; Bogaard & Wörner, 2003; Jung *et al.*, 2006, 2012). The hornblende-bearing lavas have CaO/Al₂O₃ ratios less than 1 and less pronounced LREE/HREE fractionation together with somewhat higher Lu contents (up to 0.49 ppm) relative to other lavas from elsewhere in the CEVP. This indicates a source containing less garnet than other sources of CEVP lavas. This inferred source is probably spinel peridotite rather than garnet peridotite which then must be located in the lithospheric mantle.

Most alkaline volcanic rocks from the CEVP show a characteristic depletion in K and Rb relative to elements with similar incompatibility but an enrichment of Ba with respect to primitive mantle concentrations (Fig. 5.6). These features are commonly ascribed to amphibole and/or phlogopite fractionation. However, most lavas from the CEVP do not contain amphibole or phlogopite and hence, the presence of amphibole and/or phlogopite as residual minerals in the mantle source must be considered (Griffin & Murthy, 1969; Kesson & Price, 1972; O'Reilly *et al.*, 1991; Wilson & Downes, 1991). The hornblende-bearing and hornblende-free lavas show a large variation in K/La (c. 100–400) at rather low and uniform (Ce/Yb)_N ratios between ca. 11–20 (Fig. 5.4 a) implying that partial melting of a simple four-phase peridotite is not likely because low-melt fractions from such a source have both high Ce/Yb_N and K/La ratios (Haase *et al.*, 2004). It is, therefore, possible that a residual mineral phase that fractionates K from La was present during partial melting. This mineral phase was amphibole rather than

6 Discussion

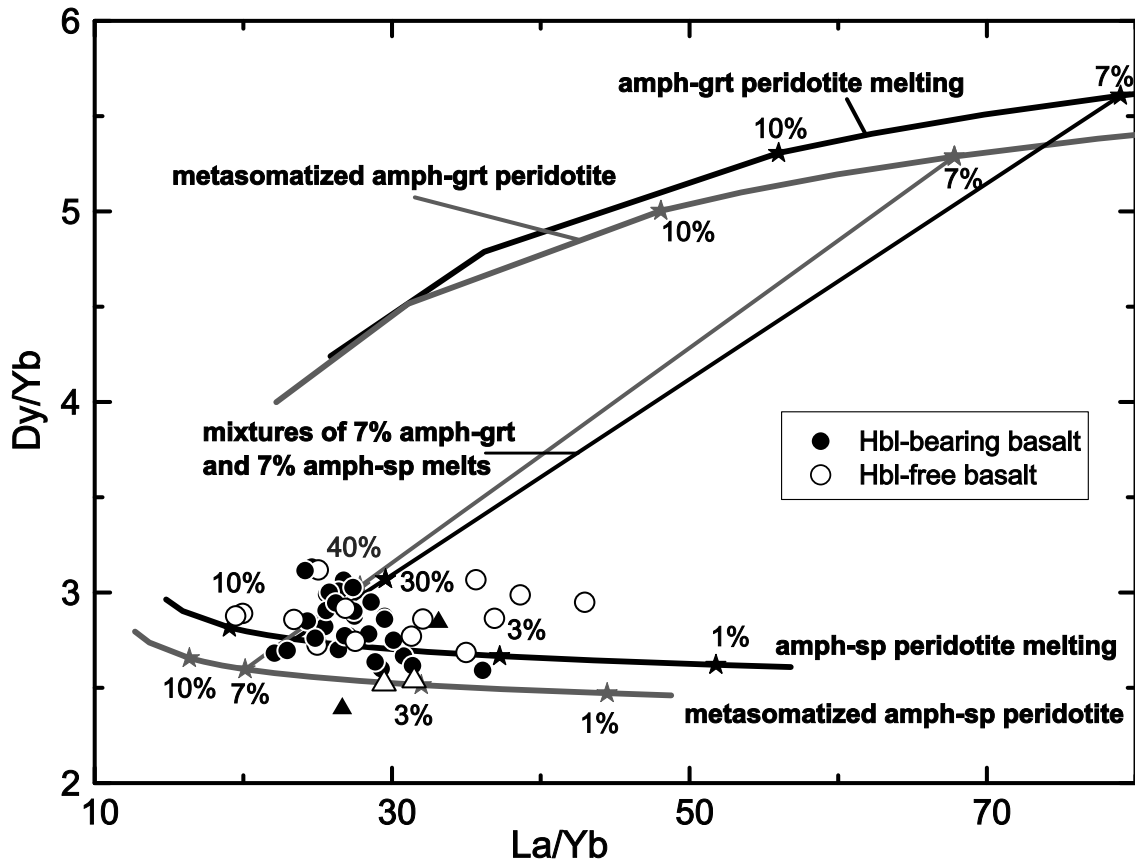


Figure 6.3: La/Yb vs. Dy/Yb covariation for the basalts from the Rhön. Partial melting curves were calculated using a non-modal fractional melting model (Shaw, 1970). Sources are grt-amph peridotite (cpx 0.07, opx 0.19, ol 0.55, grt 0.08, amph 0.11), which melts in the proportions cpx 0.25, opx 0.15, ol 0.05, grt 0.3, amph 0.25, and sp-amph peridotite (cpx 0.08, opx 0.25, ol 0.554, sp 0.033, amph 0.083), which melts in the proportions cpx 0.27, opx 0.25, ol 0.08, sp 0.13, amph 0.27. Source composition (La 2.3 ppm, Yb 0.16 ppm, Dy 0.48 ppm) represents an adjusted composition from Hartmann & Wedepohl (1990). Grey curves represent a mixture of 90% peridotite with 10% pyroxenite (sample DH 1182; Witt-Eickschen *et al.* 1993). Mineral-melt distribution coefficients are taken from LaTourrette *et al.* (1995); Adam & Green (2006). Numbers on model curves indicate the per cent melting.

phlogopite, because phlogopite fractionates K/La even more efficiently than amphibole and fractionates also Ba from La (Fig. 5.4 a). However, Ba concentrations are high in the hornblende-bearing and hornblende-free lavas which argues against significant amounts of phlogopite in the solid residue.

Previous models on the generation of primitive alkaline melts in the CEVP suggested either garnet-bearing or spinel-bearing peridotite sources. Melting of spinel or garnet peridotite upper mantle sources can be illustrated and modelled using REE systematics

6 Discussion

e.g. a plot of La/Yb vs. Dy/Yb plot (Fig. 6.3; Thirlwall *et al.*, 1994; Baker *et al.*, 1997). This plot can distinguish between melting in the garnet peridotite stability field or the spinel peridotite stability field because of the strong fractionation of HREE by garnet. In addition, melt mixing produces linear arrays that are distinguishable from partial melting trajectories. The hornblende-bearing and hornblende-free lavas from the Rhön form a coherent group near the calculated trend for melts produced in the spinel peridotite stability field (Fig. 6.3). The data indicate only a few samples lying on a mixing line between melts from garnet peridotite and melts from spinel peridotite in contrast to other studies on other Cenozoic volcanic areas of Germany (Westerwald: Haase *et al.*, 2004; Tertiary Hocheifel: Jung *et al.*, 2006). There is, however, geochemical evidence that the hornblende-bearing lavas have a significant contribution from non peridotitic sources (see below). As a consequence, we have modelled also the partial melting behaviour of non peridotitic, pyroxenitic sources (Fig. 6.3). These modelled curves are not fundamentally different to those of peridotitic material indicating that REE systematics of the lavas are not greatly influenced by the presence of non-peridotitic material such as pyroxenites.

To further constrain the melting conditions of the Rhön lavas, we have applied the new geothermobarometric calculations for basaltic magmas provided by Lee *et al.* (2009). The thermobarometer is valid for primary mantle-derived magmas that were saturated in olivine and orthopyroxene in their source regions. Although the upper mantle is believed to be largely peridotitic and hence contain both of these phases, there is growing evidence that some basaltic magmas might include a component derived from non-peridotitic sources (Foley, 1992; Hirschmann *et al.*, 2003; Kogiso *et al.*, 2003). This degree of chemical heterogeneity falls outside the applicable compositional range of the thermobarometers provided by Lee *et al.* (2009). Second, the barometer has not been calibrated for silica-undersaturated rocks (< 40 wt.% SiO₂) due to lack of sufficient experimental data, hence it is strongly advised not to apply the thermobarometer to nephelinites, leucitites and kimberlites. Finally, the barometer also does not include the effects of CO₂ on silica activity, however, CO₂ is very important in the generation of silica undersaturated magmas (Dasgupta *et al.*, 2006). Nevertheless, it is obvious from Fig. 6.4 that the calculated temperature and pressure estimates seem to fit with the experimental and geophysical data. The P-T estimates are also compatible with the generation of the lavas from predominantly spinel peridotite sources and the inferred presence of amphibole, at least in the lower temperature and pressure lavas. One important observation is that the data of the most primitive Rhön lavas intersect the garnet

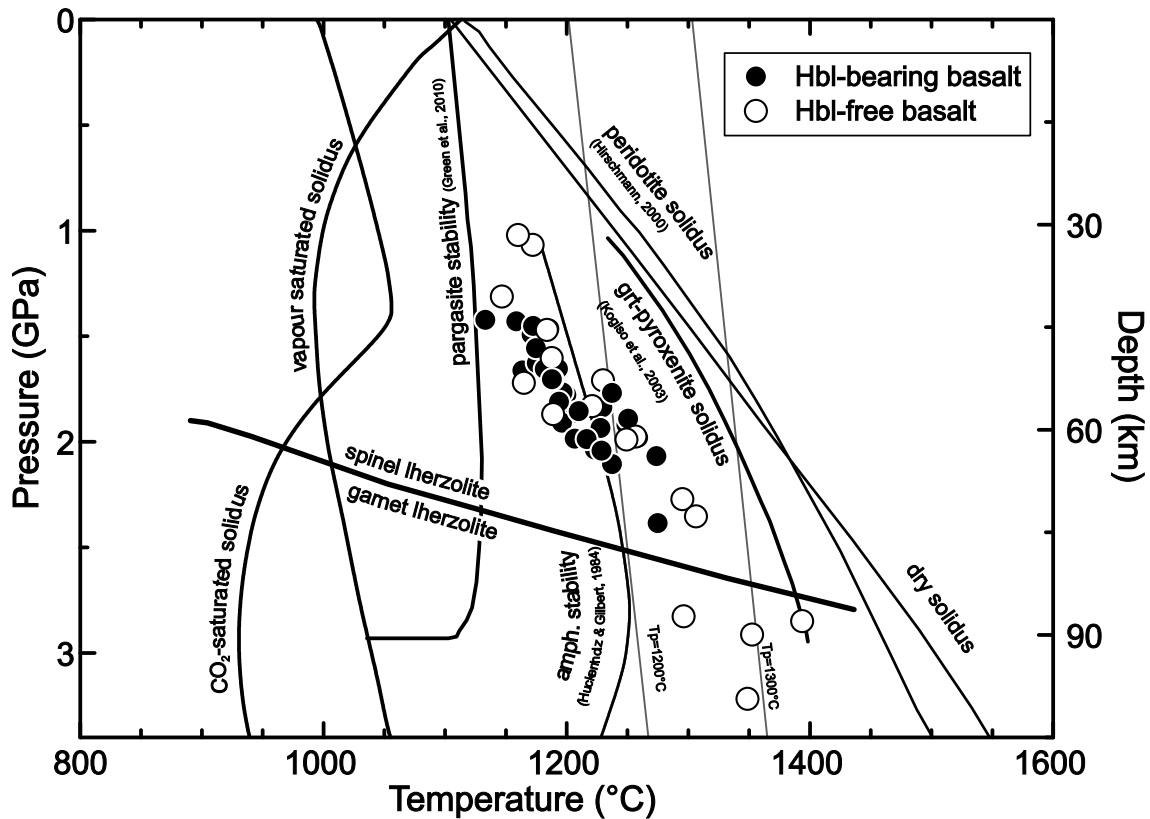


Figure 6.4: Pressure-temperature diagram to illustrate the potential source region for mafic alkaline lavas from the Rhön area. Solidi for dry mantle and CO₂-saturated mantle are from McKenzie & Bickle (1988); Falloon & Green (1990), respectively. Also shown are adiabats for various mantle potential temperatures. Stability fields for spinel and garnet peridotite and amphibole in upper mantle rocks are from Falloon & Green (1990); Foley (1991); Robinson & Wood (1998). Amphibole stability field from experimental results of Huckenholz & Gilbert (1984). Calculated temperature and pressure estimates after Lee *et al.* (2009).

pyroxenite solidus (Kogiso *et al.*, 2003) at temperatures consistent with a mantle potential temperature of ~ 1400 °C at pressure of about 3 GPa. These pressure-temperature estimates are considered to be realistic for the generation of common alkali basalts due to partial melting of volatile-rich (carbonated) peridotite (Dasgupta *et al.*, 2007). There is also geophysical evidence (Ritter *et al.*, 2001) and independent geochemical evidence (Haase *et al.*, 2004) for a deep seated "hot finger" underneath the Rhenish Massif and these inferred high temperatures are probably realistic. Beside the presence of a thermally anomalous "hot finger" beneath the area, radioactive heating of a highly metasomatized lower lithosphere at the base of the continental lithosphere must be

6 Discussion

considered. This suggestion is compatible with the view that metasomatic effects of carbonatitic melts may be greatest at 2–3 GPa (Foley *et al.*, 2009).

6.4 Nature of the source

Enrichment of the Earth's mantle can be achieved by small amounts of "metasomatic" melts. This is one mechanism for explaining the origin of enriched isotope and trace element signatures in primitive alkaline volcanic rocks. Evidence for modal or cryptic mantle metasomatism has been found in mantle xenoliths from subcontinental lithospheric mantle (e.g., Kempton *et al.*, 1988; O'Reilly *et al.*, 1991; Beyer *et al.*, 2006). Mantle enrichment is most pronounced in highly incompatible element abundances. However, even samples with considerable degrees of "re-fertilization" by metasomatic melts do not show corresponding enrichment in TiO₂ (Beyer *et al.*, 2006). This observation is consistent with TiO₂ depletion during the initial lithosphere forming melting event (Klein & Langmuir, 1987). As a consequence, the lithospheric mantle is depleted in TiO₂ compared to the primitive mantle. A possible exception is if the mantle is modally metasomatized as the result of extensive melt impregnation or accumulation of minerals (e.g., Pilet *et al.*, 2005). In addition, recycled oceanic crust, now preserved as pyroxenite, eclogite, or amphibolite may constitute parts of the lithospheric mantle (Sobolev *et al.*, 2005, 2007). The presence of these, sometimes ancient components will generate variable elemental and isotope signatures that can be transferred to the lavas upon melting.

Previous work on other mafic lavas in the CEVP (Wilson & Downes, 1991, 1992; Bogaard & Wörner, 2003; Haase *et al.*, 2004; Jung *et al.*, 2006, 2011, 2012) and xenolith studies (Hartmann & Wedepohl, 1990; Witt-Eickschen & Kramm, 1997; Witt-Eickschen *et al.*, 2003; Ackerman *et al.*, 2007) have provided geochemical evidence of a metasomatic event during the Variscan in which subduction of altered mafic crust lead to metasomatized portions of the ambient upper mantle. The most striking differences of the hornblende-bearing Rhön lavas in comparison with other CEVP lavas are their high TiO₂ contents and a large range in MgO, Al₂O₃, Ni, and Cr. These observations suggest that these lavas might contain a contribution from a non peridotite source probably a metasomatized amphibole-bearing pyroxenitic source. Experimental partial melts of garnet pyroxenite are rich in Al₂O₃ and low in MgO and show a broad similarity to the basalts studied here (Hirschmann *et al.*, 2003; Dasgupta *et al.*, 2006) although there

6 Discussion

are notable differences in absolute concentrations. The high Al_2O_3 content observed in the hornblende-bearing basalts can be modelled by partial melts of mantle material consisting of a mixture of eclogite and peridotite (Kogiso *et al.*, 1998). According to Pilet *et al.* (2010) the temperature of melting controls significantly the MgO and Al_2O_3 content of the liquid. Lower temperatures during melting cause lower MgO but higher Al_2O_3 abundances in the liquids relative to common alkali basalts with similar SiO_2 and little variation in TiO_2 . This is similar to the elemental variation seen in the Rhön lavas having high Al_2O_3 . Moreover, absolute concentrations of MgO and Al_2O_3 in the modelled liquids shown by Pilet *et al.* (2010) are similar to the concentrations in the alkali basalts from the Rhön. The CaO concentration is higher in the Rhön lavas than in the experimental melts which can be attributed to a higher clinopyroxene:amphibole ratio in the source of the Rhön lavas.

It has previously been shown that generation of alkaline SiO_2 -undersaturated melts from unmodified peridotitic mantle requires the presence of CO_2 as a fluid phase during melting (Brey & Green, 1977; Mengel & Green, 1986; Thibault *et al.*, 1992; Hirose, 1997). This CO_2 could potentially have been delivered by ascending carbonatitic melts from the deeper mantle. By carbonating anhydrous and silica-deficient garnet pyroxenites, such pyroxenites could melt without affecting the surrounding peridotite producing a Ti-enriched silica-undersaturated siliceous liquid (Dasgupta *et al.*, 2006). These TiO_2 -enriched silica-undersaturated liquids could be the potential parental liquids to common nephelinites and basanites found in oceanic and continental settings. Witt-Eickschen *et al.* (1993) has argued that enrichment of TiO_2 in mantle xenoliths from the nearby Vogelsberg volcanic complex occurred in pyroxenitic veins that were affected by intruding basaltic melts. Consequently, it can be suggested that high-Ti basanites with and without amphibole represent melts with contribution of veins which are rich in secondary pyroxene and possibly amphibole. Bogaard & Wörner (2003) observed high-Ti basanites in the nearby Vogelsberg area that are also low in MgO and rich in Al_2O_3 , similar to the basanites studied here, although these basanites do not carry amphibole. It has also been suggested that low MgO contents of alkaline lavas are not the result of fractional crystallization processes but instead point to non peridotitic sources potentially carrying hydrous minerals. Foley *et al.* (1999) performed melting experiments on hydrous mineral-bearing veins in a peridotitic or harzburgitic matrix. These experimental melts have low SiO_2 and MgO but high TiO_2 and high Al_2O_3 , which is broadly similar to the high-Ti basanites studied here. Overall, experimental evidences indicate that high-Ti basanites may originate from partial melting of pyroxene-bearing lithologies

6 Discussion

with abundant hydrous mineral phases (e.g. amphibole). For the Rhön basalts, evidence for residual amphibole is provided by negative K anomalies in primitive mantle normalized trace element patterns and the lack of K-Ba fractionation. Similarly, many Rhön basalts from this study have higher Ce/Pb ratios than the assumed range for OIBs (25 ± 5 ; Hofmann *et al.*, 1986) which is due to low Pb concentrations in the samples. It is commonly assumed that phlogopite and amphibole are the main reservoirs for Pb in the mantle (Rosenbaum, 1993). Hence, for the Rhön lavas residual amphibole in the mantle that fractionate Pb from Ce is the most likely candidate for the low Ce/Pb ratios observed here.

Enrichment of LILE and LREE is thought to be connected with (i) fluids from pyroxenite, amphibolite, or eclogite veins or (ii) layers in the subcontinental mantle formed by infiltrating fluids or (iii) melts from the underlying asthenosphere (Foley, 1992). In this model, possible types of metasomatic agents can vary in composition from carbonatitic (Rudnick *et al.*, 1993) to low degree silicate melts (Rapp *et al.*, 1999). Melt generation from carbonated pyroxenite sources requires only $\sim 1\text{--}5\%$ of partial melting to produce common alkaline magmas (Dasgupta *et al.*, 2007). This degree of partial melting is commonly accepted for alkaline basaltic magmas from the CEVP (Wilson & Downes, 2006). It should be noted, however, that the hornblende-bearing lavas from the Rhön have high Ti/Eu ratios (4300–8600) which argue against the direct participation of carbonatitic liquids (Powell *et al.*, 2004). It is more likely that the metasomatized lithospheric mantle carries abundant hydrous veins and cumulates that preferentially melted during the rifting event (Foley, 1992; Pilet *et al.*, 2008, 2010, 2011).

6.5 Origin of hornblende in basaltic lavas

In addition to evidence from whole-rock chemical and isotope compositions, a detailed reconstruction of petrogenetic processes that affected mantle-derived basaltic melts is possible through an evaluation of mineral data (Boettcher & O'Neil, 1980; Menzies & Murthy, 1980; Rosenbaum, 1993; Simonetti & Bell, 1993; Hegner *et al.*, 1995; Powell *et al.*, 2004). Previous studies on minerals of inferred comagmatic derivation show significant differences in the chemical and isotope characteristics relative to their host lavas (Simonetti & Bell, 1993, 1994; Hegner *et al.*, 1995; Molina *et al.*, 2009). Especially megacrysts as recorders of high-pressure crystallization (Best, 1970, 1974; Binns *et al.*, 1970; Irving, 1974; Wilkinson, 1975; Ellis, 1976; Gutmann, 1977; Wass, 1979; Irving & Frey, 1984; Shaw

6 Discussion

& Eyzaguirre, 2000) and near liquidus phases (Green & Hibberson, 1970; Bultitude & Green, 1971) can provide important information on the early stages of magma evolution (Simonetti & Bell, 1993). However, their relationship to the host lava is controversial (Binns, 1969; Binns *et al.*, 1970; Irving, 1974; Stuckless & Irving, 1976; Ellis, 1976; Irving & Frey, 1984; Wilkinson & Hensel, 1991). Distinct phenocrysts (clinopyroxene, amphibole, phlogopite) can have different chemical and isotope compositions. However, hydrous phases are more prone to record the presence of metasomatic agents than nominally anhydrous mineral phases such as clinopyroxene (Ben Othman *et al.*, 1990). Thus, detailed chemical and isotope work on hydrous phases may be more helpful in elucidating metasomatic processes in the mantle (Boettcher & O'Neil, 1980; Menzies & Murthy, 1980; Rosenbaum, 1993; Powell *et al.*, 2004). Before constraining the implications of amphibole for processes occurring in the upper mantle, we determined whether the hornblende represent incorporated xenocrystic material from the mantle or the crust or if they represent comagmatic liquidus phases derived from the host basaltic lava.

A first indication as to whether an amphibole is comagmatic is high Mg# which is typical for primitive basaltic melts (Mg# > 0.68) and a positive correlation of Mg# in the amphibole and the corresponding rock (Bedard, 1988). Although the investigated kaersutite has somewhat lower Mg# (~0.6) which is positively correlated with the Mg# in the host lava. Although the incompatible trace element pattern of the host rock and the amphibole is different they show a relationship which can be used to constrain whether these minerals are in chemical equilibrium with the host rock. For this purpose the trace element concentration of an amphibole is calculated using a mineral-melt relationship with the equation for fractional crystallization. The calculated trace element concentration of an amphibole of inferred igneous origin is shown in Fig. 6.5 a-c in comparison with the host rock and the measured trace element concentration of the phenocrysts. A best fit can be obtained for a weight fraction of amphibole (F) of about 30%. It can be seen that absolute trace element concentration and the resulting trace element patterns of the calculated composition are similar to the measured kaersutite values. Together with the petrographic observations this is ample evidence that the kaersutite are comagmatic and crystallized from the host lava of known composition.

Two distinct types of amphibole have been reported from mantle environments (Kesson & Price, 1972; Wilshire *et al.*, 1980; Witt & Seck, 1989; Downes *et al.*, 1991; Ionov & Hofmann, 1995; Vannucci *et al.*, 1995; Ionov *et al.*, 1997; Tiepolo *et al.*, 2000; Witt-Eickschen *et al.*, 2003). First, disseminated amphibole from peridotite may show undulatory extinction and is typical in textural equilibrium with the host peridotite. These amphibole

6 Discussion

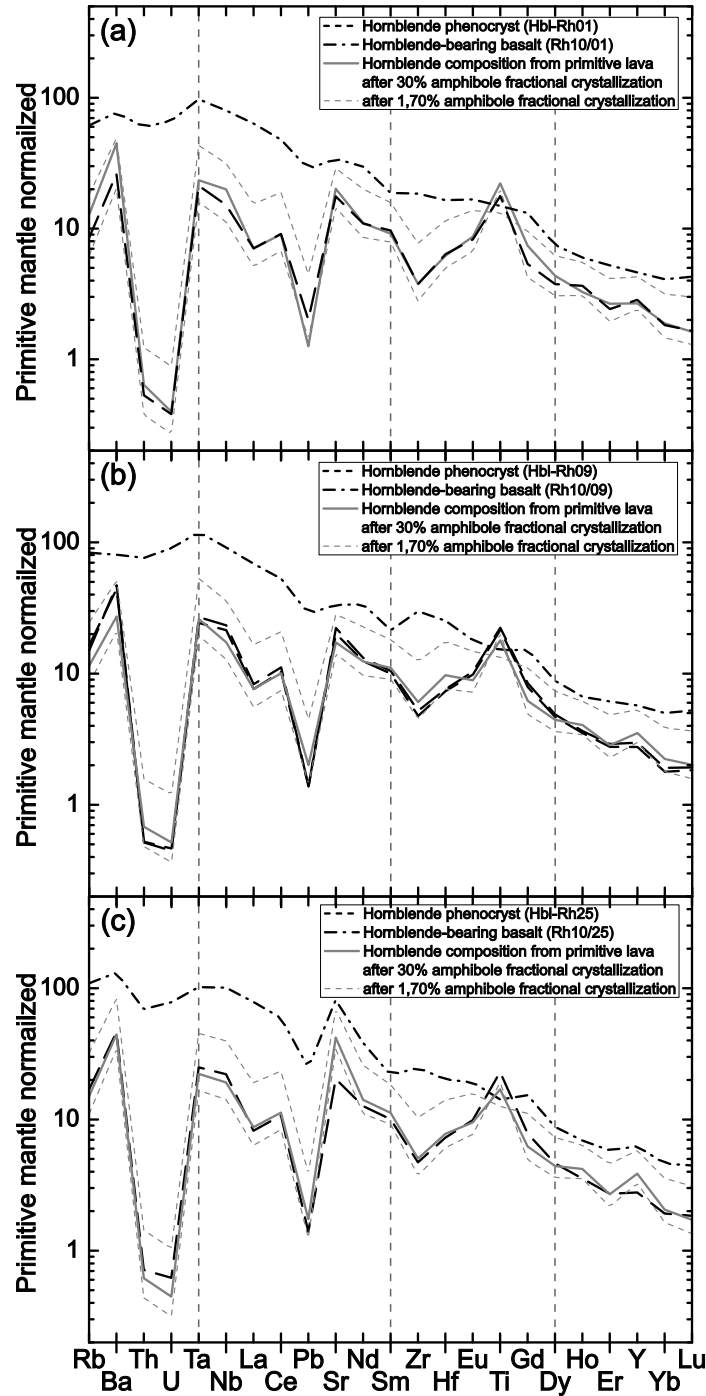


Figure 6.5: Calculated incompatible trace element concentrations of amphibole after fractional crystallization of amphibole using whole-rock composition of (a) Rh10/01; (b) Rh10/09; (c) Rh10/25 in comparison to corresponding analysed hornblende concentrations. The equation for the calculated amphibole concentrations is the fractional crystallization equation: $C_s = C_0 * D * F^{D-1}$, where C_s is the concentration of an element in the crystal for a weight fraction of crystallized F and C_0 is the concentration of the element in the primary parent liquid. D is the partition coefficient. For the calculation the corresponding host lava was used as an approximation of the composition of the liquid. Partition coefficients are taken from LaTourrette *et al.* (1995); Adam & Green (2006).

6 Discussion

have high Mg# (0.8–0.9; Ionov & Hofmann, 1995; Witt-Eickschen *et al.*, 2003; Powell *et al.*, 2004) and a flat REE pattern with a slight enrichment of LREE over HREE. This amphibole shows no pronounced Ta enrichment, and Zr and Hf concentrations show negative anomalies in primitive mantle normalized diagrams (Kesson & Price, 1972; Witt & Seck, 1989; Ionov & Hofmann, 1995; Tiepolo *et al.*, 2000; Witt-Eickschen *et al.*, 2003). In addition, disseminated amphibole from peridotite has low Al and Ti contents (Bedard, 1988). The second type of amphibole is associated with veins in mantle rocks. Due to the reaction of migrating melts and fluids with the ambient peridotite these vein amphibole shows distinct geochemical signatures different to amphibole which is in textural equilibrium with peridotite. In general, vein amphibole has lower Mg# (0.5–0.6; Ionov & Hofmann, 1995; Shaw & Eyzaguirre, 2000; Witt-Eickschen *et al.*, 2003), a convex REE pattern with an enrichment of MREE over LREE and HREE and higher Nb, Ta, Zr, and Hf concentrations relative to elements with similar incompatibility (Ionov & Hofmann, 1995; Vannucci *et al.*, 1995; Ionov *et al.*, 1997; Tiepolo *et al.*, 2000; Witt-Eickschen *et al.*, 2003). These differences of HREE and HFSE between the two amphibole types can be used for the hornblende in the hornblende-bearing lavas from the Rhön area. The kaersutite are similar e.g. in their Lu/Hf and Nb/Th ratio (Fig. 5.13) to vein amphibole.

6.6 Implications from isotope compositions

Chemical and probably isotope equilibrium between kaersutite and the host lavas during crystallization of the amphibole can be constrained by the isotope composition of the hornblende. For some hornblende-lava pairs (Hbl-Rh10/01, Hbl-Rh10/13, Hbl-Rh10/25, Hbl-Rh10/33) the Nd-Sr-Pb isotope compositions between phenocryst and host rock are similar. An exception is Hbl-Rh10/25 where the measured and calculated Sr concentrations deviate by a factor of 2 (Fig. 6.5 c). For most kaersutite analyses the $^{207}\text{Pb}/^{204}\text{Pb}$ and $^{208}\text{Pb}/^{204}\text{Pb}$ ratios are higher than the $^{207}\text{Pb}/^{204}\text{Pb}$ and $^{208}\text{Pb}/^{204}\text{Pb}$ ratios of the corresponding lava although phenocrysts and lavas have the same $^{206}\text{Pb}/^{204}\text{Pb}$ ratio. This radiogenic signature could be attributed to the involvement of ancient material (continental crust or ancient lithospheric mantle). Similar radiogenic $^{207}\text{Pb}/^{204}\text{Pb}$ and $^{208}\text{Pb}/^{204}\text{Pb}$ ratios are also observed in the hornblende-bearing lavas and in mantle xenoliths from the CEVP (Witt-Eickschen *et al.*, 2003) which were also explained by the presence of ancient components having higher U/Pb and Th/Pb ratios. The isotope and trace element composition of these peridotite xenoliths suggested that mantle

6 Discussion

metasomatism of the lithospheric mantle was due to percolation of melts from an ancient, HIMU-like (high time-integrated $\mu = {}^{238}\text{U}/{}^{204}\text{Pb}$) mantle source (Witt-Eickschen *et al.*, 2003). The HIMU-like component had a more radiogenic Pb isotope composition (${}^{206}\text{Pb}/{}^{204}\text{Pb} > 21$) than EAR (${}^{206}\text{Pb}/{}^{204}\text{Pb} \sim 20$) and may be linked to reactivation of ancient subducted crustal domains during the Variscan orogeny.

The kaersutite Hbl-Rh10/07 and Hbl-Rh10/09 have less radiogenic Nd and Pb isotope compositions than their host lava; an observation that has not been reported for any other alkaline lava from the CEVP. In the Urach volcanic field, most phlogopite and amphibole have Pb, Nd and Sr isotope ratios similar to the isotope composition of the corresponding melilitic lava (Hegner *et al.*, 1995). Only rare phlogopite of inferred comagmatic parentage from these melilitites show unradiogenic isotope characteristics similar to that of hornblende from the Rhön area. In the case of the Urach samples unradiogenic isotope characteristics of the phlogopite are also not matched by the corresponding host melilitites (Hegner *et al.*, 1995). In addition, an unradiogenic Pb and Nd isotope composition has not been observed in peridotite or pyroxenite xenoliths from the CEVP. Thus, there is no possibility to produce such unradiogenic isotope compositions by simple mixing of two or more distinct mantle endmembers. However, similar variations of isotope compositions from mantle-like values towards unradiogenic Nd isotope compositions are observed in minerals from peridotite xenoliths from the Eifel area (Witt-Eickschen *et al.*, 1998, 2003). In these spinel peridotite and pyroxenite xenoliths secondary amphibole and clinopyroxene minerals have ϵNd values (recalculated to 24 Ma) ranging from +3.5 to -2.4. These phenocrysts are present in an equigranular recrystallized peridotite adjacent to hornblende veins and were formed during an episode of modal metasomatism (Witt-Eickschen *et al.*, 1998). This modal metasomatism led to the formation of amphibole and clinopyroxene caused by aqueous fluids from an isotopically enriched (EMI-like) mantle reservoir during deformation in the shallow continental lithospheric mantle and may be subduction related (Witt-Eickschen *et al.*, 2003). Hegner *et al.* (1995) suggested for the unusual Urach phlogopite an involvement of ancient continental crust similar in composition to Variscan basement outcropping in the Vosges and Black Forest. Due to high concentrations of Pb in crustal domains it is possible to change the Pb isotope compositions of phenocrysts towards less radiogenic compositions. However, in the case of hornblende from the Rhön lavas, it is unlikely that the unusual unradiogenic ("crustal" like) isotope composition of the kaersutite is caused by crustal contamination during ascent because the host lavas do not show any crustal contamination (see section 6.2). Ionov *et al.*

6 Discussion

(1997) suggested that amphibole and mica from upper mantle domains cannot produce radiogenic isotope ratios due to a low U/Pb ratio in these minerals, even though Pb can be incorporated to a limited extent. As kaersutite is assumed to be comagmatic (see above) and amphibole (and phlogopite; Rosenbaum, 1993) are expected to be the main repository of Pb in the mantle, early crystallized amphibole may have incorporated Pb of distinct isotope composition from distinct parts of the ambient lithospheric mantle beneath the CEVP.

It has been shown that the SCLM beneath the CEVP is probably not only composed of peridotite but contains also significant proportions of pyroxenite and eclogite which can be interpreted as remnants from ancient subducted crust (Bogaard & Wörner, 2003; Haase *et al.*, 2004; Jung *et al.*, 2006, 2012). High $^{207}\text{Pb}/^{204}\text{Pb}$ and $^{208}\text{Pb}/^{204}\text{Pb}$ ratios for kaersutite can be interpreted through involvement of aged crust having U/Pb ratio higher than $\mu = 9.9$ (e.g. $\mu = ^{238}\text{U}/^{204}\text{Pb} = 11$; Fig. 5.15 b). The phlogopite from the Urach volcanic field and the kaersutite with negative εNd values from this study are similar to a crustal domain with a μ value of about 9.9, or the most unradiogenic kaersutite probably record involvement of an EM I component (Zindler & Hart, 1986).

Oxygen isotope studies on mantle minerals imply a $\delta^{18}\text{O}$ value of about 5.2 ‰ for the upper mantle (Mattey *et al.*, 1994). Oxygen isotope composition of the upper mantle based on analyses of basaltic lavas has been estimated to ca. 5.5 ‰ (Mattey *et al.*, 1994). However, analyses of basaltic lavas of different compositions reveal heterogeneity of oxygen isotope values in the mantle between 3.6 and 8.7 ‰ (Harmon & Hoefs, 1995). Especially LILE-enriched basalts associated with subduction at convergent plate margins are slightly enriched in $\delta^{18}\text{O}$ (Harmon & Hoefs, 1995). Oxygen isotope values obtained on amphibole from other localities (Dobosi *et al.*, 1998) are similar to the host rock or are lower than the corresponding lava if low temperature alteration has increased the $\delta^{18}\text{O}$ value of the host lava. Some studies have emphasized that in peridotite carrying OH-bearing minerals the $\delta^{18}\text{O}$ value obtained on minerals is positively correlated with LREE enrichment due to metasomatic processes (Kempton *et al.*, 1988). The $\delta^{18}\text{O}$ values of the four kaersutite with $\delta^{18}\text{O} > 6$ ‰ (this study) are similar to alteration-corrected $\delta^{18}\text{O}$ values of basaltic lavas from the Rhön area (Fig. 5.16; Freerk-Parpatt, 1990; Jung & Hoernes, 2000). The phenocrysts as well as the alteration-corrected whole-rocks have slightly higher $\delta^{18}\text{O}$ values than the inferred oxygen isotope composition of the mantle (ca. 5.5 ‰; Mattey *et al.*, 1994). This can be attributed to a metasomatized source of these rocks and minerals since some studies have showed such relationship between higher $\delta^{18}\text{O}$ values and metasomatic processes (Kempton *et al.*, 1988). For the Urach

6 Discussion

volcanic rocks and associated minerals the O isotope composition of phlogopite is less than 6 ‰. Together with relatively unradiogenic Sr isotope composition this has been interpreted to be indicative for the isotope composition of the SCLM beneath Europe (Hegner & Vennemann, 1997). The higher O isotope values of the kaersutite from this study relative to the phlogopite samples from the Urach volcanic field and to the mantle range can be attributed to the inferred metasomatic processes (Kempton *et al.*, 1988). Compared to phlogopite from the Urach area, the kaersutite from this study has lower Sr isotope ratios. This can be attributed to the high Rb/Sr ratio associated with low Sr abundances in phlogopite which are more susceptible to contamination than amphibole (Ionov *et al.*, 1997). The unusual composition of hornblende Hbl-Rh10/25 with low $\delta^{18}\text{O}$, radiogenic Sr isotope ratios, and relatively lower Sr concentration of the phenocrysts in comparison to the host rock can be attributed to alteration with seawater or meteoric water (Simonetti & Bell, 1993; Hegner & Vennemann, 1997). Some phlogopite from the Urach volcanic field with similar isotope composition to Hbl-Rh10/25 have high δD (-25) values which indicate involvement of recycled seawater probably during melt formation in the lithospheric mantle (Hegner & Vennemann, 1997).

6.7 Hornblende implications for petrogenetic settings

The hornblende-bearing lavas and other mafic lavas from the Rhön and the CEVP show negative K and Rb and positive Ba anomalies in primitive mantle normalized patterns. These depletions and enrichments are commonly ascribed to residual phlogopite or amphibole in the mantle. These secondary minerals are important hosts for Large Ion Lithophile Elements (LILE; Rb, Ba) and Light Rare Earth Elements (LREE; La, Ce, Nd). Hence, pronounced fractionation of LILE and LREE may occur when these minerals are involved in partial melting processes (Griffin & Murthy, 1969; Kesson & Price, 1972; Witt & Seck, 1989; Francis & Ludden, 1995). The lack of Ba/La fractionation, which would have been caused by residual phlogopite, suggests that amphibole is the dominant residual phase in the lithospheric mantle beneath the CEVP (Griffin & Murthy, 1969; Kesson & Price, 1972; O'Reilly *et al.*, 1991; Wilson & Downes, 1991; Haase *et al.*, 2004). In addition, secondary minerals produced by modal mantle metasomatism may concentrate and probably fractionate High Field Strength Elements (HFSE; Nb, Ta, Zr, Hf, Ti) (Witt-Eickschen & Harte, 1994; Ionov & Hofmann, 1995; Moine *et al.*, 2001).

6 Discussion

Breakdown of residual amphibole and release of water to the ambient mantle at pressures greater than 1.2 GPa is a likely process to produce silica undersaturated melts (Francis & Ludden, 1995; Molina *et al.*, 2009). The conditions of melting can be constrained by modeling and P-T estimates either with whole-rock or hornblende compositions. From whole-rock geochemistry, a petrogenetic model and P-T conditions can be approached. As seen in section 6.3, the hornblende-bearing lavas of the Rhön were produced from spinel peridotite containing a significant amount of pyroxenite and whole-rock geothermobarometer indicate pressures ranging from 2.3 to 1.4 GPa and temperatures between 1290 °C and 1170 °C (section 6.4). Application of the clinopyroxene-whole-rock thermobarometer proposed by Putirka *et al.* (1996) suggests that clinopyroxene fractionation occurred at temperatures between 1150 °C and 1300 °C at pressures between 1.0 GPa and 1.8 GPa. Based on the Ti incorporation into amphibole temperatures between 1100 °C to 1300 °C (see inset to Fig. 6.6 a) can be estimated (Helz, 1973; Otten, 1984). However, the stability of amphibole is restricted to lower temperatures and temperatures of amphibole above 1200 °C are considered to be unlikely. A temperature lower than 1200 °C is confirmed by several studies on amphibole stability which estimated a P-T stability field of amphibole between 1100 °C and 1200 °C and 1–3 GPa (Huckenholz & Gilbert, 1984; Foley, 1991; Wallace & Green, 1991; Witt-Eickschen *et al.*, 1998; Niida & Green, 1999). An experimental study (Pilet *et al.*, 2010) showed that amphibole with similar geochemical composition as kaersutite from the Rhön is stable at rather low temperatures of ca. 1000–1100 °C (Fig. 6.6 a-d). Therefore, we used the TiO_2 , MgO, and FeO correlation with temperature of these experimental results ($T[^\circ\text{C}] = 17.4\text{TiO}_2 + 7.8\text{MgO} - 4.4\text{FeO} + 971.6$) and calculate a temperature range of 1100 °C to 1150 °C for crystallization of the kaersutite from the Rhön (Fig. 6.6 a-d). These calculated temperatures are consistent with the occurrence of Ti-rich amphibole crystallizing from a basanitic lava system between 1100–1200 °C (Huckenholz & Gilbert, 1984; Green *et al.*, 2010). The newly formulated geochemical thermometer for amphibole is consistent with the other approaches for temperature estimates using modeling of whole-rock and mineral composition and the stability field of amphibole. The temperature estimate of ca. 1100 °C is somewhat lower than the highest temperature estimated based on whole-rock compositions but is consistent with the onset of amphibole crystallization in the metasomatized upper mantle (Pilet *et al.*, 2010). A comparison of experimental results (Pilet *et al.*, 2010) with the modal abundance of hornblende, clinopyroxene, and olivine in the hornblende-bearing basalts suggest also that the lavas were generated at temperatures between 1050 and 1150 °C.

6 Discussion

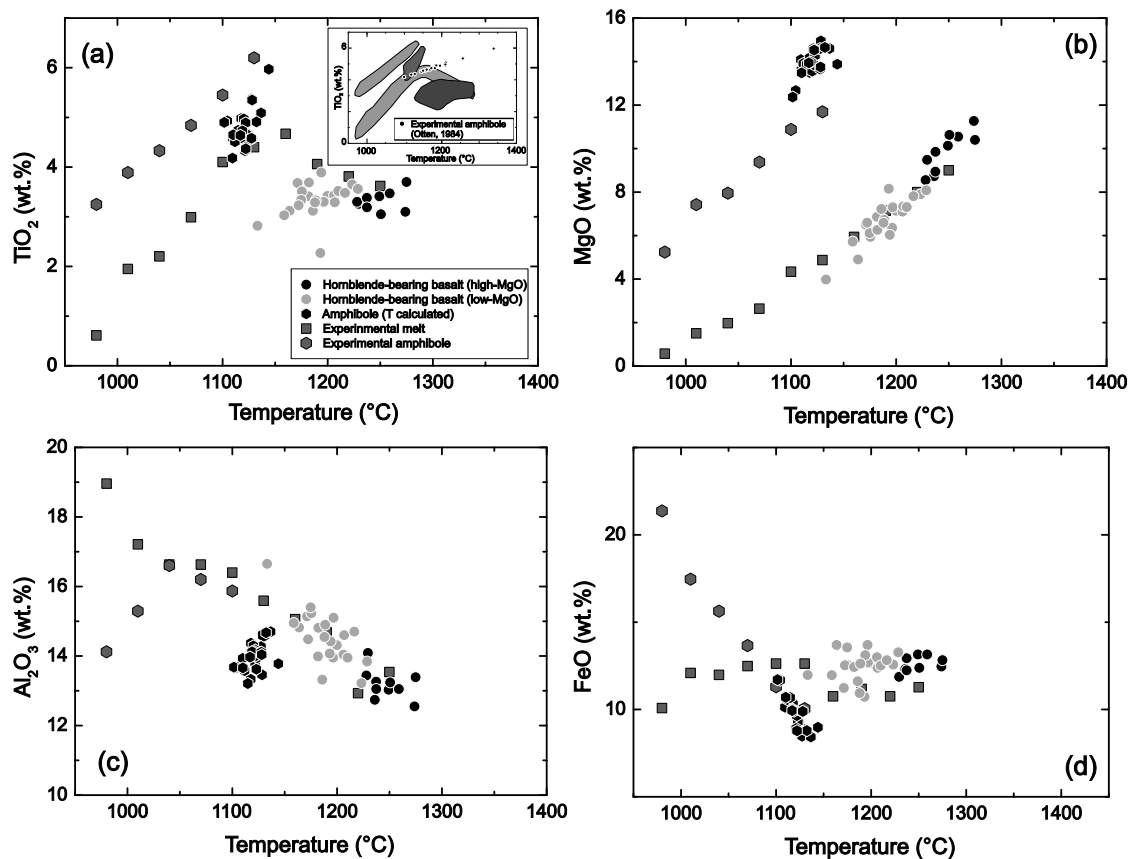


Figure 6.6: Geochemical compositions vs. calculated temperatures of hornblende (see text) and hornblende-bearing lavas (after Lee *et al.*, 2009): (a) TiO₂, (b) MgO, (c) Al₂O₃, (d) FeO^T. Inlet in (a) show temperature calculation based on Ti-temperature correlation after Helz (1973); Otten (1984). Experimental data for amphibole and melt from Pilet *et al.* (2010).

Early geochronological data indicated that the volcanic activity in the Rhön area lasted from 26–11 Ma (Lippolt, 1982). The new ⁴⁰Ar/³⁹Ar ages of ca. 24 Ma (Fig. 5.17; Table A.7) obtained in this study indicate that the hornblende-bearing basalts in the Rhön area are likely the earliest melts in this area marking the onset of rift-related volcanism of this volcanic sub-province within the CEVP. Later, hornblende-free lavas with ⁴⁰Ar/³⁹Ar whole-rock ages of 18–19 Ma were erupted (Pfänder *et al.*, 2012). These results are consistent with the inferred process of breakdown of amphibole in the mantle early in the magmatic history (Francis & Ludden, 1995). In addition, the view is consistent that upon heating or uplift of the lithosphere-asthenosphere boundary hydrous veins with a solidus temperature lower than the ambient mantle will be the first to melt and will initially generate hydrous phase-bearing mafic lavas (Hawkesworth & Gallagher, 1993).

7 Conclusion

Geochemical and isotope studies on the Miocene hornblende-bearing basanites, alkali basalts, and more differentiated lavas from the Rhön (CEVP) and the hornblende phenocrysts provide the following constraints on the evolution of these rocks and the SCLM (Fig. 7.1).

- (1) Most of the investigated samples are relatively primitive with moderate high Mg# (mostly > 0.50) and moderately high Cr (70–443 ppm) and Ni (60–211 ppm) contents. All basaltic lavas have high TiO₂ contents and basanites as well as alkali basalts can be distinguished by different MgO abundances at similar SiO₂ contents. At 40–45 wt.% SiO₂, lavas with 8–12 wt.% MgO have lower Al₂O₃ abundances (< 14 wt.%) than low MgO lavas which have > 14 wt.% Al₂O₃ at 4–8 wt.% MgO. Some samples represent more differentiated magmas with even lower MgO and lower Cr and Ni contents. These melts have undergone polybaric fractionation of olivine + clinopyroxene + amphibole ± Fe-Ti oxides.
- (2) The high Ti-hornblende are comagmatic kaersutite and paragasite crystallizing from an alkaline lavas. They show a geochemical composition similar to amphibole from magmatic veins.
- (3) Incompatible trace element abundances are broadly similar for basanites and alkali basalts and both rock types have similar K/Nb, Rb/Nb, Zr/Nb, La/Nb, Ba/Nb, K/La, and Ba/La ratios. Variations in REE abundances and correlations between REE ratios are compatible with partial melting of amphibole-bearing spinel peridotite containing a significant fraction of non peridotitic material, e.g. pyroxenite. The presence of residual amphibole requires melting close to the asthenosphere-lithosphere boundary or within the lithospheric mantle.
- (4) Strontium, Nd, and Pb isotope data for the basanites and alkali basalts overlap and are broadly similar to other mafic lavas from the CEVP. In Pb isotope composition all lavas plot above the NHRL in the ²⁰⁶Pb/²⁰⁴Pb-²⁰⁷Pb/²⁰⁴Pb-²⁰⁸Pb/²⁰⁴Pb space. The isotope features imply the existence of a common mantle source for the Rhön lavas with a slightly higher U/Pb and Th/Pb ratio than the reference source; broadly similar to an asthenospheric OIB-type source (EAR: Cebriá & Wilson, 1995; LVC: Hoernle *et al.*, 1995) which may contain an additional crustal component.

7 Conclusion

- (5) Although the spread in isotope composition is limited, $^{87}\text{Sr}/^{86}\text{Sr}$ - $^{206}\text{Pb}/^{204}\text{Pb}$ isotope modelling suggests that minor assimilation of lower crustal rocks for few samples may have occurred. This suggestion is compatible with somewhat lower Ce/Pb and Nb/U ratios in some lavas.
- (6) The host rock isotope composition is similar to other mafic basalts in the CEVP and close to the inferred isotope composition of the European Asthenospheric Reservoir (EAR) which is assumed to be located at the lithosphere-asthenosphere boundary (Wilson *et al.*, 1995). The observed variation of the isotope ratios is attributed either to crustal contamination processes or effects related to metasomatism. The kaersutite, on the other hand, show a much larger variation in the isotope composition and are decoupled from their host rock. The phenocrysts with similar $^{87}\text{Sr}/^{86}\text{Sr}$, $^{143}\text{Nd}/^{144}\text{Nd}$, and $^{206}\text{Pb}/^{204}\text{Pb}$ ratios but higher $^{207}\text{Pb}/^{204}\text{Pb}$ and $^{208}\text{Pb}/^{204}\text{Pb}$ than their host rock may have incorporate some Pb from ancient recycled domain. The hornblende with negative ϵNd values and low Pb isotope ratios may record the involvement of an old crustal component. This heterogeneity of the SCLM is also observed in the oxygen isotope composition where kaersutite record $\delta^{18}\text{O}$ values between 6.4–7.5 ‰.
- (7) Volcanism in the CEVP is considered to be related to mantle metasomatism *sensu lato* (Wilson & Downes, 1991). It has recently been shown that mantle metasomatism related to carbonatite-peridotite interaction produces carbonated silicate partial melts with compositions that have many of the features of primitive alkaline volcanic rocks (Dasgupta *et al.*, 2006, 2007). Carbonated silicate melts are potentially parental to alkaline volcanic rocks and may be produced at small degrees (1–5 %) of partial melting from garnet peridotite with 0.1–0.25 wt.% CO_2 . These melts may form at ~ 1350 – 1450 °C at 3 GPa (Dasgupta *et al.*, 2007), conditions which could be encountered along a colder periphery of mantle plumes at about 90 km depth. Such melts potentially freeze at the LAB producing "enriched" veins and layers of probably non peridotitic, e.g. pyroxenitic material with abundant hydrous minerals. Products derived from remelting of such veins together with parts of the ambient mantle may be parental to the hornblende-bearing basalts studied here. High TiO_2 abundances of the hornblende-bearing basalts can be explained by derivation from a pyroxenitic source containing hydrous minerals (e.g. high Ti-amphibole).
- (8) The metasomatic process probably occurred during the Variscan orogeny where Cadomian or even older crust was recycled into the upper mantle beneath Europe.

7 Conclusion

This recycling produced large scale as well as regional geochemical variations in the SCLM. Alkaline volcanic rocks show the regional heterogeneity of the SCLM, but hydrous phenocrysts may highlight the local heterogeneities within a small volume of the mantle. Such heterogeneities are shown by the decoupling of isotope compositions between host rock and the comagmatic kaersutite.

- (9) Thermobarometric calculations using whole-rock compositions (Lee *et al.*, 2009) constrained a P-T range (2.3–1.4 GPa; 1290–1170 °C) for the primitive hornblende-bearing lavas corresponding to a depth of melting at ~ 80 km. It is important to note that the hornblende-bearing lavas evolved at pressures lower than 2.4 GPa which is the boundary between spinel peridotite and garnet peridotite in the temperature range 1200–1300 °C. This observation is in accordance with the trace element modeling that indicate sources containing only minor amounts of garnet. The occurrence of the comagmatic kaersutite provide also important information of the petrogenesis of alkaline rocks. Hydrous mineral assemblages have lower solidus temperatures than normal mantle peridotite. The stability field of amphibole is constrained at temperature ranging from 1050–1250 °C at 1.5–2.5 GPa (Huckenholz & Gilbert, 1984) or slightly lower temperatures of < 1100 °C at pressures up to 3 GPa; Green *et al.*, 2010). The newly formulated thermometric calculation using the amphibole chemistry constrained a temperature of ~ 1120 °C for the hornblende from this study. This is consistent with the estimated stability range of amphibole in the upper mantle.
- (10) Upon heating or uplift of the lithosphere-asthenosphere boundary hydrous veins with a solidus temperature lower than the ambient mantle will be the first to melt (Hawkesworth & Gallagher, 1993). In this context, it is important to note that the hornblende basalts from the Rhön are considered to be the earliest melts in this area (Ehrenberg & Hickethier, 1994) marking the onset of rift-related volcanism of this volcanic sub-province within the CEVP. This consideration is confirmed by new high-precision $^{40}\text{Ar}/^{39}\text{Ar}$ ages obtained on these comagmatic kaersutite which yield ages about 24 Ma. Other new $^{40}\text{Ar}/^{39}\text{Ar}$ ages in the Rhön area gave slightly younger ages (~ 18 Ma). Therefore, the hornblende-bearing lavas may represent the first products of "wet melting" of a metasomatized SCLM.

7 Conclusion

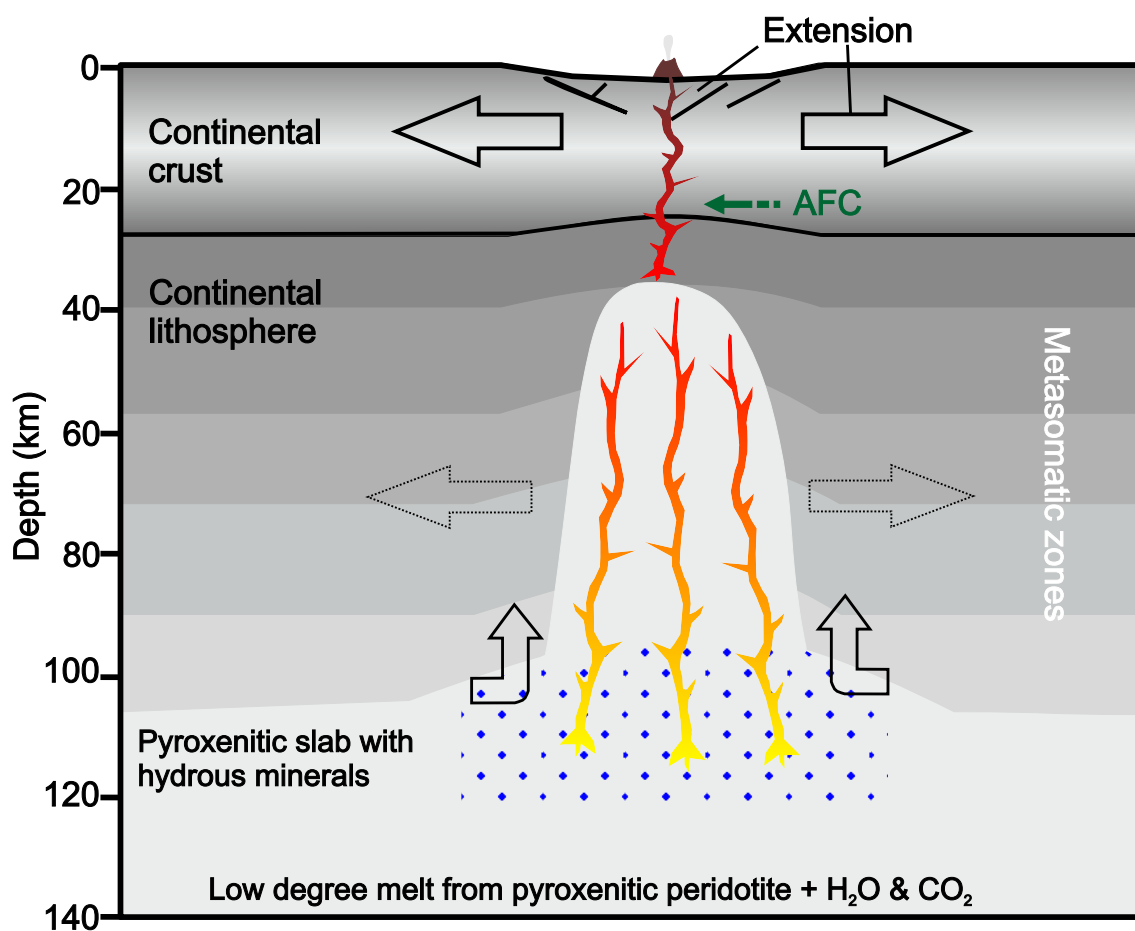


Figure 7.1: Possible model for the petrogenesis of hornblende-bearing lavas from the Rhön area. Enrichment of the upper mantle by subduction of oceanic/continental crust leads to vein generation and later metasomatism in the SCLM. During rifting melting of the metasomatized SCLM leads to genesis of hornblende-bearing lavas in the Rhön area.

Bibliography

- Ackerman, L., Mahlen, N., Jelinek, E., Medaris, G., Ulrych, J., Strnad, L., & Mihaljevic, M. (2007). Geochemistry and evolution of subcontinental lithospheric mantle in Central Europe: evidence from peridotite xenoliths of the Kozakov Volcano, Czech Republic. *Journal of Petrology*, **48**(12), 2235–2260.
- Adam, J. & Green, T. (2006). Trace element partitioning between mica- and amphibole-bearing garnet lherzolite and hydrous basanitic melt: 1. Experimental results and the investigation of controls on partitioning behaviour. *Contributions to Mineralogy and Petrology*, **152**(1), 1–17.
- Alibert, C., Leterrier, J., Panasiuk, M., & Zimmermann, J. (1987). Trace and isotope geochemistry of the alkaline Tertiary volcanism in southwestern Poland. *Lithos*, **20**(4), 311–321.
- Asprey, L.B. (1976). The preparation of very pure fluorine gas. *Journal of Fluorine Chemistry*, **7**(1-3), 359–361.
- Babuška, V. & Plomerová, J. (1988). Subcrustal continental lithosphere: a model of its thickness and anisotropic structure. *Physics of the Earth and Planetary Interiors*, **51**(1-3), 130–132.
- Babuška, V. & Plomerová, J. (2006). European mantle lithosphere assembled from rigid microplates with inherited seismic anisotropy. *Physics of the Earth and Planetary Interiors*, **158**(2-4), 264–280.
- Baker, J., Menzies, M., Thirlwall, M., & MacPherson, C. (1997). Petrogenesis of Quaternary intraplate volcanism, Sana'a, Yemen: Implications for plume-lithosphere interaction and polybaric melt hybridization. *Journal of Petrology*, **38**(10), 1359–1390.
- Bedard, J.H. (1988). Comparative amphibole chemistry of the Monteregian and White Mountain alkaline suites, and the origin of amphibole megacrysts in alkali basalts and lamprophyres. *Mineralogical Magazine*, **52**(364), 91–103.
- Ben Othman, D., Tilton, G., & Menzies, M. (1990). Pb, Nd and Sr isotopic investigations of kaersutite and clinopyroxene from ultramafic nodules, and their host basalts: The nature of the subcontinental mantle. *Geochimica et Cosmochimica Acta*, **54**(12), 3449–3460.

Bibliography

- Best, M. (1970). Kaersutite-peridotite inclusions and kindred megacrysts in basanitic lavas, Grand Canyon, Arizona. *Contributions to Mineralogy and Petrology*, **27**, 25–44.
- Best, M. (1974). Mantle-derived amphibole within inclusions in alkalic-basaltic lavas. *Journal of Geophysical Research-Solid Earth*, **79**(14), 2107–2113.
- Beyer, E.E., Griffin, W.L., & O'Reilly, S.Y. (2006). Transformation of archaean lithospheric mantle by refertilization: evidence from exposed peridotites in the Western Gneiss Region, Norway. *Journal of Petrology*, **47**(8), 1611–1636.
- Binns, R. (1969). High-pressure megacrysts in basanitic lavas near Armidale New South Wales. *American Journal of Science*, **267**(I), 33.
- Binns, R., Duggan, M.B., & Wilkinson, J.F.G. (1970). High pressure megacrysts in alkaline lavas from northeastern New South Wales. *American Journal of Science*, **269**(2), 132–168.
- Blusztajn, J. & Hart, S.R. (1989). Sr, Nd, and Pb isotopic character of Tertiary basalts from southwest Poland. *Geochimica et Cosmochimica Acta*, **53**(10), 2689–2696.
- Blusztajn, J. & Hegner, E. (2002). Osmium isotopic systematics of melilitites from the Tertiary Central European Volcanic Province in SW Germany. *Chemical Geology*, **189**(1-2), 91–103.
- Boettcher, A. & O'Neil, J. (1980). Stable isotope, chemical, and petrographic studies of high-pressure amphiboles and micas – evidence for metasomatism in the mantle source regions of alkali basalts and kimberlites. *American Journal of Science*, **280**(SI), 594–621.
- Bogaard, P.J.F. & Wörner, G. (2003). Petrogenesis of basanitic to tholeiitic volcanic rocks from the Miocene Vogelsberg, Central Germany. *Journal of Petrology*, **44**(3), 569–602.
- Bradshaw, T., Hawkesworth, C., & Gallagher, K. (1993). Basaltic volcanism in the Southern Basin and Range: no role for a mantle plume. *Earth and Planetary Science Letters*, **116**(1-4), 45–62.
- Brey, G. & Green, D.H. (1977). Systematic study of liquidus phase relations in olivine melilitite +H₂O +CO₂ at high pressures and petrogenesis of an olivine melilitite magma. *Contributions to Mineralogy and Petrology*, **61**(2), 141–162.

Bibliography

- Bultitude, R. & Green, D. (1971). Experimental study of crystal-liquid relationships at high pressures in olivine nephelinite and basanite compositions. *Journal of Petrology*, **12**(1), 121–147.
- Cebriá, J.M. & Wilson, M. (1995). Cenozoic mafic magmatism in Western/Central Europe: a common European asthenospheric reservoir? *Terra Nova, Abstracts Supplement*, **7**, 162.
- Class, C. & Goldstein, S.L. (1997). Plume-lithosphere interactions in the ocean basins: constraints from the source mineralogy. *Earth and Planetary Science Letters*, **150**(3-4), 245–260.
- Colville, A.A. & Novak, G.A. (1991). Kaersutite megacrysts and associated crystal inclusions from the Cima volcanic field, San Bernardino County, California. *Lithos*, **27**(2), 107–114.
- Dasgupta, R., Hirschmann, M.M., & Smith, N.D. (2007). Partial melting experiments of peridotite + CO₂ at 3 GPa and genesis of alkalic ocean island basalts. *Journal of Petrology*, **48**(11), 2093–2124.
- Dasgupta, R., Hirschmann, M.M., & Stalker, K. (2006). Immiscible transition from carbonate-rich to silicate-rich melts in the 3GPa melting interval of eclogite + CO₂ and genesis of silica-undersaturated ocean island lavas. *Journal of Petrology*, **47**(4), 647–671.
- Dobosi, G., Downes, H., Matthey, D., & Embey-Isztin, A. (1998). Oxygen isotope ratios of phenocrysts from alkali basalts of the Pannonian basin: Evidence for an O-isotopically homogeneous upper mantle beneath a subduction-influenced area. *Lithos*, **42**(3-4), 213–223.
- Downes, H. (1984). Sr and Nd isotope geochemistry of coexisting alkaline magma series, Cantal, Massif Central, France. *Earth and Planetary Science Letters*, **69**(2), 321–334.
- Downes, H., Bodinier, J.L., Thirlwall, M.F., Lorand, J.P., & Fabries, J. (1991). REE and Sr-Nd isotopic geochemistry of Eastern Pyrenean peridotite massifs: Sub-continental lithospheric mantle modified by continental magmatism. *Journal of Petrology*, **Special Volume**(2), 97–115.
- Downes, H., Seghedi, I., Szakacs, A., Dobosi, G., James, D.E., Vaselli, O., Rigby, I.J., Ingram, G.A., Rex, D., & Pecsckay, Z. (1995). Petrology and geochemistry of late Tertiary/Quaternary mafic alkaline volcanism in Romania. *Lithos*, **35**(1-2), 65–81.

Bibliography

- Duda, A. & Schmincke, H.U. (1985). Polybaric differentiation of alkali basaltic magmas: evidence from green-core clinopyroxenes (Eifel, FRG). *Contributions to Mineralogy and Petrology*, **91**(4), 340–353.
- Ehrenberg, K.H. & Hickethier, H. (1994). Tertiärer Vulkanismus der Wasserkuppenrhön und Kuppenrhön. (Exkursion D1 am 7. und Exkursion D2 am 8. April 1994). *Jahresberichte und Mitteilungen des Oberrheinischen Geologischen Vereins*, **76**, 83–146.
- Ellis, D. (1976). High pressure cognate inclusions in the Newer Volcanics of Victoria. *Contributions to Mineralogy and Petrology*, **58**, 149–180.
- Falloon, T.J. & Green, D.H. (1990). Solidus of carbonated fertile peridotite under fluid-saturated conditions. *Geology*, **18**(3), 195–199.
- Foley, S. (1991). High-pressure stability of the fluor- and hydroxy-endmembers of pargasite and K-richterite. *Geochimica et Cosmochimica Acta*, **55**(9), 2689–2694.
- Foley, S. (1992). Vein-plus-wall-rock melting mechanisms in the lithosphere and the origin of potassic alkaline magmas. *Lithos*, **28**(3-6), 435–453.
- Foley, S., Yaxley, G., Rosenthal, A., Buhre, S., Kiseeva, E., Rapp, R., & Jacob, D. (2009). The composition of near-solidus melts of peridotite in the presence of CO₂ and H₂O between 40 and 60 kbar. *Lithos*, **112**(Supplement 1), 274–283.
- Foley, S.F., Musselwhite, D.S., & van der Laan, S.R. (1999). Melt compositions from ultramafic vein assemblages in the lithospheric mantle: a comparison of cratonic and non-cratonic settings. In: *Proceedings of the 7th International Kimberlite Conference*, (Eds.) J.J. Gurney, J.L. Gurney, M.D. Pascoe, & S.H. Richardson. Cape Town: Red Roof Design, 238–246.
- Francis, D. & Ludden, J. (1995). The signature of amphibole in mafic alkaline lavas, a study in the Northern Canadian Cordillera. *Journal of Petrology*, **36**(5), 1171–1191.
- Freerk-Parpatt, M. (1990). Geochemie Amphibol-führender Nephelinbasalte und Alkali-olivinbasalte aus der Rhön. PhD-thesis, University Göttingen.
- Frey, F.A., Green, D.H., & Roy, S.D. (1978). Integrated models of basalt petrogenesis: A study of quartz tholeiites to olivine melilitites from South Eastern Australia utilizing geochemical and experimental petrological data. *Journal of Petrology*, **19**(3), 463–513.
- Garbe-Schönberg, C.D. (1993). Simultaneous determination of 37 trace elements in 28 international rock standards by ICP-MS. *Geostandards Newsletter*, **17**(1), 81–97.

Bibliography

- Gehler, A., Tütken, T., & Pack, A. (in press). Oxygen and carbon isotope variations in a modern rodent community - implications for palaeoenvironmental reconstructions. *PlosONE*.
- Gerstenberger, H. & Haase, G. (1997). A highly effective emitter substance for mass spectrometric Pb isotope ratio determinations. *Chemical Geology*, **136**(3-4), 309–312.
- Goes, S., Spakman, W., & Bijwaard, H. (1999). A lower mantle source for Central European Volcanism. *Science*, **286**(5446), 1928–1931.
- Granet, M., Wilson, M., & Achauer, U. (1995). Imaging a mantle plume beneath the French Massif Central. *Earth and Planetary Science Letters*, **136**(3-4), 281–296.
- Green, D. & Hibberson, W. (1970). Experimental duplication of conditions of precipitation of high-pressure phenocrysts in a basaltic magma. *Physics of the Earth and Planetary Interiors*, **3**, 247–254.
- Green, D.H., Hibberson, W.O., Kovacs, I., & Rosenthal, A. (2010). Water and its influence on the lithosphere-asthenosphere boundary. *Nature*, **467**(7314), 448–451.
- Griffin, W. & Murthy, V.R. (1969). Distribution of K, Rb, Sr and Ba in some minerals relevant to basalt genesis. *Geochimica et Cosmochimica Acta*, **33**(11), 1389–1414.
- Griffiths, R.W. & Campbell, I.H. (1990). Stirring and structure in mantle starting plumes. *Earth and Planetary Science Letters*, **99**(1-2), 66–78.
- Gutmann, J. (1977). Textures and genesis of phenocrysts and megacrysts in basaltic lavas from the Pinacate volcanic field. *American Journal of Science*, **277**(7), 833–861.
- Haase, K.M., Goldschmidt, B., & Garbe-Schönberg, C.D. (2004). Petrogenesis of Tertiary continental intra-plate lavas from the Westerwald region, Germany. *Journal of Petrology*, **45**(5), 883–905.
- Haase, K.M. & Renno, A.D. (2008). Variation of magma generation and mantle sources during continental rifting observed in Cenozoic lavas from the Eger Rift, Central Europe. *Chemical Geology*, **257**(3-4), 192–202.
- Harmon, R.S. & Hoefs, J. (1995). Oxygen isotope heterogeneity of the mantle deduced from global ¹⁸O systematics of basalts from different geotectonic settings. *Contributions to Mineralogy and Petrology*, **120**(1), 95–114.
- Hart, S.R. (1984). A large-scale isotope anomaly in the Southern Hemisphere mantle. *Nature*, **309**(5971), 753–757.

Bibliography

- Hart, S.R. & Davis, K.E. (1978). Nickel partitioning between olivine and silicate melt. *Earth and Planetary Science Letters*, **40**(2), 203–219.
- Hartmann, G. & Wedepohl, K. (1990). Metasomatically altered peridotite xenoliths from the hessian depression (Northwest Germany). *Geochimica et Cosmochimica Acta*, **54**(1), 71–86.
- Hawkesworth, C., Kempton, P., Rogers, N., Ellam, R., & van Calsteren, P. (1990). Continental mantle lithosphere, and shallow level enrichment processes in the Earth's mantle. *Earth and Planetary Science Letters*, **96**(3-4), 256–268.
- Hawkesworth, C.J. & Gallagher, K. (1993). Mantle hotspots, plumes and regional tectonics as causes of intraplate magmatism. *Terra Nova*, **5**(6), 552–559.
- Hawkesworth, C.J. & Vollmer, R. (1979). Crustal contamination versus enriched mantle: $^{143}\text{Nd}/^{144}\text{Nd}$ and $^{87}\text{Sr}/^{86}\text{Sr}$ evidence from the Italian volcanics. *Contributions to Mineralogy and Petrology*, **69**(2), 151–165.
- Hawthorne, F.C., Oberti, R., Harlow, G.E., Maresch, W.V., Martin, R.F., Schumacher, J.C., & Welch, M.D. (2012). Nomenclature of the amphibole supergroup. *American Mineralogist*, **97**(11-12), 2031–2048.
- Hegner, E. & Vennemann, T.W. (1997). Role of fluids in the origin of Tertiary European intraplate volcanism: Evidence from O, H, and Sr isotopes in melilitites. *Geology*, **25**(11), 1035–1038.
- Hegner, E., Walter, H.J., & Satir, M. (1995). Pb-Sr-Nd isotopic compositions and trace element geochemistry of megacrysts and melilitites from the Tertiary Urach volcanic field: source composition of small volume melts under SW Germany. *Contributions to Mineralogy and Petrology*, **122**(3), 322–335.
- Helz, R.T. (1973). Phase relations of basalts in their melting range at $P_{\text{H}_2\text{O}} = 5 \text{ kb}$ as a function of oxygen fugacity. *Journal of Petrology*, **14**(2), 249–302.
- Hirose, K. (1997). Partial melt compositions of carbonated peridotite at 3 GPa and role of CO_2 in alkali-basalt magma generation. *Geophysical Research Letters*, **24**(22), 2837–2840.
- Hirschmann, M.M., Kogiso, T., Baker, M.B., & Stolper, E.M. (2003). Alkalic magmas generated by partial melting of garnet pyroxenite. *Geology*, **31**(6), 481–484.

Bibliography

- Hoernle, K.A., Zhang, Y.S., & Graham, D. (1995). Seismic and geochemical evidence for large-scale mantle upwelling beneath the eastern Atlantic and western and central Europe. *Nature*, **374**(6517), 34–39.
- Hofmann, A. (1997). Mantle geochemistry: The message from oceanic volcanism. *Nature*, **385**(6613), 219–229.
- Hofmann, A., Jochum, K., Seufert, M., & White, W. (1986). Nb and Pb in oceanic basalts: new constraints on mantle evolution. *Earth and Planetary Science Letters*, **79**(1-2), 33–45.
- Huckenholz, H.G. & Gilbert, M.C. (1984). Stabilität von Ca-Amphibol in Alkalibasalten der Hoheifel. *Fortschritte der Mineralogie*, **62**(Beiheft 1), 106–107.
- Ionov, D. & Hofmann, A. (1995). Nb-Ta-rich mantle amphiboles and micas: Implications for subduction-related metasomatic trace element fractionations. *Earth and Planetary Science Letters*, **131**(3-4), 341–356.
- Ionov, D.A., Griffin, W.L., & O'Reilly, S.Y. (1997). Volatile-bearing minerals and lithophile trace elements in the upper mantle. *Chemical Geology*, **141**(3-4), 153–184.
- Irving, A. (1974). Megacrysts from the Newer basalts and other basaltic rocks of South-eastern Australia. *Geological Society of America Bulletin*, **85**(10), 1503–1514.
- Irving, A.J. & Frey, F.A. (1984). Trace element abundances in megacrysts and their host basalts: Constraints on partition coefficients and megacryst genesis. *Geochimica et Cosmochimica Acta*, **48**(6), 1201–1221.
- Jochum, K.P., Dingwell, D.B., Rocholl, A., Stoll, B., Hofmann, A.W., Becker, S., Besmehn, A., Bessette, D., Dietze, H.J., Dulski, P., Erzinger, J., Hellebrand, E., Hoppe, P., Horn, I., Janssens, K., Jenner, G., Klein, M., McDonough, W., Maetz, M., Mezger, K., Mürer, C., Nikogosian, I., Pickhardt, C., Raczek, I., Rhede, D., Seufert, H., Simakin, S., Sobolev, A., Spettel, B., Straub, S., Vincze, L., Wallianos, A., Weckwerth, G., Weyer, S., Wolf, D., & Zimmer, M. (2000). The preparation and preliminary characterisation of eight geological MPI-DING reference glasses for in-situ microanalysis. *Geostandards Newsletter*, **24**(1), 87–133.
- Jochum, K.P., Stoll, B., Herwig, K., Willbold, M., Hofmann, A.W., Amini, M., Aarburg, S., Abouchami, W., Hellebrand, E., Mocek, B., Raczek, I., Stracke, A., Alard, O., Bouman, C., Becker, S., Duecking, M., Braetz, H., Klemm, R., de Bruin, D., Canil, D., Cornell, D., de Hoog, C.J., Dalpe, C., Danyushevsky, L., Eisenhauer, A., Gao, Y., Snow, J.E., Goschopf,

Bibliography

- N., Gunther, D., Latkoczy, C., Guillong, M., Hauri, E.H., Hofer, H.E., Lahaye, Y., Horz, K., Jacob, D.E., Kasemann, S.A., Kent, A.J.R., Ludwig, T., Zack, T., Mason, P.R.D., Meixner, A., Rosner, M., Misawa, K., Nash, B.P., Pfaender, J., Premo, W.R., Sun, W., Tiepolo, M., Vannucci, R., Vennemann, T., Wayne, D., & Woodhead, J.D. (2006). MPI-DING reference glasses for in situ microanalysis: New reference values for element concentrations and isotope ratios. *Geochemistry Geophysics Geosystems*, **7**.
- Jones, A.M., Iacumin, P., & Young, E.D. (1999). High-resolution $\delta^{18}\text{O}$ analysis of tooth enamel phosphate by isotope ratio monitoring gas chromatography mass spectrometry and ultraviolet laser fluorination. *Chemical Geology*, **153**(1-4), 241–248.
- Jung, C., Jung, S., Hoffer, E., & Berndt, J. (2006). Petrogenesis of Tertiary mafic alkaline magmas in the Hoheifel, Germany. *Journal of Petrology*, **47**(8), 1637–1671.
- Jung, S. (1995). Geochemistry and petrogenesis of rift-related Tertiary alkaline rocks from the Rhön area (Central Germany). *Neues Jahrbuch für Mineralogie-Abhandlungen*, **169**(3), 193–226.
- Jung, S. & Hoernes, S. (2000). The major- and trace-element and isotope (Sr, Nd, O) geochemistry of Cenozoic alkaline rift-type volcanic rocks from the Rhön area (central Germany): petrology, mantle source characteristics and implications for asthenosphere-lithosphere interactions. *Journal of Volcanology and Geothermal Research*, **99**(1-4), 27–53.
- Jung, S. & Masberg, P. (1998). Major- and trace-element systematics and isotope geochemistry of Cenozoic mafic volcanic rocks from the Vogelsberg (central Germany): Constraints on the origin of continental alkaline and tholeiitic basalts and their mantle sources. *Journal of Volcanology and Geothermal Research*, **86**(1-4), 151–177.
- Jung, S., Pfänder, J., Brauns, M., & Maas, R. (2011). Crustal contamination and mantle source characteristics in continental intra-plate volcanic rocks: Pb, Hf and Os isotopes from central European volcanic province basalts. *Geochimica et Cosmochimica Acta*, **75**(10), 2664–2683.
- Jung, S., Pfänder, J., Brüggemann, G., & Stracke, A. (2005). Sources of primitive alkaline volcanic rocks from the Central European Volcanic Province (Rhön, Germany) inferred from Hf, Os and Pb isotopes. *Contributions to Mineralogy and Petrology*, **150**(5), 546–559.

Bibliography

- Jung, S., Vieten, K., Romer, R.L., Mezger, K., Hoernes, S., & Satir, M. (2012). Petrogenesis of Tertiary alkaline magmas in the Siebengebirge, Germany. *Journal of Petrology*, **53**(11), 2381–2409.
- Kempton, P., Harmon, R., Stosch, H.G., Hoefs, J., & Hawkesworth, C. (1988). Open-system O-isotope behaviour and trace element enrichment in the sub-Eifel mantle. *Earth and Planetary Science Letters*, **89**(3-4), 273–287.
- Kesson, S. & Price, R.C. (1972). The major and trace element chemistry of kaersutite and its bearing on the petrogenesis of alkaline rocks. *Contributions to Mineralogy and Petrology*, **35**(2), 119–124.
- Klein, E.M. & Langmuir, C.H. (1987). Global correlations of ocean ridge basalt chemistry with axial depth and crustal thickness. *Journal of Geophysical Research-Solid Earth*, **92**(B8), 8089–8115.
- Kogiso, T., Hirose, K., & Takahashi, E. (1998). Melting experiments on homogeneous mixtures of peridotite and basalt: application to the genesis of ocean island basalts. *Earth and Planetary Science Letters*, **162**(1-4), 45–61.
- Kogiso, T., Hirschmann, M.M., & Frost, D.J. (2003). High-pressure partial melting of garnet pyroxenite: possible mafic lithologies in the source of ocean island basalts. *Earth and Planetary Science Letters*, **216**(4), 603–617.
- Kroner, U., Romer, R.L., & Linnemann, U. (2010). The Saxo-Thuringia zone of the Variscan orogen as part of Pangea. In: *Pre-Mesozoic geology of Saxo-Thuringia - From the Cadomian active margin to the Variscan orogen*, (Eds.) U. Linnemann & R.L. Romer. Schweizerbart, Stuttgart, 3–16.
- LaTourrette, T., Hervig, R.L., & Holloway, J.R. (1995). Trace element partitioning between amphibole, phlogopite, and basanite melt. *Earth and Planetary Science Letters*, **135**(1-4), 13–30.
- Leake, B., Woolley, A., Arps, C., Birch, W., Gilbert, M., Grice, J., Hawthorne, F., Kato, A., Kisch, H., Krivovichev, V., Linthout, K., Laird, J., Mandarino, J., Maresch, W., Nickel, E., Rock, N., Schumacher, J., Smith, D., Stephenson, N., Ungaretti, L., Whittaker, E., & Guo, Y. (1997). Nomenclature of amphiboles: Report of the subcommittee on amphiboles of the International Mineralogical Association, commission on new minerals and mineral names. *American Mineralogist*, **82**(9-10), 1019–1037.

Bibliography

- LeBas, M.J., Maitre, R.W.L., Streckeisen, A., Zanettin, B., & IUGS Subcommittee on the Systematics of Igneous Rocks (1986). A chemical classification of volcanic rocks based on the total alkali-silica diagram. *Journal of Petrology*, **27**(3), 745–750.
- Lechler, P. & Desilets, M. (1987). A review of the use of loss on ignition as a measurement of total volatiles in whole-rock analysis. *Chemical Geology*, **63**(3-4), 341–344.
- Lee, C.T.A., Luffi, P., Plank, T., Dalton, H., & Leeman, W.P. (2009). Constraints on the depths and temperatures of basaltic magma generation on Earth and other terrestrial planets using new thermobarometers for mafic magmas. *Earth and Planetary Science Letters*, **279**(1-2), 20–33.
- Lippolt, H.J. (1982). K/Ar age determinations and the correlation of Tertiary volcanic activity in Central Europe. *Geologisches Jahrbuch Hannover*, **52**, 113–135.
- Loock, G., Stosch, H.G., & Seck, H.A. (1990). Granulite facies lower crustal xenoliths from the Eifel, West Germany: petrological and geochemical aspects. *Contributions to Mineralogy and Petrology*, **105**(1), 25–41.
- Ludwig, K. (2008). Isoplot 3.70. A geochronological toolkit for Microsoft Excel. *Berkeley Geochronology Center Special Publication*, **4**, 1–76.
- Lustrino, M. & Wilson, M. (2007). The circum-Mediterranean anorogenic Cenozoic igneous province. *Earth-Science Reviews*, **81**(1-2), 1–65.
- Mattey, D., Lowry, D., & Macpherson, C. (1994). Oxygen isotope composition of mantle peridotite. *Earth and Planetary Science Letters*, **128**(3-4), 231–241.
- McDonough, W. & Sun, S.S. (1995). The composition of the Earth. *Chemical Geology*, **120**(3-4), 223–253.
- McDonough, W., Sun, S.S., Ringwood, A., Jagoutz, E., & Hofmann, A. (1992). Potassium, rubidium, and cesium in the Earth and Moon and the evolution of the mantle of the Earth. *Geochimica et Cosmochimica Acta*, **56**(3), 1001–1012.
- McKenzie, D. & Bickle, M.J. (1988). The volume and composition of melt generated by extension of the lithosphere. *Journal of Petrology*, **29**(3), 625–679.
- Mengel, K. & Green, D.H. (1986). Stability of amphibole and phlogopite in metasomatised peridotite under water-saturated and water-undersaturated conditions. In: *Kimberlites and Related Rocks*, (Eds.) J. Ross, A.L. Jaques, J. Ferguson, D.H. Green,

Bibliography

- Y. O'Reilly Suzanne, R.V. Danchin, & A.J.A. Janse, volume 1. Oxford: Blackwell Scientific, 571–581.
- Mengel, K., Sachs, P.M., Stosch, H.G., Wörner, G., & Loock, G. (1991). Crustal xenoliths from Cenozoic volcanic fields of West Germany: Implications for structure and composition of the continental crust. *Tectonophysics*, **195**(2-4), 271–289.
- Menzies, M. & Murthy, V.R. (1980). Mantle metasomatism as a precursor to the genesis of aklaline magmas - isotopic evidence. *American Journal of Science*, **280**(SI), 622–638.
- Moine, B.N., Grégoire, M., O'Reilly, Suzanne Y., S.Y., Sheppard, S.M.F., & Cottin, J.Y. (2001). High field strength element fractionation in the upper mantle: Evidence from amphibole-rich composite mantle xenoliths from the Kerguelen Islands (Indian Ocean). *Journal of Petrology*, **42**(11), 2145–2167.
- Molina, J., Scarrow, J., Montero, P., & Bea, F. (2009). High-Ti amphibole as a petrogenetic indicator of magma chemistry: evidence for mildly alkalic-hybrid melts during evolution of Variscan basic-ultrabasic magmatism of Central Iberia. *Contributions to Mineralogy and Petrology*, **158**, 69–98.
- Neumann, H., Mead, J., & Vitaliano, C. (1954). Trace element variation during fractional crystallization as calculated from the distribution law. *Geochimica et Cosmochimica Acta*, **6**(2-3), 90–99.
- Niida, K. & Green, D. (1999). Stability and chemical composition of pargasitic amphibole in MORB pyrolite under upper mantle conditions. *Contributions to Mineralogy and Petrology*, **135**(1), 18–40.
- Niu, Y., Wilson, M., Humphreys, E.R., & O'Hara, M.J. (2011). The origin of intra-plate Ocean Island Basalts (OIB): the lid effect and its geodynamic implications. *Journal of Petrology*, **52**(7-8), 1443–1468.
- O'Reilly, S.Y., Griffin, W.L., & Ryan, C.G. (1991). Residence of trace elements in metasomatized spinel lherzolite xenoliths: a proton-microprobe study. *Contributions to Mineralogy and Petrology*, **109**(1), 98–113.
- Otten, M.T. (1984). The origin of brown hornblende in the Artfjället gabbro and dolerites. *Contributions to Mineralogy and Petrology*, **86**(2), 189–199.
- Pearce, N.J., Perkins, W.T., Westgate, J.A., Gorton, M.P., Jackson, S.E., Neal, C.R., & Chener, S.P. (1997). A compilation of new and published major and trace element data for

Bibliography

- NIST SRM 610 and NIST SRM 612 glass reference materials. *Geostandards Newsletter*, **21**(1), 115–144.
- Peccerillo, A. (1999). Multiple mantle metasomatism in central-southern Italy: Geochemical effects, timing and geodynamic implications. *Geology*, **27**(4), 315–318.
- Pfänder, J., Sperner, B., Ratschbacher, L., Jung, S., Freidlein, V., Geyer, G., Krause, T., Rohrmüller, J., & Kunzmann, T. (2012). High-resolution Ar-Ar dating of volcanic rocks from Central and Southern Germany - methodical limitations and a (preliminary) re-evaluation of timing of volcanic activity within Central Europe. *European Mineralogical Conference*, **abstract**, 538.
- Pilet, S., Baker, M.B., Müntener, O., & Stolper, E.M. (2011). Monte Carlo simulations of metasomatic enrichment in the lithosphere and implications for the source of alkaline basalts. *Journal of Petrology*, **52**(7-8), 1415–1442.
- Pilet, S., Baker, M.B., & Stolper, E.M. (2008). Metasomatized lithosphere and the origin of alkaline lavas. *Science*, **320**(5878), 916–919.
- Pilet, S., Hernandez, J., Sylvester, P., & Poujol, M. (2005). The metasomatic alternative for ocean island basalt chemical heterogeneity. *Earth and Planetary Science Letters*, **236**(1-2), 148–166.
- Pilet, S., Ulmer, P., & Villiger, S. (2010). Liquid line of descent of a basanitic liquid at 1.5 GPa: Constraints on the formation of metasomatic veins. *Contrib. Mineral. Petrol.*, **159**(5), 621–643.
- Powell, W., Zhang, M., O'Reilly, S.Y., & Tiepolo, M. (2004). Mantle amphibole trace-element and isotopic signatures trace multiple metasomatic episodes in lithospheric mantle, western Victoria, Australia. *Lithos*, **75**(1-2), 141–171.
- Prodehl, C. (1981). Structure of the crust and upper mantle beneath the Central European rift system. *Tectonophysics*, **80**(1-4), 255–269.
- Prodehl, C., Mueller, S., Glahn, A., Gutscher, M., & Haak, V. (1992). Lithospheric cross-sections of the European Cenozoic rift system. *Tectonophysics*, **208**(1-3), 113–138.
- Putirka, K., Johnson, M., Kinzler, R., Longhi, J., & Walker, D. (1996). Thermobarometry of mafic igneous rocks based on clinopyroxene-liquid equilibria, 0-30 kbar. *Contributions to Mineralogy and Petrology*, **123**(1), 92–108.

Bibliography

- Rapp, R.P., Shimizu, N., Norman, M.D., & Applegate, G.S. (1999). Reaction between slab-derived melts and peridotite in the mantle wedge: experimental constraints at 3.8 GPa. *Chemical Geology*, **160**(4), 335–356.
- Renne, P.R., Mundil, R., Balco, G., Min, K., & Ludwig, K.R. (2010). Joint determination of ^{40}K decay constants and $^{40}\text{Ar}^*/^{40}\text{K}$ for the Fish Canyon sanidine standard, and improved accuracy for $^{40}\text{Ar}/^{39}\text{Ar}$ geochronology. *Geochimica et Cosmochimica Acta*, **74**(18), 5349–5367.
- Renne, P.R. & Norman, E.B. (2001). Determination of the half-life of ^{37}Ar by mass spectrometry. *Phys. Rev. C*, **63**, 047302.
- Ritter, J.R., Jordan, M., Christensen, U.R., & Achauer, U. (2001). A mantle plume below the Eifel volcanic fields, Germany. *Earth and Planetary Science Letters*, **186**(1), 7–14.
- Robinson, J.C. & Wood, B.J. (1998). The depth of the spinel to garnet transition at the peridotite solidus. *Earth and Planetary Science Letters*, **164**(1-2), 277–284.
- Romer, R.L., Heinrich, W., Schröder-Smeibidl, B., Meixner, A., Fischer, C.O., & Schulz, C. (2005). Elemental dispersion and stable isotope fractionation during reactive fluid-flow and fluid immiscibility in the Bufa del Diente aureole, NE-Mexico: evidence from radiographies and Li, B, Sr, Nd, and Pb isotope systematics. *Contributions to Mineralogy and Petrology*, **149**(4), 400–429.
- Rosenbaum, J.M. (1993). Mantle phlogopite: A significant lead repository? *Chemical Geology*, **106**(3-4), 475–483.
- Rudnick, R.L. & Fountain, D.M. (1995). Nature and composition of the continental crust: A lower crustal perspective. *Reviews of Geophysics*, **33**(3), 267–309.
- Rudnick, R.L. & Goldstein, S.L. (1990). The Pb isotopic compositions of lower crustal xenoliths and the evolution of lower crustal Pb. *Earth and Planetary Science Letters*, **98**(2), 192–207.
- Rudnick, R.L., McDonough, W.F., & Chappell, B.W. (1993). Carbonatite metasomatism in the northern Tanzanian mantle: Petrographic and geochemical characteristics. *Earth and Planetary Science Letters*, **114**(4), 463–475.
- Sachs, P.M. & Hansteen, T.H. (2000). Pleistocene underplating and metasomatism of the lower continental crust: A xenolith study. *Journal of Petrology*, **41**(3), 331–356.

Bibliography

- Sharp, Z.D. (1990). A laser-based microanalytical method for the in situ determination of oxygen isotope ratios of silicates and oxides. *Geochimica et Cosmochimica Acta*, **54**(5), 1353–1357.
- Shaw, C.S. & Eyzaguirre, J. (2000). Origin of megacrysts in the mafic alkaline lavas of the West Eifel volcanic field, Germany. *Lithos*, **50**(1-3), 75–95.
- Shaw, D. (1970). Trace element fractionation during anatexis. *Geochimica et Cosmochimica Acta*, **34**(2), 237–243.
- Shimizu, N., Semet, M., & Allégre, C. (1978). Geochemical applications of quantitative ion-microprobe analysis. *Geochimica et Cosmochimica Acta*, **42**(9), 1321–1334.
- Simonetti, A. & Bell, K. (1993). Isotopic disequilibrium in clinopyroxenes from nephelinitic lavas, Napak volcano, eastern Uganda. *Geology*, **21**(3), 243–246.
- Simonetti, A. & Bell, K. (1994). Nd, Pb and Sr isotopic data from the Napak carbonatite-nephelinite centre, eastern Uganda: an example of open-system crystal fractionation. *Contributions to Mineralogy and Petrology*, **115**, 356–366.
- Sobolev, A.V., Hofmann, A.W., Kuzmin, D.V., Yaxley, G.M., Arndt, N.T., Chung, S.L., Danyushkevsky, L.V., Elliott, T., Frey, F.A., Garcia, M.O., Gurenko, A.A., Kamenetsky, V.S., Kerr, A.C., Krivolutsкая, N.A., Matvienkov, V.V., Nikogosian, I.K., Rocholl, A., Sigurdsson, I.A., Sushchevskaya, N.M., & Teklay, M. (2007). The amount of recycled crust in sources of mantle-derived melts. *Science*, **316**(5823), 412–417.
- Sobolev, A.V., Hofmann, A.W., Sobolev, S.V., & Nikogosian, I.K. (2005). An olivine-free mantle source of Hawaiian shield basalts. *Nature*, **434**(7033), 590–597.
- Spera, F.J. & Bohron, W.A. (2001). Energy-constrained open-system magmatic processes I: General model and energy-constrained assimilation and fractional crystallization (EC-AFC) formulation. *Journal of Petrology*, **42**(5), 999–1018.
- Stacey, J. & Kramers, J. (1975). Approximation of terrestrial lead isotope evolution by a two-stage model. *Earth and Planetary Science Letters*, **26**(2), 207–221.
- Stosch, H.G. & Lugmair, G.W. (1984). Evolution of the lower continental crust: granulite facies xenoliths from the Eifel, West Germany. *Nature*, **311**(5984), 368–370.
- Stosch, H.G., Lugmair, G.W., & Seck, H. (1986). Geochemistry of granulite-facies lower crustal xenoliths: implications for the geological history of the lower continental crust

Bibliography

- below the Eifel, West Germany. *Geological Society, London, Special Publications*, **24**(1), 309–317.
- Stosch, H.G., Schmucker, A., & Reys, C. (1992). The nature and geological history of the deep crust under the Eifel, Germany. *Terra Nova*, **4**(1), 53–62.
- Stracke, A., Hofmann, A., & Hart, S. (2005). FOZO, HIMU, and the rest of the mantle zoo. *Geochemistry Geophysics Geosystems*, **6**, Q05007.
- Stuckless, J.S. & Irving, A.J. (1976). Strontium isotope geochemistry of megacrysts and host basalts from southeastern Australia. *Geochimica et Cosmochimica Acta*, **40**(2), 209–213.
- Thibault, Y., Edgar, A., & Lloyd, F. (1992). Experimental investigation of melts from a carbonated phlogopite lherzolite - implications for metasomatism in the continental lithospheric mantle. *American Mineralogist*, **77**(7-8), 784–794.
- Thirlwall, M.F., Upton, B.G.J., & Jenkins, C. (1994). Interaction between continental lithosphere and the iceland plume – Sr-Nd-Pb isotope geochemistry of Tertiary basalts, NE Greenland. *Journal of Petrology*, **35**(3), 839–879.
- Tiepolo, M., Vannucci, R., Oberti, R., Foley, S., Bottazzi, P., & Zanetti, A. (2000). Nb and Ta incorporation and fractionation in titanite pargasite and kaersutite: crystal-chemical constraints and implications for natural systems. *Earth and Planetary Science Letters*, **176**(2), 185–201.
- Vannucci, R., Piccardo, G., Rivalenti, G., Zanetti, A., Rampone, E., Ottolini, L., Oberti, R., Mazzucchelli, M., & Bottazzi, P. (1995). Origin of LREE-depleted amphiboles in the subcontinental mantle. *Geochimica et Cosmochimica Acta*, **59**(9), 1763–1771.
- Villemant, B., Jaffrezic, H., Joron, J.L., & Treuil, M. (1981). Distribution coefficients of major and trace elements; fractional crystallization in the alkali basalt series of Chaîne des Puys (Massif Central, France). *Geochimica et Cosmochimica Acta*, **45**(11), 1997–2016.
- Vinx, R. & Jung, D. (1977). Pargasitic-kaersutitic amphibole from a basanitic diatreme at the Rosenberg, North of Kassel (North Germany). *Contributions to Mineralogy and Petrology*, **65**, 135–142.
- Vogel, W. & Kuipers, G. (1987). A pre-calibrated program for geological applications. *Phillips New Developments in X-Ray Spectrometry*, **11**, 2–8.

Bibliography

- Wallace, M. & Green, D. (1991). The effect of bulk rock composition on the stability of amphibole in the upper mantle - implications for solidus positions and mantle metasomatism. *Mineralogy and Petrology*, **44**(1-2), 1–19.
- Wass, S.Y. (1979). Multiple origins of clinopyroxenes in alkali basaltic rocks. *Lithos*, **12**(2), 115–132.
- Wedepohl, K.H. & Baumann, A. (1999). Central European Cenozoic plume volcanism with OIB characteristics and indications of a lower mantle source. *Contributions to Mineralogy and Petrology*, **136**(3), 225–239.
- Wedepohl, K.H., Gohn, E., & Hartmann, G. (1994). Cenozoic alkali basaltic magmas of Western Germany and their products of Differentiation. *Contributions to Mineralogy and Petrology*, **115**(3), 253–278.
- Wilkinson, J. (1975). Ultramafic inclusions and high pressure megacrysts from a nephelinite sill, Nandewar Mountains, north-eastern New South Wales, and their bearing on the origin of certain ultramafic inclusions in alkaline volcanic rocks. *Contributions to Mineralogy and Petrology*, **51**, 235–262.
- Wilkinson, J.F.G. & Hensel, H.D. (1991). An analcime mugearite-megacryst association from north-eastern New South Wales: implications for high-pressure amphibole-dominated fractionation of alkaline magmas. *Contributions to Mineralogy and Petrology*, **109**(2), 240–251.
- Wilshire, H., Pike, J., Meyer, C., & Schwarzmann, E. (1980). Amphibole-rich veins in lherzolite xenoliths, Dish Hill and Deadman lake, California. *American Journal of Science*, **280**(SI), 576–593.
- Wilson, M. & Downes, H. (1991). Tertiary-Quaternary extension-related alkaline magmatism in Western and Central Europe. *Journal of Petrology*, **32**(4), 811–849.
- Wilson, M. & Downes, H. (1992). Mafic alkaline magmatism associated with the European Cenozoic rift system. *Tectonophysics*, **208**(1-3), 173–182.
- Wilson, M. & Downes, H. (2006). Tertiary-Quaternary intra-plate magmatism in Europe and its relationship to mantle dynamics. *Geological Society, London, Memoirs*, **32**(1), 147–166.
- Wilson, M., Rosenbaum, J.M., & Dunworth, E.A. (1995). Melilitites: partial melts of the thermal boundary layer? *Contributions to Mineralogy and Petrology*, **119**(2-3), 181–196.

Bibliography

- Witt, G. & Seck, H. (1989). Origin of amphibole in recrystallized and porphyroclastic mantle xenoliths from the Rhenish Massif: Implications for the nature of mantle metasomatism. *Earth and Planetary Science Letters*, **91**(3-4), 327–340.
- Witt-Eickschen, G. & Harte, B. (1994). Distribution of trace elements between amphibole and clinopyroxene from mantle peridotites of the Eifel (western Germany): An ion-microprobe study. *Chemical Geology*, **117**(1-4), 235–250.
- Witt-Eickschen, G., Kaminsky, W., Kramm, U., & Harte, B. (1998). The nature of young vein metasomatism in the lithosphere of the West Eifel (Germany): Geochemical and isotopic constraints from composite mantle xenoliths from the Meerfelder Maar. *Journal of Petrology*, **39**(1), 155–185.
- Witt-Eickschen, G. & Kramm, U. (1997). Mantle upwelling and metasomatism beneath Central Europe: Geochemical and isotopic constraints from mantle xenoliths from the Rhön (Germany). *Journal of Petrology*, **38**(4), 479–493.
- Witt-Eickschen, G., Seck, H.A., Mezger, K., Eggins, S.M., & Altherr, R. (2003). Lithospheric mantle evolution beneath the Eifel (Germany): Constraints from Sr-Nd-Pb isotopes and trace element abundances in spinel peridotite and pyroxenite xenoliths. *Journal of Petrology*, **44**(6), 1077–1095.
- Witt-Eickschen, G., Seck, H.A., & Reys, C. (1993). Multiple enrichment processes and their relationships in the subcrustal lithosphere beneath the Eifel (Germany). *Journal of Petrology*, **34**(1), 1–22.
- Wörner, G., Zindler, A., Staudigel, H., & Schmincke, H.U. (1986). Sr, Nd, and Pb isotope geochemistry of Tertiary and Quaternary alkaline volcanics from West Germany. *Earth and Planetary Science Letters*, **79**(1-2), 107–119.
- Ziegler, P.A. (1990). Geological atlas of Eastern and Central Europe. *Shell Int. Pet. Mij. and Geol. Soc.*, 238pp.
- Ziegler, P.A. (1992). European Cenozoic rift system. *Tectonophysics*, **208**(1-3), 91–111.
- Zindler, A. & Hart, S. (1986). Chemical geodynamics. *Annual Review of Earth and Planetary Sciences*, **14**(1), 493–571.
- Zinner, E. & Crozaz, G. (1986). A method for the quantitative measurement of rare earth elements in the ion microprobe. *International Journal of Mass Spectrometry and Ion Processes*, **69**(1), 17–38.

A Appendix

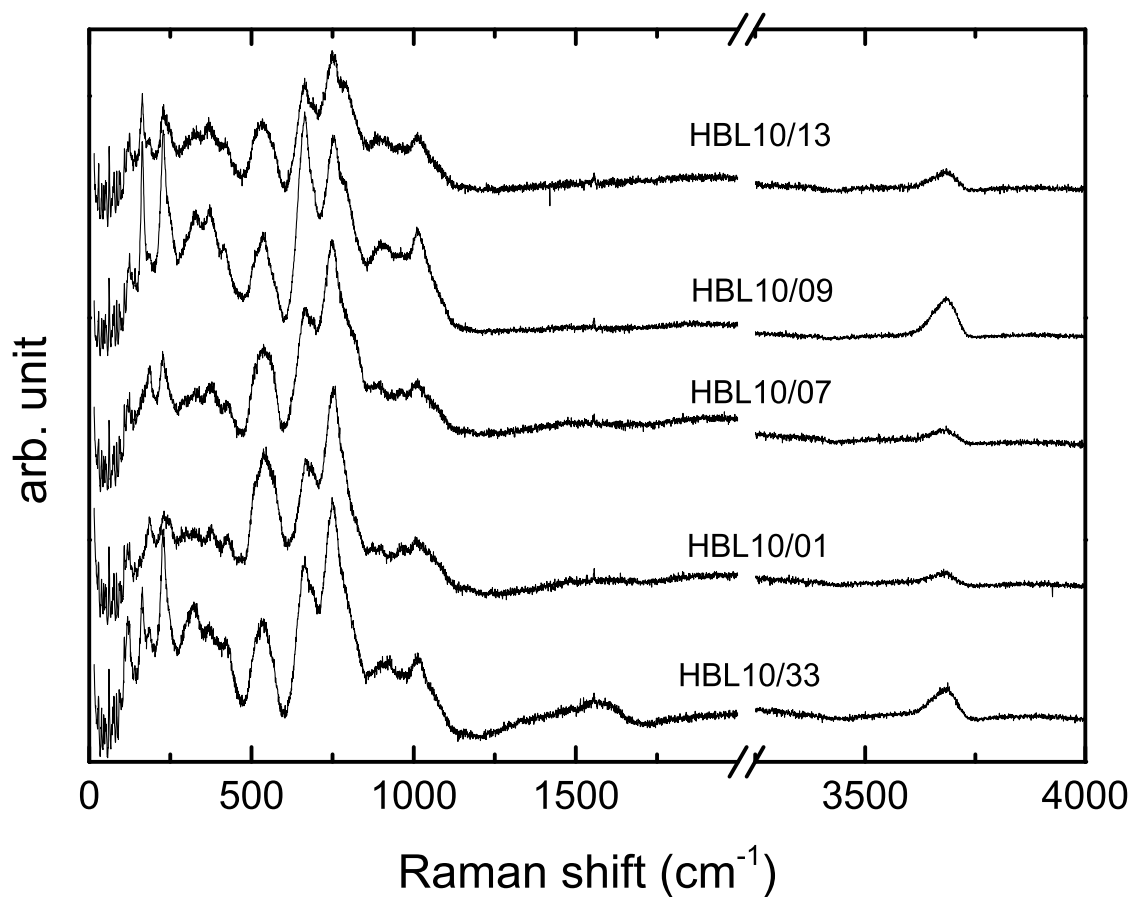


Figure A.1: Raman spectroscopic analyses of hornblende from the Rhön area in the spectra range from 15 to 4000 cm^{-1} . The Raman spectra show the fingerprint spectrum of kaersutite and pargasite and the specific OH-bonding vibration at $\sim 3400 \text{ cm}^{-1}$.

Table A.1: Chemical compositions of Rhön lavas; the prefix "Hbl" indicates the presence of hornblende as phenocrysts; Hbl-phonteph.: hornblende-bearing phonotephrite; Hbl-trachybas.: hornblende-bearing trachybasalt; *a*: all major elements and Sc measured by XRF from Universität Hamburg; *b*: trace elements measured by Actlabs; *c*: trace elements measured by ICP-MS Universität Kiel.

| Sample | Rh10/01 ^b | Rh10/02 ^b | Rh10/03 ^b | Rh10/04 ^c | Rh10/05 ^c | Rh10/06 ^b | Rh10/07 ^b | Rh10/08 ^b | Rh10/09 ^b | Rh10/10 ^c | Rh10/11 ^c | Rh10/12 ^b |
|--------------------------------|----------------------|----------------------|----------------------|----------------------|----------------------|----------------------|----------------------|----------------------|----------------------|----------------------|----------------------|----------------------|
| Rock type | Hbl-Basanite | Hbl-Basanite | Hbl alk basalt | Hbl-Basanite | Hbl-Basanite | Hbl-phont. | Hbl-Basanite | Hbl-Basanite | Hbl-Basanite | Hbl-Basanite | Hbl-Basanite | Hbl-Basanite |
| Location | Danzwiesen | Biebertal | Kl Ziegenk. | Lothar Mai Hüt. | Kl. Grubenh. | Sandberg | S Teufelsberg | Hauk | W Sparbrod | S Gersfeld | Todtenköpfchen | Wachtküppel |
| Latitude (°N) | 50.55 | 50.54 | 50.56 | 50.56 | 50.58 | 50.59 | 50.42 | 50.42 | 50.44 | 50.44 | 50.45 | 50.47 |
| Longitude (°E) | 9.91 | 9.89 | 9.89 | 9.90 | 9.92 | 9.89 | 9.95 | 9.84 | 9.90 | 9.90 | 9.89 | 9.89 |
| SiO ₂ | 43.7 | 42.1 | 43.1 | 41.8 | 42.7 | 49.6 | 40.2 | 43.1 | 43.1 | 43.9 | 42.0 | 46.4 |
| TiO ₂ | 3.26 | 3.41 | 3.41 | 3.47 | 3.42 | 2.04 | 3.34 | 3.29 | 3.30 | 3.05 | 3.10 | 2.82 |
| Al ₂ O ₃ | 14.1 | 13.0 | 14.0 | 13.1 | 14.3 | 17.5 | 12.7 | 15.1 | 13.4 | 13.2 | 12.6 | 16.7 |
| FeO ^T | 11.9 | 13.2 | 12.4 | 13.2 | 12.7 | 9.10 | 12.3 | 12.7 | 13.3 | 12.4 | 12.5 | 12.0 |
| MnO | 0.16 | 0.17 | 0.20 | 0.18 | 0.20 | 0.27 | 0.18 | 0.22 | 0.18 | 0.19 | 0.18 | 0.24 |
| MgO | 9.48 | 10.1 | 6.86 | 10.6 | 7.14 | 2.40 | 8.73 | 7.30 | 8.55 | 10.6 | 11.3 | 3.98 |
| CaO | 11.6 | 11.8 | 10.3 | 11.9 | 11.4 | 7.58 | 12.6 | 11.1 | 11.7 | 11.7 | 12.1 | 9.52 |
| Na ₂ O | 3.16 | 2.81 | 3.24 | 2.68 | 3.74 | 5.22 | 2.91 | 2.25 | 3.18 | 3.12 | 2.52 | 4.42 |
| K ₂ O | 0.89 | 0.51 | 1.21 | 0.46 | 0.79 | 3.21 | 0.85 | 1.82 | 1.32 | 0.80 | 0.79 | 1.74 |
| P ₂ O ₅ | 0.44 | 0.49 | 0.59 | 0.49 | 0.67 | 0.85 | 0.56 | 0.67 | 0.64 | 0.48 | 0.49 | 1.11 |
| H ₂ O ^f | 2.46 | 3.20 | 6.05 | 2.89 | 3.01 | 2.15 | 6.62 | 3.39 | 1.78 | 1.77 | 2.01 | 1.60 |
| Total | 101.1 | 100.8 | 101.3 | 100.6 | 100.1 | 100.2 | 101.2 | 100.9 | 100.6 | 101.3 | 99.5 | 100.5 |
| Sc | 38 | 36 | 30 | 34 | 29 | 8 | 38 | 28 | 38 | 33 | 36 | 13 |
| V | 325 | 336 | 333 | 378 | 324 | 106 | 322 | 307 | 307 | 316 | 327 | 207 |
| Cr | 320 | 260 | 190 | 319 | 82.7 | d.l | 250 | 120 | 250 | 371 | 435 | d.l |
| Co | 51.0 | 58.0 | 47.0 | 57.6 | 43.9 | 13.0 | 51.0 | 45.0 | 49.0 | 53.3 | 56.9 | 25.0 |
| Ni | 150 | 130 | 70.0 | 134 | 50.2 | d.l | 140 | 70.0 | 100 | 174 | 177 | d.l |
| Cu | 50.0 | 50.0 | 80.0 | 42.8 | 45.8 | d.l | 110 | 40.0 | 80.0 | 65.8 | 59.8 | 20.0 |
| Zn | 70.0 | 100 | 130 | 95.9 | 107 | 140 | 100 | 100 | 90.0 | 98.5 | 93.2 | 160 |
| Ga | 20.0 | 20.0 | 21.0 | 19.9 | 22.3 | 25.0 | 20.0 | 23.0 | 23.0 | 19.6 | 19.1 | 25.0 |
| Rb | 39.0 | 30.0 | 47.0 | 24.9 | 74.7 | 69.0 | 25.0 | 48.0 | 53.0 | 57.8 | 32.3 | 68.0 |
| Sr | 720 | 708 | 529 | 712 | 928 | 2380 | 831 | 2090 | 706 | 835 | 936 | 1100 |
| Y | 21.0 | 23.0 | 27.0 | 22.8 | 28.2 | 40.0 | 22.0 | 27.0 | 26.0 | 24.0 | 23.0 | 36.0 |
| Zr | 207 | 225 | 304 | 224 | 301 | 484 | 224 | 297 | 334 | 246 | 232 | 409 |
| Nb | 57.0 | 64.0 | 80.0 | 59.2 | 81.3 | 128.0 | 59.0 | 78.0 | 65.0 | 67.2 | 62.5 | 102 |
| Cs | d.l | d.l | d.l | 0.383 | 3.21 | 1.10 | 3.60 | 0.700 | 0.500 | 0.428 | 0.399 | 0.900 |
| Ba | 540 | 610 | 583 | 505 | 710 | 1930 | 562 | 1090 | 562 | 651 | 632 | 841 |
| La | 45.0 | 47.2 | 52.8 | 38.8 | 57.5 | 106 | 46.4 | 59.6 | 48.6 | 52.3 | 43.4 | 83.1 |
| Ce | 87.7 | 95.4 | 109 | 82.2 | 118 | 215 | 94.1 | 119 | 96.8 | 103 | 89.5 | 174 |
| Pr | 10.3 | 10.8 | 12.5 | 9.90 | 14.1 | 24.9 | 11.3 | 14.2 | 11.6 | 11.9 | 10.7 | 19.7 |
| Nd | 40.6 | 39.9 | 46.9 | 40.3 | 55.4 | 94.3 | 44.4 | 54.6 | 45.9 | 45.6 | 42.1 | 72.6 |
| Sm | 8.30 | 7.80 | 9.10 | 7.95 | 10.2 | 17.3 | 9.00 | 10.5 | 9.50 | 8.35 | 8.09 | 13.0 |
| Eu | 2.50 | 2.31 | 2.63 | 2.44 | 3.04 | 5.25 | 2.71 | 3.13 | 2.69 | 2.51 | 2.46 | 3.79 |
| Gd | 7.10 | 6.50 | 7.40 | 6.92 | 8.55 | 13.30 | 7.60 | 8.70 | 8.20 | 7.12 | 7.01 | 10.20 |
| Tb | 1.00 | 0.900 | 1.10 | 0.953 | 1.16 | 1.80 | 1.00 | 1.20 | 1.10 | 0.973 | 0.960 | 1.40 |
| Dy | 5.00 | 4.60 | 5.40 | 4.93 | 6.02 | 9.10 | 5.30 | 6.10 | 5.90 | 5.07 | 4.97 | 7.20 |
| Ho | 0.900 | 0.800 | 0.900 | 0.859 | 1.06 | 1.60 | 0.900 | 1.10 | 1.00 | 0.898 | 0.867 | 1.30 |
| Er | 2.30 | 2.10 | 2.40 | 2.05 | 2.60 | 4.10 | 2.30 | 2.80 | 2.70 | 2.22 | 2.10 | 3.40 |
| Tm | 0.300 | 0.270 | 0.330 | 0.266 | 0.342 | 0.540 | 0.300 | 0.370 | 0.350 | 0.293 | 0.274 | 0.450 |
| Yb | 1.80 | 1.60 | 2.00 | 1.58 | 2.09 | 3.20 | 1.80 | 2.20 | 2.20 | 1.77 | 1.62 | 2.70 |
| Lu | 0.270 | 0.220 | 0.290 | 0.218 | 0.291 | 0.490 | 0.270 | 0.340 | 0.330 | 0.249 | 0.225 | 0.410 |
| Hf | 5.10 | 4.80 | 6.60 | 5.13 | 6.73 | 9.60 | 5.50 | 6.90 | 7.80 | 5.51 | 5.18 | 8.50 |
| Ta | 4.00 | 4.00 | 5.10 | 3.42 | 4.69 | 9.70 | 4.20 | 5.40 | 4.90 | 3.87 | 3.56 | 6.80 |
| Pb | 5.00 | 6.00 | d.l | 2.60 | 2.11 | 11.0 | 7.00 | 7.00 | 5.00 | 3.57 | 2.72 | 6.00 |
| Th | 5.00 | 5.00 | 5.70 | 4.19 | 6.26 | 9.80 | 4.90 | 6.80 | 6.40 | 5.60 | 4.49 | 8.10 |
| U | 1.40 | 1.40 | 1.60 | 1.09 | 1.65 | 2.70 | 1.40 | 1.70 | 1.90 | 1.51 | 1.26 | 2.40 |

Table A.1: (continued)

| Sample | Rh10/13 ^b | Rh10/14 ^c | Rh10/15 ^b | Rh10/17 ^b | Rh10/20 ^c | Rh10/21 ^b | Rh10/22 ^c | Rh10/23 ^b | Rh10/25 ^c | Rh10/26 ^b | Rh10/27 ^c | Rh10/28 ^c |
|--------------------------------|----------------------|----------------------|----------------------|----------------------|----------------------|----------------------|----------------------|----------------------|----------------------|----------------------|----------------------|----------------------|
| Rock type | Hbl-Basanite | Hbl-Basanite | Hbl-Basanite | Hbl-trachyb. | Hbl-Basanite | Hbl-Basanite | Hbl alk basalt | Hbl alk basalt | Hbl alk basalt | Hbl-Basanite | Hbl-Basanite | Hbl-Basanite |
| Location | Kühküppel | Billstein | Schwarzenhauk | Wasserkuppe | Mosbach | R. Eberstein | Wittges | Egelmes | Fohlenweide | Schröcksküppel | Schwarzehauk | Alter Berg |
| Latitude (°N) | 50.48 | 50.50 | 50.50 | 50.50 | 50.45 | 50.54 | 50.59 | 50.59 | 50.56 | 50.61 | 50.62 | 50.63 |
| Longitude (°E) | 9.87 | 9.87 | 9.89 | 9.93 | 9.95 | 9.97 | 9.88 | 9.85 | 9.86 | 9.89 | 9.87 | 9.88 |
| SiO ₂ | 41.2 | 40.9 | 42.4 | 47.3 | 39.1 | 44.4 | 44.7 | 43.6 | 43.1 | 43.2 | 40.2 | 41.5 |
| TiO ₂ | 3.43 | 3.38 | 3.30 | 2.11 | 3.65 | 3.12 | 3.03 | 3.68 | 3.12 | 3.29 | 3.70 | 3.52 |
| Al ₂ O ₃ | 14.0 | 13.3 | 14.0 | 14.7 | 13.2 | 14.8 | 15.0 | 15.1 | 13.3 | 14.6 | 13.4 | 14.0 |
| FeO ^T | 13.0 | 12.9 | 13.7 | 10.7 | 12.6 | 13.7 | 12.0 | 11.2 | 11.6 | 12.4 | 12.8 | 12.5 |
| MnO | 0.20 | 0.18 | 0.24 | 0.21 | 0.17 | 0.26 | 0.22 | 0.14 | 0.18 | 0.20 | 0.16 | 0.17 |
| MgO | 7.10 | 8.94 | 6.36 | 7.49 | 7.90 | 4.90 | 5.72 | 6.49 | 7.22 | 7.34 | 10.4 | 7.31 |
| CaO | 12.2 | 12.0 | 10.8 | 9.10 | 12.4 | 10.3 | 10.4 | 11.6 | 12.0 | 10.7 | 11.5 | 13.1 |
| Na ₂ O | 2.43 | 1.46 | 2.93 | 3.84 | 2.60 | 3.59 | 3.56 | 2.20 | 2.36 | 2.99 | 2.33 | 3.16 |
| K ₂ O | 1.35 | 2.04 | 2.13 | 1.69 | 0.65 | 2.14 | 1.19 | 1.46 | 1.18 | 2.29 | 1.27 | 0.67 |
| P ₂ O ₅ | 0.68 | 0.61 | 1.02 | 0.58 | 0.53 | 0.98 | 0.75 | 0.63 | 0.62 | 0.72 | 0.45 | 0.52 |
| H ₂ O ^f | 4.19 | 5.06 | 3.03 | 1.79 | 7.78 | 1.78 | 3.61 | 4.24 | 3.97 | 2.17 | 2.41 | 4.17 |
| Total | 99.9 | 100.8 | 99.9 | 99.5 | 100.6 | 100.0 | 100.1 | 100.5 | 98.8 | 99.9 | 98.8 | 100.6 |
| Sc | 31 | 30 | 23 | 15 | 42 | 19 | 24 | 30 | 32 | 32 | 40 | 33 |
| V | 318 | 336 | 291 | 196 | 361 | 277 | 275 | 353 | 313 | 313 | 380 | 358 |
| Cr | 150 | 212 | 90.0 | 290 | 173 | 30.0 | 140 | 73.5 | 220 | 130 | 190 | 184 |
| Co | 51.0 | 48.8 | 42.0 | 41.0 | 51.9 | 36.0 | 37.0 | 43.9 | 52.2 | 46.0 | 55.9 | 49.9 |
| Ni | 100 | 85.4 | 60.0 | 150 | 83.7 | 40.0 | 65.2 | 47.7 | 111 | 90.0 | 87.4 | 102 |
| Cu | 90.0 | 54.9 | 40.0 | 40.0 | 71.3 | 30.0 | 49.2 | 54.0 | 84.5 | 60.0 | 73.3 | 84.1 |
| Zn | 110 | 98.6 | 160 | 120 | 90 | 130 | 118 | 103 | 106 | 100 | 90.0 | 94.8 |
| Ga | 22.0 | 20.5 | 25.0 | 22.0 | 19.3 | 27.0 | 22.8 | 22.1 | 20.6 | 24.0 | 19.8 | 20.8 |
| Rb | 76.0 | 86.2 | 67.0 | 87.0 | 36.2 | 43.0 | 48.4 | 40.4 | 69.2 | 53.0 | 25.4 | 74.2 |
| Sr | 989 | 802 | 999 | 892 | 807 | 1160 | 976 | 908 | 1718 | 967 | 719 | 858 |
| Y | 25.0 | 25.5 | 34.0 | 25.0 | 23.2 | 34.0 | 31.1 | 28.8 | 28.5 | 28.0 | 22.8 | 25.1 |
| Zr | 271 | 258 | 421 | 285 | 209 | 413 | 309 | 264 | 278 | 312 | 207 | 248 |
| Nb | 76.0 | 66.8 | 105 | 91.0 | 56.5 | 118 | 77.6 | 70.2 | 72.0 | 88.0 | 57.1 | 64.4 |
| Cs | 6.10 | 0.774 | 0.600 | 0.900 | 0.389 | 1.20 | 2.14 | 1.16 | 4.83 | 0.600 | 0.435 | 4.16 |
| Ba | 782 | 705 | 904 | 792 | 634 | 899 | 739 | 727 | 918 | 755 | 548 | 640 |
| La | 57.2 | 48.0 | 81.6 | 61.3 | 39.6 | 87.8 | 58.8 | 52.2 | 55.6 | 65.4 | 38.6 | 46.0 |
| Ce | 113 | 101 | 168 | 113 | 85.3 | 172 | 122 | 108 | 109 | 128 | 82.5 | 96.8 |
| Pr | 13.5 | 12.2 | 18.7 | 12.1 | 10.5 | 19.9 | 14.7 | 13.3 | 13.4 | 15.1 | 10.2 | 11.7 |
| Nd | 52.4 | 48.9 | 67.7 | 44.8 | 43.0 | 75.1 | 58.0 | 53.4 | 52.4 | 57.8 | 41.7 | 46.5 |
| Sm | 10.3 | 9.16 | 12.2 | 8.60 | 8.33 | 13.9 | 10.8 | 10.1 | 9.66 | 11.1 | 8.18 | 8.84 |
| Eu | 3.02 | 2.76 | 3.53 | 2.58 | 2.53 | 4.02 | 3.21 | 3.01 | 2.88 | 3.29 | 2.50 | 2.67 |
| Gd | 8.60 | 7.78 | 9.50 | 7.30 | 7.17 | 11.20 | 9.10 | 8.59 | 8.26 | 9.20 | 7.07 | 7.57 |
| Tb | 1.20 | 1.06 | 1.40 | 1.10 | 0.98 | 1.50 | 1.25 | 1.18 | 1.13 | 1.30 | 0.962 | 1.03 |
| Dy | 5.90 | 5.46 | 6.80 | 5.50 | 5.05 | 7.80 | 6.50 | 6.10 | 5.88 | 6.40 | 4.98 | 5.36 |
| Ho | 1.00 | 0.953 | 1.20 | 1.00 | 0.882 | 1.40 | 1.15 | 1.07 | 1.04 | 1.10 | 0.865 | 0.940 |
| Er | 2.60 | 2.34 | 3.10 | 2.60 | 2.12 | 3.60 | 2.86 | 2.60 | 2.56 | 2.90 | 2.09 | 2.29 |
| Tm | 0.350 | 0.304 | 0.410 | 0.360 | 0.271 | 0.490 | 0.376 | 0.338 | 0.334 | 0.390 | 0.268 | 0.297 |
| Yb | 2.00 | 1.82 | 2.60 | 2.30 | 1.61 | 3.00 | 2.31 | 2.04 | 2.03 | 2.30 | 1.60 | 1.79 |
| Lu | 0.300 | 0.254 | 0.370 | 0.350 | 0.223 | 0.450 | 0.320 | 0.284 | 0.281 | 0.360 | 0.221 | 0.248 |
| Hf | 6.50 | 5.86 | 8.90 | 6.30 | 5.00 | 9.10 | 6.62 | 6.18 | 6.23 | 7.30 | 5.03 | 5.70 |
| Ta | 5.30 | 3.90 | 7.00 | 6.20 | 3.34 | 8.00 | 4.46 | 4.10 | 4.19 | 6.10 | 3.36 | 3.72 |
| Pb | 8.00 | 3.19 | 6.00 | 9.00 | 2.21 | 10.0 | 4.14 | 2.59 | 4.34 | 7.00 | 2.14 | 2.65 |
| Th | 6.40 | 4.93 | 8.40 | 9.30 | 3.89 | 10.6 | 6.32 | 5.57 | 5.82 | 7.40 | 3.93 | 4.87 |
| U | 1.70 | 1.33 | 2.60 | 2.30 | 0.978 | 2.80 | 1.69 | 1.89 | 1.64 | 1.90 | 1.07 | 1.22 |

Table A.1: (continued)

| Sample | Rh10/29 ^b | Rh10/30 ^b | Rh10/31 ^b | Rh10/32 ^b | Rh10/33 ^c | Rh10/34 ^b | Rh10/35 ^b | Rh10/36 ^b | Rh10/38 ^b | 27377 ^c | Rh10/16 ^a | Rh10/18 ^a |
|--------------------------------|----------------------|----------------------|----------------------|----------------------|----------------------|----------------------|----------------------|----------------------|----------------------|--------------------|----------------------|----------------------|
| Rock type | Hbl-Basanite | Hbl-Basanite | Hbl alk basalt | Hbl-Basanite | Hbl-Basanite | Hbl-Basanite | Hbl alk basalt | Hbl-Basanite | Hbl-Basanite | Hbl-basanite | Basanite | Basanite |
| Location | Spahler Berg | Pietzelsberg | Teufelsberg | Kl. Ganskuppe | Ransbach | Tannenküppel | Maulküppel | Eselsbrunn | Sternsküppel | Sternsküppel | Heidigsküppel | Guckaisee |
| Latitude (°N) | 50.63 | 50.66 | 50.68 | 50.68 | 50.82 | 50.63 | 50.53 | 50.53 | 50.53 | 50.53 | 50.51 | 50.49 |
| Longitude (°E) | 9.89 | 9.90 | 9.89 | 9.87 | 9.87 | 9.95 | 9.88 | 9.89 | 9.90 | | 9.90 | 9.92 |
| SiO ₂ | 43.4 | 43.8 | 44.1 | 42.7 | 41.5 | 41.1 | 44.2 | 42.5 | 43.0 | 42.6 | 42.4 | 42.1 |
| TiO ₂ | 3.51 | 3.34 | 3.23 | 3.48 | 3.56 | 3.89 | 2.27 | 3.69 | 3.33 | 3.29 | 2.90 | 3.04 |
| Al ₂ O ₃ | 15.2 | 15.4 | 14.5 | 14.7 | 13.8 | 14.4 | 14.1 | 14.8 | 14.9 | 14.5 | 13.4 | 12.5 |
| FeO ^T | 12.5 | 13.6 | 12.5 | 12.8 | 13.3 | 13.1 | 10.7 | 12.4 | 12.6 | 10.9 | 11.9 | 12.1 |
| MnO | 0.19 | 0.22 | 0.19 | 0.21 | 0.19 | 0.26 | 0.20 | 0.22 | 0.18 | 0.18 | 0.19 | 0.18 |
| MgO | 5.94 | 6.11 | 6.59 | 7.81 | 8.08 | 6.03 | 8.15 | 6.26 | 6.72 | 6.58 | 8.77 | 10.2 |
| CaO | 11.1 | 10.5 | 10.7 | 11.3 | 11.7 | 13.5 | 10.1 | 12.1 | 11.0 | 11.2 | 11.9 | 12.8 |
| Na ₂ O | 4.03 | 3.42 | 2.94 | 2.90 | 3.29 | 2.97 | 2.22 | 2.94 | 3.31 | 4.10 | 2.10 | 2.99 |
| K ₂ O | 0.70 | 0.92 | 1.12 | 1.70 | 1.01 | 0.72 | 2.35 | 0.99 | 1.11 | 0.82 | 1.65 | 0.63 |
| P ₂ O ₅ | 0.63 | 0.91 | 0.63 | 0.68 | 0.69 | 0.56 | 0.71 | 0.60 | 0.54 | 0.54 | 0.65 | 0.44 |
| H ₂ O ^f | 2.79 | 2.63 | 4.15 | 2.15 | 2.60 | 4.62 | 4.85 | 4.13 | 3.21 | 1.86 | 3.93 | 2.45 |
| Total | 100.1 | 100.7 | 100.7 | 100.5 | 99.8 | 101.2 | 99.8 | 100.7 | 99.9 | 99.1 | 99.9 | 99.4 |
| Sc | 29 | 29 | 30 | 33 | 34 | 36 | 21 | 38 | 34 | 31 | 24 | 38 |
| V | 334 | 334 | 338 | 212 | 340 | 385 | 277 | 344 | 325 | 326 | 284 | 313 |
| Cr | 100 | 130 | 140 | 250 | 139 | 130 | 140 | 100 | 170 | 186 | 381 | 439 |
| Co | 46.0 | 49.0 | 50.0 | 41.0 | 48.6 | 47.0 | 42.0 | 44.0 | 49.0 | 46.3 | 60.0 | 63.0 |
| Ni | 90.0 | 80.0 | 90.0 | 150 | 71.1 | 50.0 | 70.0 | 60.0 | 110 | 104 | 194 | 191 |
| Cu | 50.0 | 90.0 | 70.0 | 50.0 | 71.3 | 60.0 | 60.0 | 60.0 | 70.0 | 60.8 | 53.0 | 57.0 |
| Zn | 110 | 110 | 90.0 | 110 | 107 | 120 | 130 | 120 | 90.0 | 101 | 108 | 85.0 |
| Ga | 24.0 | 23.0 | 22.0 | 21.0 | 21.6 | 22.0 | 22.0 | 22.0 | 23.0 | 22.7 | 13.0 | 14.0 |
| Rb | 70.0 | 50.0 | 12.0 | 71.0 | 12.2 | 51.0 | 64.0 | 42.0 | 31.0 | 16.2 | 53.0 | 68.0 |
| Sr | 887 | 1680 | 876 | 1290 | 900 | 751 | 846 | 804 | 889 | 965 | 947 | 711 |
| Y | 26.0 | 26.0 | 25.0 | 25.0 | 28.0 | 25.0 | 28.0 | 28.0 | 25.0 | 27.0 | 27.0 | 22.0 |
| Zr | 271 | 280 | 254 | 305 | 271 | 246 | 319 | 290 | 245 | 272 | 278 | 202 |
| Nb | 70.0 | 76.0 | 72.0 | 108 | 75.0 | 65.0 | 79.0 | 75.0 | 65.0 | 73.6 | 77.0 | 51.0 |
| Cs | 0.600 | 0.600 | 1.70 | 1.20 | 1.68 | d.l | 0.800 | d.l | 1.50 | 0.546 | n.a | n.a |
| Ba | 661 | 825 | 665 | 946 | 679 | 626 | 704 | 728 | 673 | 640 | 767 | 562 |
| La | 52.8 | 59.0 | 53.7 | 79.4 | 54.4 | 47.2 | 63.5 | 60.2 | 48.6 | 50.9 | 77.0 | 51.0 |
| Ce | 106 | 117 | 110 | 139 | 112 | 101 | 130 | 123 | 96.0 | 112 | 127 | 85.0 |
| Pr | 12.8 | 14.0 | 13.4 | 14.9 | 13.8 | 11.8 | 14.4 | 13.9 | 11.5 | 13.0 | n.a | n.a |
| Nd | 50.0 | 54.4 | 52.6 | 53.5 | 54.7 | 45.1 | 52.4 | 51.4 | 45.8 | 48.3 | 50.0 | 35.0 |
| Sm | 10.1 | 10.7 | 10.5 | 10.0 | 10.2 | 8.90 | 9.80 | 9.70 | 9.40 | 9.30 | n.a | n.a |
| Eu | 3.03 | 3.16 | 3.13 | 2.93 | 3.05 | 2.72 | 2.91 | 2.79 | 2.82 | 2.53 | n.a | n.a |
| Gd | 8.60 | 8.90 | 8.80 | 8.20 | 8.58 | 7.50 | 7.90 | 8.00 | 8.20 | 7.98 | n.a | n.a |
| Tb | 1.20 | 1.20 | 1.20 | 1.10 | 1.16 | 1.10 | 1.10 | 1.10 | 1.10 | 1.12 | n.a | n.a |
| Dy | 6.20 | 6.10 | 6.10 | 5.70 | 6.01 | 5.30 | 5.80 | 5.50 | 5.70 | 5.66 | n.a | n.a |
| Ho | 1.10 | 1.10 | 1.00 | 1.00 | 1.05 | 0.900 | 1.00 | 1.00 | 1.00 | 1.03 | n.a | n.a |
| Er | 2.80 | 2.80 | 2.70 | 2.70 | 2.56 | 2.30 | 2.60 | 2.50 | 2.60 | 2.57 | n.a | n.a |
| Tm | 0.370 | 0.370 | 0.350 | 0.360 | 0.331 | 0.300 | 0.350 | 0.340 | 0.340 | 0.333 | n.a | n.a |
| Yb | 2.30 | 2.20 | 2.10 | 2.20 | 1.99 | 1.80 | 2.20 | 2.00 | 2.00 | 2.05 | n.a | n.a |
| Lu | 0.340 | 0.340 | 0.310 | 0.340 | 0.280 | 0.250 | 0.320 | 0.290 | 0.310 | 0.283 | n.a | n.a |
| Hf | 6.50 | 6.60 | 6.30 | 6.60 | 6.22 | 5.60 | 6.80 | 6.40 | 5.80 | 6.26 | n.a | n.a |
| Ta | 4.80 | 5.30 | 5.30 | 6.70 | 4.59 | 4.20 | 5.20 | 4.90 | 4.50 | 3.78 | n.a | n.a |
| Pb | 5.00 | 8.00 | 8.00 | 10.0 | 3.09 | d.l | 8.00 | 5.00 | 6.00 | 2.88 | 2.00 | 9.00 |
| Th | 5.70 | 6.70 | 5.70 | 10.0 | 5.43 | 4.70 | 6.50 | 6.00 | 5.40 | 4.62 | 16.0 | 12.0 |
| U | 1.40 | 1.70 | 1.50 | 2.30 | 1.46 | 1.40 | 1.90 | 1.70 | 1.90 | 1.83 | d.l | 1.00 |

Table A.1: (continued)

| Sample | Rh10/19 ^a | Rh10/24 ^a | 28327 ^c | 27797 ^c | 27557 ^c | 27403 ^c | 26199 ^c | 27370 ^c | 27401 ^c | 27611 ^c | 28223 ^c | 28317 ^c |
|--------------------------------|----------------------|----------------------|--------------------|--------------------|--------------------|--------------------|--------------------|--------------------|--------------------|--------------------|--------------------|--------------------|
| Rock type | Basanite | Basanite | Basanite | Basanite | Basanite | Basanite | Basanite | Basanite | Basanite | Alk. basalt | Alk. basalt | Alk. basalt |
| Location | Glaswald | Hofbieber | Pferdskopf | Wasserkuppe | Königstein | Bubenbäder St. | E Wickers | Silberhauck | Biebertal | Abtsroder Kup. | Schafstein | Gr. Grubenhauck |
| Latitude (°N) | 50.48 | 50.59 | | | | | | | | | | |
| Longitude (°E) | 9.94 | 9.85 | | | | | | | | | | |
| SiO ₂ | 41.5 | 43.0 | 40.7 | 42.5 | 41.5 | 42.8 | 41.9 | 42.7 | 43.1 | 49.7 | 48.9 | 44.9 |
| TiO ₂ | 3.13 | 3.20 | 2.64 | 2.44 | 2.40 | 2.14 | 2.66 | 3.73 | 3.26 | 2.06 | 2.08 | 3.19 |
| Al ₂ O ₃ | 12.3 | 13.1 | 11.4 | 11.9 | 11.2 | 10.1 | 12.3 | 15.4 | 13.7 | 14.2 | 14.4 | 15.5 |
| FeO ^T | 12.3 | 12.6 | 11.9 | 11.1 | 10.8 | 10.5 | 11.1 | 11.9 | 10.8 | 10.4 | 10.3 | 11.5 |
| MnO | 0.17 | 0.18 | 0.21 | 0.20 | 0.18 | 0.20 | 0.21 | 0.20 | 0.18 | 0.17 | 0.17 | 0.19 |
| MgO | 12.0 | 9.59 | 13.2 | 13.0 | 15.0 | 18.4 | 11.0 | 6.24 | 10.5 | 8.29 | 7.53 | 7.35 |
| CaO | 12.4 | 11.7 | 11.8 | 11.2 | 11.0 | 10.1 | 12.3 | 11.4 | 11.2 | 9.02 | 9.24 | 10.6 |
| Na ₂ O | 2.42 | 2.48 | 3.77 | 3.71 | 2.85 | 2.28 | 3.91 | 3.10 | 2.22 | 3.59 | 3.22 | 2.49 |
| K ₂ O | 0.89 | 0.78 | 1.49 | 0.74 | 1.60 | 1.22 | 2.08 | 1.81 | 1.81 | 1.13 | 1.13 | 1.51 |
| P ₂ O ₅ | 0.41 | 0.52 | 1.01 | 0.80 | 0.60 | 0.66 | 0.87 | 0.85 | 0.54 | 0.48 | 0.43 | 0.48 |
| H ₂ O ^f | 1.59 | 3.24 | 0.97 | 0.94 | 1.26 | 1.23 | 1.21 | 2.22 | 1.25 | 0.69 | 1.58 | 0.77 |
| Total | 99.1 | 100.4 | 99.7 | 99.0 | 98.9 | 100.2 | 100.3 | 100.2 | 99.7 | 100.1 | 99.6 | 100.4 |
| Sc | 34 | 28 | 32 | 31 | 30 | 23 | 33 | 31 | 33 | 27 | 26 | 35 |
| V | 324 | 392 | 252 | 234 | 250 | 209 | 273 | 384 | 326 | 189 | 187 | 303 |
| Cr | 443 | 145 | 535 | 640 | 642 | 834 | 464 | 16.7 | 304 | 327 | 232 | 75.6 |
| Co | 67.0 | 46.6 | 57.2 | 56.4 | 61.3 | 62.8 | 51.1 | 44.0 | 49.6 | 43.4 | 45.2 | 46.5 |
| Ni | 190 | 55.7 | 340 | 367 | 426 | 716 | 212 | 24.8 | 161 | 198 | 151 | 58.8 |
| Cu | 43.0 | 55.3 | 55.2 | 56.4 | 66.0 | 51.6 | 58.7 | 46.8 | 57.1 | 43.1 | 48.2 | 37.4 |
| Zn | 82.0 | 97.3 | 118 | 118 | 105 | 85.8 | 113 | 125 | 90.2 | 123 | 114 | 111 |
| Ga | 13.0 | 21.2 | 20.2 | 20.1 | 17.8 | 15.3 | 20.9 | 25.0 | 20.2 | 21.1 | 20.5 | 22.8 |
| Rb | 47.0 | 54.5 | 50.8 | 68.1 | 78.9 | 21.4 | 61.3 | 68.3 | 36.2 | 33.6 | 23.7 | 28.6 |
| Sr | 656 | 811 | 1025 | 978 | 819 | 779 | 1043 | 1237 | 824 | 705 | 832 | 701 |
| Y | 20.0 | 25.0 | 29.1 | 28.7 | 22.4 | 21.1 | 28.6 | 29.5 | 24.1 | 24.4 | 21.9 | 25.3 |
| Zr | 175 | 235 | 301 | 288 | 196 | 233 | 308 | 289 | 245 | 171 | 145 | 219 |
| Nb | 49.0 | 61.1 | 103 | 97.1 | 76.5 | 83.1 | 115 | 74.6 | 69.7 | 46.8 | 45.9 | 48.5 |
| Cs | n.a | 0.525 | 0.586 | 0.569 | 0.655 | 0.363 | 0.711 | 0.667 | 0.319 | 0.310 | 0.162 | 0.307 |
| Ba | 492 | 616 | 772 | 780 | 746 | 535 | 916 | 686 | 581 | 522 | 609 | 469 |
| La | 50.0 | 43.7 | 79.5 | 76.2 | 55.8 | 58.1 | 88.1 | 56.9 | 51.0 | 46.2 | 36.4 | 36.3 |
| Ce | 87.0 | 92.2 | 153 | 145 | 105 | 119 | 158 | 118 | 112 | 86.1 | 69.0 | 75.1 |
| Pr | n.a | 11.4 | 17.9 | 16.9 | 12.2 | 12.9 | 18.1 | 14.7 | 12.7 | 9.90 | 8.20 | 9.50 |
| Nd | 36.0 | 46.1 | 65.1 | 61.0 | 45.2 | 45.3 | 64.7 | 57.0 | 46.2 | 37.7 | 31.4 | 37.7 |
| Sm | n.a | 8.99 | 11.0 | 10.4 | 8.12 | 7.88 | 10.8 | 10.6 | 8.61 | 7.50 | 6.31 | 7.76 |
| Eu | n.a | 2.71 | 2.95 | 2.77 | 2.16 | 2.05 | 2.81 | 2.91 | 2.30 | 2.20 | 1.90 | 2.30 |
| Gd | n.a | 7.73 | 8.84 | 8.25 | 6.76 | 6.50 | 8.64 | 8.69 | 7.29 | 6.55 | 5.70 | 6.85 |
| Tb | n.a | 1.05 | 1.22 | 1.16 | 0.942 | 0.893 | 1.19 | 1.22 | 1.01 | 0.956 | 0.831 | 0.993 |
| Dy | n.a | 5.45 | 6.15 | 5.92 | 4.80 | 4.46 | 6.05 | 6.18 | 5.08 | 5.05 | 4.45 | 5.26 |
| Ho | n.a | 0.943 | 1.07 | 1.03 | 0.818 | 0.813 | 1.04 | 1.07 | 0.927 | 0.888 | 0.780 | 0.915 |
| Er | n.a | 2.28 | 2.61 | 2.57 | 2.02 | 2.06 | 2.57 | 2.64 | 2.32 | 2.23 | 1.93 | 2.29 |
| Tm | n.a | 0.293 | 0.340 | 0.335 | 0.258 | 0.268 | 0.335 | 0.345 | 0.302 | 0.297 | 0.256 | 0.296 |
| Yb | n.a | 1.75 | 2.06 | 2.07 | 1.57 | 1.66 | 2.05 | 2.12 | 1.85 | 1.85 | 1.56 | 1.82 |
| Lu | n.a | 0.240 | 0.281 | 0.289 | 0.213 | 0.232 | 0.281 | 0.289 | 0.258 | 0.252 | 0.217 | 0.250 |
| Hf | n.a | 5.65 | 6.53 | 6.23 | 4.36 | 5.30 | 6.56 | 6.76 | 5.99 | 3.91 | 3.36 | 5.06 |
| Ta | n.a | 3.56 | 5.14 | 4.84 | 3.86 | 4.21 | 5.66 | 4.03 | 3.68 | 2.30 | 2.42 | 2.52 |
| Pb | d.l. | 2.79 | 9.11 | 4.20 | 6.22 | 3.12 | 5.29 | 3.76 | 2.92 | 2.66 | 2.47 | 2.46 |
| Th | 1.00 | 4.57 | 8.77 | 7.50 | 5.96 | 5.89 | 10.6 | 5.96 | 4.82 | 4.52 | 3.33 | 3.82 |
| U | d.l. | 1.20 | 2.39 | 1.97 | 1.59 | 1.69 | 2.87 | 1.76 | 1.47 | 0.813 | 0.797 | 1.00 |

Table A.1: (continued)

| Sample | 26450 ^c | 26383 ^c | 28343 ^c | 27606 ^c | 27799 ^c | JGb-1 ^a | JGb-1 ^a | JGb-1 ^a | |
|--------------------------------|--------------------|--------------------|--------------------|--------------------|--------------------|--------------------|------------------------------|---------------------|-------------------------------|
| Rock type | Alk. basalt | Alk. basalt | Alk. basalt | Trachybasalt | Trachybasalt | rec. value | this study | this study | |
| Location | Gr. Grubenh. | Kl. Grubenh. | Schackau | Wasserkuppe | Wasserkuppe | | n=18 | 2 σ | |
| Latitude (°N) | | | | | | | | | |
| Longitude (°E) | | | | | | | | | |
| SiO ₂ | 44.2 | 43.4 | 43.5 | 47.6 | 47.5 | 43.4 | 44.0 | 0.64 | |
| TiO ₂ | 3.12 | 3.10 | 3.41 | 2.10 | 2.06 | 1.62 | 1.61 | 0.02 | |
| Al ₂ O ₃ | 15.1 | 14.9 | 14.4 | 14.9 | 14.9 | 17.7 | 17.7 | 0.20 | |
| FeO ^T | 11.3 | 11.3 | 12.6 | 9.4 | 9.3 | 15.2 | 15.3 | 0.25 | |
| MnO | 0.20 | 0.23 | 0.24 | 0.18 | 0.17 | 0.17 | 0.19 | 0.00 | |
| MgO | 7.07 | 5.02 | 4.75 | 7.26 | 7.29 | 7.83 | 7.95 | 0.26 | |
| CaO | 10.9 | 10.2 | 10.8 | 8.92 | 9.21 | 12.0 | 11.9 | 0.14 | |
| Na ₂ O | 3.10 | 4.68 | 3.41 | 4.41 | 4.28 | 1.23 | 1.28 | 0.06 | |
| K ₂ O | 1.49 | 1.54 | 0.83 | 1.90 | 1.72 | 0.24 | 0.23 | 0.02 | |
| P ₂ O ₅ | 0.46 | 0.92 | 1.05 | 0.55 | 0.56 | 0.05 | 0.06 | 0.01 | |
| H ₂ O ^f | 0.65 | 1.73 | 3.38 | 1.18 | 2.05 | 1.27 | 0.85 | 0.00 | |
| Total | 100.0 | 99.0 | 99.7 | 99.0 | 99.7 | 100.7 | 101.4 | 1.3 | |
| | | | | | | BIR-1 rec. val. | BIR-1 this study (n=4) | BHVO-2 rec. val. | BHVO-2 this study (n=2) |
| Sc | 36 | 27 | 25 | 27 | 26 | 37 | 34.7 | 7.4 | |
| V | 304 | 288 | 293 | 198 | 192 | 310 | 321 | 317 | 319 |
| Cr | 82.8 | 28.2 | 12.9 | 295 | 277 | 370 | 375 | 289 | 293 |
| Co | 47.1 | 35.0 | 34.8 | 38.4 | 36.9 | 52.0 | 53.8 | 45.0 | 44.4 |
| Ni | 63.6 | 23.2 | 15.2 | 141 | 136 | 170 | 165 | 119 | 120 |
| Cu | 37.5 | 26.1 | 30.1 | 40.8 | 46.9 | 125 | 133 | 127 | 130 |
| Zn | 112 | 134 | 163 | 134 | 117 | 70.0 | 80.0 | 103 | 104 |
| Ga | 22.9 | 26.4 | 27.0 | 22.2 | 22.2 | 16.0 | 15.5 | 21.7 | 21.2 |
| Rb | 27.7 | 43.0 | 58.2 | 69.2 | 74.6 | 0.250 | < 1 | 9.20 | 9.05 |
| Sr | 688 | 1070 | 1170 | 892 | 1054 | 110 | 111 | 395 | 397 |
| Y | 25.6 | 33.4 | 36.2 | 26.3 | 26.2 | 16.0 | 15.7 | 25.5 | 25.8 |
| Zr | 218 | 381 | 404 | 289 | 300 | 15.5 | 17.8 | 174 | 171 |
| Nb | 48.2 | 101 | 109 | 87.7 | 92.3 | 0.550 | 0.700 | 18.0 | 17.8 |
| Cs | 0.273 | 0.941 | 7.48 | 0.881 | 0.905 | 0.007 | < 0.1 | 0.110 | 0.113 |
| Ba | 476 | 809 | 843 | 764 | 802 | 7.14 | < 3 | 130 | 131 |
| La | 35.8 | 78.5 | 84.3 | 60.8 | 64.7 | 0.615 | 0.360 | 15.2 | 15.1 |
| Ce | 73.5 | 156 | 168 | 110 | 115 | 1.92 | 2.25 | 38.0 | 37.5 |
| Pr | 9.40 | 18.9 | 20.3 | 12.5 | 12.8 | 0.000 | 0.103 | 5.30 | 5.33 |
| Nd | 37.5 | 70.4 | 75.7 | 44.9 | 45.8 | 0.370 | 2.47 | 25.0 | 24.5 |
| Sm | 7.76 | 12.3 | 13.3 | 8.10 | 8.10 | 1.12 | 1.12 | 6.20 | 6.09 |
| Eu | 2.30 | 3.29 | 3.61 | 2.14 | 2.11 | 0.530 | 0.531 | 2.06 | 2.07 |
| Gd | 6.96 | 9.66 | 10.64 | 6.81 | 6.81 | 1.87 | 1.91 | 6.30 | 6.14 |
| Tb | 1.00 | 1.36 | 1.48 | 0.986 | 0.993 | 0.360 | 2.28 | 0.930 | 0.941 |
| Dy | 5.29 | 6.95 | 7.51 | 5.20 | 5.21 | 2.51 | 2.57 | 5.25 | 5.33 |
| Ho | 0.922 | 1.20 | 1.30 | 0.934 | 0.927 | 0.560 | 0.590 | 0.990 | 0.984 |
| Er | 2.29 | 3.05 | 3.22 | 2.38 | 2.37 | 1.66 | 1.66 | 2.50 | 2.44 |
| Tm | 0.304 | 0.399 | 0.424 | 0.325 | 0.325 | 0.250 | 0.294 | 0.340 | 0.327 |
| Yb | 1.84 | 2.51 | 2.63 | 2.06 | 2.05 | 1.70 | 1.68 | 2.00 | 2.00 |
| Lu | 0.251 | 0.350 | 0.362 | 0.294 | 0.294 | 0.250 | 0.287 | 0.280 | 0.278 |
| Hf | 5.13 | 8.40 | 8.99 | 6.09 | 6.25 | 0.582 | 0.575 | 4.07 | 4.25 |
| Ta | 2.50 | 5.42 | 5.86 | 4.65 | 4.86 | 0.036 | 0.030 | 1.13 | 1.13 |
| Pb | 2.48 | 4.89 | 4.46 | 4.89 | 5.35 | 3.10 | < 5 | 1.70 | 1.56 |
| Th | 3.81 | 8.10 | 8.35 | 8.15 | 9.25 | 0.032 | 0.050 | 1.21 | 1.20 |
| U | 1.01 | 2.39 | 2.23 | 2.17 | 2.44 | 0.010 | 0.020 | 0.410 | 0.413 |

Table A.2: Sr, Nd, and Pb isotope compositions of Rhön lavas. Measured Sr, Nd, and Pb isotope data were recalculated using the concentrations given in Table A.1 and an age of 24 Ma. Numbers in parentheses are 2σ in-run deviations of the deviations of the measurements.

| Sample | Rock type | $^{87}\text{Sr}/$ | $^{87}\text{Sr}/$ | $^{143}\text{Nd}/$ | $^{143}\text{Nd}/$ | $^{206}\text{Pb}/$ | $^{207}\text{Pb}/$ | $^{208}\text{Pb}/$ | $^{206}\text{Pb}/$ | $^{207}\text{Pb}/$ | $^{208}\text{Pb}/$ |
|---------|----------------|------------------------|------------------------|-------------------------|-------------------------|-------------------------|-------------------------|-------------------------|-------------------------|-------------------------|-------------------------|
| | | $^{86}\text{Sr}_{(m)}$ | $^{86}\text{Sr}_{(i)}$ | $^{144}\text{Nd}_{(m)}$ | $^{144}\text{Nd}_{(i)}$ | $^{204}\text{Pb}_{(m)}$ | $^{204}\text{Pb}_{(m)}$ | $^{204}\text{Pb}_{(m)}$ | $^{204}\text{Pb}_{(i)}$ | $^{204}\text{Pb}_{(i)}$ | $^{204}\text{Pb}_{(i)}$ |
| Rh10/01 | Hbl-Basanite | 0.703623(8) | 0.70357 | 0.512827(9) | 0.51281 | 19.44 | 15.62 | 39.18 | 19.38 | 15.61 | 39.10 |
| Rh10/02 | Hbl-Basanite | 0.703593(7) | 0.70355 | 0.512824(3) | 0.51281 | | | | | | |
| Rh10/09 | Hbl-Basanite | 0.703615(7) | 0.70354 | 0.512819(5) | 0.51280 | 19.32 | 15.62 | 39.08 | 19.22 | 15.61 | 38.98 |
| Rh10/10 | Hbl-Basanite | 0.703796(6) | 0.70372 | 0.512811(6) | 0.51279 | | | | | | |
| Rh10/11 | Hbl-Basanite | 0.703738(8) | 0.70370 | 0.512852(5) | 0.51283 | 19.41 | 15.64 | 39.21 | 19.33 | 15.63 | 39.11 |
| Rh10/14 | Hbl-Basanite | 0.703857(7) | 0.70375 | 0.512845(5) | 0.51283 | 19.46 | 15.63 | 39.24 | 19.38 | 15.62 | 39.14 |
| Rh10/27 | Hbl-Basanite | 0.703499(6) | 0.70347 | 0.512821(5) | 0.51280 | 19.46 | 15.63 | 39.24 | 19.39 | 15.63 | 39.16 |
| Rh10/05 | Hbl-Basanite | 0.703592(7) | 0.70352 | 0.512806(5) | 0.51279 | 19.47 | 15.63 | 39.24 | 19.36 | 15.62 | 39.10 |
| Rh10/07 | Hbl-Basanite | 0.703694(7) | 0.70366 | 0.512808(2) | 0.51279 | 19.47 | 15.63 | 39.26 | 19.42 | 15.63 | 39.20 |
| Rh10/08 | Hbl-Basanite | 0.703870(6) | 0.70385 | 0.512816(9) | 0.51280 | | | | | | |
| Rh10/12 | Hbl-Basanite | 0.703860(7) | 0.70380 | 0.512806(5) | 0.51279 | | | | | | |
| Rh10/13 | Hbl-Basanite | 0.703667(8) | 0.70359 | 0.512826(2) | 0.51281 | 19.25 | 15.61 | 39.01 | 19.20 | 15.61 | 38.95 |
| Rh10/20 | Hbl-Basanite | 0.703639(7) | 0.70360 | 0.512823(1) | 0.51280 | 19.44 | 15.64 | 39.28 | 19.38 | 15.63 | 39.20 |
| Rh10/21 | Hbl-Basanite | 0.703613(8) | 0.70358 | 0.512809(3) | 0.51279 | 19.31 | 15.62 | 39.10 | 19.24 | 15.62 | 39.02 |
| Rh10/26 | Hbl-Basanite | 0.703645(6) | 0.70359 | 0.512811(3) | 0.51279 | | | | | | |
| Rh10/28 | Hbl-Basanite | 0.703571(7) | 0.70348 | 0.512824(2) | 0.51281 | | | | | | |
| Rh10/29 | Hbl-Basanite | 0.703791(7) | 0.70371 | 0.512812(2) | 0.51279 | 19.32 | 15.61 | 39.09 | 19.25 | 15.61 | 39.00 |
| Rh10/32 | Hbl-Basanite | 0.704074(7) | 0.70402 | 0.512800(2) | 0.51278 | | | | | | |
| Rh10/33 | Hbl-Basanite | 0.703676(6) | 0.70365 | 0.512827(5) | 0.51281 | 19.29 | 15.61 | 39.06 | 19.18 | 15.61 | 38.94 |
| Rh10/36 | Hbl-Basanite | 0.703681(7) | 0.70363 | 0.512811(3) | 0.51279 | | | | | | |
| Rh10/38 | Hbl-Basanite | 0.703672(7) | 0.70364 | 0.512830(2) | 0.51281 | 19.37 | 15.63 | 39.14 | 19.30 | 15.62 | 39.06 |
| Rh10/03 | Hbl-alk basalt | 0.703660(6) | 0.70357 | 0.512834(3) | 0.51282 | | | | | | |
| Rh10/23 | Hbl-alk basalt | 0.703706(7) | 0.70366 | 0.512807(6) | 0.51279 | 19.26 | 15.63 | 39.13 | 19.15 | 15.63 | 39.01 |
| Rh10/25 | Hbl-alk basalt | 0.704022(7) | 0.70398 | 0.512813(6) | 0.51279 | 19.24 | 15.64 | 39.08 | 19.18 | 15.63 | 39.01 |
| Rh10/35 | Hbl-alk basalt | 0.704121(7) | 0.70405 | 0.512855(4) | 0.51284 | 19.23 | 15.64 | 39.14 | 19.17 | 15.63 | 39.08 |
| Rh10/17 | Hbl-trachybas. | 0.703434(7) | 0.70334 | 0.512831(3) | 0.51281 | 19.28 | 15.62 | 39.08 | 19.22 | 15.62 | 38.99 |
| Rh10/06 | Hbl-phonot. | 0.703665(7) | 0.70364 | 0.512818(4) | 0.51280 | 19.14 | 15.61 | 38.99 | 19.08 | 15.61 | 38.92 |
| 27797 | Basanite | 0.703425(8) | 0.70336 | 0.512827(5) | 0.51282 | 19.21 | 15.62 | 39.09 | 19.10 | 15.62 | 38.95 |
| 26199 | Basanite | 0.703507(8) | 0.70345 | 0.512824(5) | 0.51279 | 19.43 | 15.62 | 39.28 | 19.29 | 15.61 | 39.12 |
| 27370b | Basanite | 0.704253(8) | 0.70420 | 0.512819(5) | 0.51279 | 19.29 | 15.62 | 39.11 | 19.18 | 15.61 | 38.99 |
| 27611 | Alk. basalt | 0.703458(8) | 0.70341 | 0.512811(5) | 0.51280 | 19.11 | 15.61 | 38.91 | 19.03 | 15.61 | 38.78 |
| 26450 | Alk. basalt | 0.703730(8) | 0.70369 | 0.512852(5) | 0.51281 | 19.38 | 15.61 | 39.21 | 19.29 | 15.61 | 39.09 |
| 26383 | Alk. basalt | 0.703682(8) | 0.70364 | | | 19.37 | 15.61 | 39.15 | 19.25 | 15.60 | 39.01 |

A Appendix

Table A.3: Compositions and parameters used for the EC-AFC model calculations (Spera & Bohrson, 2001).

| | | | | |
|--|----------|----------|---------------------------------|-----------------------------------|
| Magma liquidus temperature | 1250 | °C | | |
| Magma temperature t_{m0} | 1250 | °C | | |
| Assimilant liquidus temperature | 980 | °C | | |
| Country rock temperature t_{a0} | 900 | °C | | |
| Solidus temperature t_s | 950 | °C | | |
| Magma specific heat capacity C_{pm} | 1484 | J/kg K | | |
| Assimilant specific heat capacity C_{pa} | 1388 | J/kg K | | |
| Crystallization enthalpy | 396000 | J/kg | | |
| Fusion enthalpy | 354000 | J/kg | | |
| Equilibration temperature | 979 | °C | | |
| | Sr (ppm) | Pb (ppm) | $^{87}\text{Sr}/^{86}\text{Sr}$ | $^{207}\text{Pb}/^{204}\text{Pb}$ |
| Magma Rh10/07 | 831 | 7 | 0.70367 | 19.43 |
| Magma 26199 | 1040 | 5.29 | 0.70346 | 19.33 |
| Bulk distribution coefficient D_0 | 0.1 | 0.4 | | |
| Enthalpy | 0 | 0 | | |
| Assimilant S30 | 916 | 4.6 | 0.70579 | 18.87 |
| Assimilant S35 | 916 | 4.6 | 0.70546 | 18.30 |
| Bulk distribution coefficient D_0 | 1.2 | 0.1 | | |
| Enthalpy | 0 | 0 | | |

Table A.4: Representative hornblende major element compositions from the Rhön area measured by EMPA and atomic proportions for amphibole formula were calculated for 23O according to Leake *et al.* (1997).

| | Hbl-Rh10/01 | | Hbl-Rh10/07 | | Hbl-Rh10/08 | | Hbl-Rh10/09 | | Hbl-Rh10/13a | | Hbl-Rh10/13b | | Hbl-Rh10/20 | |
|--------------------------------|-------------|------|-------------|------|-------------|------|-------------|------|--------------|--------|--------------|------|-------------|------|
| | rim | core | rim | core | rim | core | rim | core | rim | core | rim | core | rim | core |
| SiO ₂ | 39.6 | 39.9 | 39.4 | 39.4 | 39.7 | 39.9 | 39.4 | 39.3 | 38.6 | 38.7 | 39.4 | 39.3 | 39.8 | 40.0 |
| TiO ₂ | 4.58 | 4.18 | 4.58 | 4.98 | 4.53 | 4.56 | 4.59 | 4.51 | 4.93 | 4.90 | 4.67 | 4.66 | 4.58 | 4.71 |
| Al ₂ O ₃ | 13.5 | 13.7 | 13.9 | 14.4 | 13.8 | 13.6 | 13.3 | 13.6 | 13.7 | 13.7 | 14.0 | 14.0 | 14.3 | 14.3 |
| FeO ^T | 8.89 | 10.1 | 10.7 | 10.3 | 9.33 | 9.22 | 10.0 | 10.6 | 11.7 | 11.711 | 9.27 | 9.28 | 8.47 | 8.69 |
| MgO | 15.0 | 14.1 | 13.6 | 13.5 | 14.5 | 14.5 | 14.2 | 13.9 | 12.7 | 12.4 | 14.4 | 14.3 | 14.6 | 14.5 |
| CaO | 11.4 | 10.7 | 11.5 | 11.7 | 11.6 | 11.7 | 11.6 | 11.6 | 11.8 | 11.9 | 11.5 | 11.7 | 11.7 | 11.8 |
| Na ₂ O | 2.27 | 2.22 | 2.16 | 2.18 | 2.14 | 2.14 | 2.11 | 2.12 | 2.25 | 2.23 | 2.06 | 2.05 | 2.02 | 1.99 |
| K ₂ O | 1.58 | 1.73 | 1.80 | 1.79 | 1.99 | 1.98 | 1.93 | 1.85 | 1.68 | 1.71 | 1.90 | 1.99 | 2.05 | 2.02 |
| F | 0.20 | 0.07 | 0.20 | 0.10 | 0.16 | 0.15 | 0.21 | 0.07 | 0.13 | 0.03 | 0.20 | 0.08 | 0.13 | 0.00 |
| Total | 97.4 | 97.2 | 98.1 | 98.8 | 98.1 | 98.0 | 97.8 | 97.8 | 97.8 | 97.5 | 97.7 | 97.7 | 97.9 | 98.5 |
| Si | 5.79 | 5.84 | 5.78 | 5.80 | 5.80 | 5.84 | 5.81 | 5.78 | 5.75 | 5.79 | 5.78 | 5.78 | 5.79 | 5.81 |
| Ti | 0.50 | 0.46 | 0.51 | 0.55 | 0.50 | 0.50 | 0.51 | 0.50 | 0.55 | 0.55 | 0.52 | 0.51 | 0.66 | 0.50 |
| Al | 2.32 | 2.36 | 2.41 | 2.49 | 2.38 | 2.35 | 2.31 | 2.35 | 2.40 | 2.41 | 2.41 | 2.43 | 2.39 | 2.45 |
| Cr | 0.02 | 0.01 | 0.00 | 0.00 | 0.02 | 0.00 | 0.01 | 0.01 | 0.00 | 0.00 | 0.00 | 0.01 | 0.02 | 0.01 |
| Fe ³⁺ | 0.54 | 0.71 | 0.44 | 0.15 | 0.39 | 0.32 | 0.41 | 0.48 | 0.25 | 0.11 | 0.43 | 0.35 | 0.00 | 0.28 |
| Fe ²⁺ | 0.54 | 0.53 | 0.88 | 1.12 | 0.75 | 0.81 | 0.82 | 0.82 | 1.21 | 1.36 | 0.71 | 0.79 | 1.10 | 0.75 |
| Mn | 0.01 | 0.02 | 0.01 | 0.00 | 0.01 | 0.01 | 0.02 | 0.01 | 0.02 | 0.01 | 0.02 | 0.01 | 0.01 | 0.01 |
| Mg | 3.26 | 3.07 | 2.98 | 2.96 | 3.16 | 3.16 | 3.11 | 3.05 | 2.82 | 2.76 | 3.14 | 3.13 | 3.04 | 3.18 |
| Ca | 1.79 | 1.68 | 1.81 | 1.85 | 1.82 | 1.83 | 1.83 | 1.83 | 1.88 | 1.91 | 1.81 | 1.84 | 1.90 | 1.84 |
| Na | 0.64 | 0.63 | 0.61 | 0.62 | 0.61 | 0.61 | 0.60 | 0.60 | 0.65 | 0.65 | 0.58 | 0.58 | 0.61 | 0.57 |
| K | 0.30 | 0.32 | 0.34 | 0.34 | 0.37 | 0.37 | 0.36 | 0.35 | 0.32 | 0.33 | 0.36 | 0.37 | 0.34 | 0.38 |
| F | 0.09 | 0.04 | 0.09 | 0.05 | 0.08 | 0.07 | 0.10 | 0.04 | 0.06 | 0.02 | 0.09 | 0.04 | 0.28 | 0.06 |

Table A.4: (continued)

| | Hbl-Rh10/21 | | Hbl-Rh10/23 | | Hb-Rhl10/25 | | Hbl-Rh10/27 | | Hbl-Rh10/33 | | Hbl-Rh10/38 | |
|--------------------------------|-------------|-------|-------------|------|-------------|------|-------------|------|-------------|------|-------------|------|
| | rim | core | rim | core | rim | core | rim | core | rim | core | rim | core |
| SiO ₂ | 38.8 | 38.9 | 39.95 | 39.8 | 38.8 | 39.2 | 39.7 | 39.5 | 39.4 | 39.8 | 39.3 | 39.1 |
| TiO ₂ | 4.74 | 4.65 | 5.09 | 4.91 | 4.97 | 4.89 | 4.33 | 4.37 | 4.73 | 4.64 | 5.37 | 5.35 |
| Al ₂ O ₃ | 13.2 | 13.7 | 14.7 | 14.7 | 14.3 | 14.2 | 14.1 | 14.0 | 14.1 | 14.0 | 14.1 | 14.0 |
| FeO ^T | 10.68 | 10.70 | 8.43 | 8.79 | 9.81 | 9.65 | 8.91 | 8.78 | 9.91 | 9.94 | 9.88 | 9.89 |
| MgO | 13.9 | 13.5 | 14.6 | 14.7 | 13.6 | 13.9 | 14.6 | 14.5 | 14.0 | 14.0 | 13.7 | 13.8 |
| CaO | 11.7 | 11.6 | 11.8 | 11.8 | 12.0 | 11.8 | 11.0 | 11.0 | 11.7 | 11.8 | 11.5 | 11.6 |
| Na ₂ O | 2.21 | 2.10 | 1.96 | 2.01 | 2.20 | 2.13 | 2.15 | 2.06 | 2.14 | 2.12 | 2.36 | 2.34 |
| K ₂ O | 1.72 | 1.86 | 2.08 | 2.14 | 1.81 | 1.81 | 1.81 | 1.81 | 1.86 | 1.79 | 1.38 | 1.46 |
| F | 0.14 | 0.07 | 0.22 | 0.12 | 0.21 | 0.08 | 0.34 | 0.08 | 0.17 | 0.13 | 0.18 | 0.12 |
| Total | 97.4 | 97.4 | 99.1 | 99.3 | 97.9 | 98.0 | 97.3 | 96.3 | 98.3 | 98.3 | 98.0 | 97.9 |
| Si | 5.76 | 5.77 | 5.76 | 5.74 | 5.74 | 5.77 | 5.81 | 5.81 | 5.76 | 5.82 | 5.75 | 5.74 |
| Ti | 0.53 | 0.52 | 0.55 | 0.53 | 0.55 | 0.54 | 0.48 | 0.48 | 0.52 | 0.51 | 0.59 | 0.59 |
| Al | 2.31 | 2.39 | 2.50 | 2.49 | 2.49 | 2.46 | 2.43 | 2.43 | 2.44 | 2.41 | 2.44 | 2.43 |
| Cr | 0.00 | 0.01 | 0.01 | 0.01 | 0.00 | 0.01 | 0.00 | 0.00 | 0.00 | 0.00 | 0.01 | 0.00 |
| Fe ³⁺ | 0.42 | 0.38 | 0.27 | 0.35 | 0.17 | 0.26 | 0.61 | 0.58 | 0.37 | 0.29 | 0.33 | 0.33 |
| Fe ²⁺ | 0.91 | 0.95 | 0.75 | 0.71 | 1.04 | 0.93 | 0.48 | 0.50 | 0.85 | 0.92 | 0.88 | 0.89 |
| Mn | 0.01 | 0.01 | 0.01 | 0.01 | 0.02 | 0.01 | 0.01 | 0.01 | 0.01 | 0.00 | 0.01 | 0.01 |
| Mg | 3.07 | 2.98 | 3.15 | 3.15 | 2.99 | 3.04 | 3.18 | 3.19 | 3.05 | 3.04 | 2.99 | 3.01 |
| Ca | 1.87 | 1.85 | 1.83 | 1.83 | 1.89 | 1.86 | 1.72 | 1.73 | 1.83 | 1.85 | 1.80 | 1.82 |
| Na | 0.63 | 0.60 | 0.55 | 0.56 | 0.63 | 0.61 | 0.61 | 0.59 | 0.61 | 0.60 | 0.67 | 0.67 |
| K | 0.33 | 0.35 | 0.38 | 0.39 | 0.34 | 0.34 | 0.34 | 0.34 | 0.35 | 0.33 | 0.26 | 0.27 |
| F | 0.07 | 0.03 | 0.10 | 0.05 | 0.10 | 0.04 | 0.16 | 0.04 | 0.08 | 0.06 | 0.09 | 0.05 |

Table A.5: Representative hornblende compositions of trace elements from the Rhön area measured by SIMS.

| | Hbl-Rh10/01 | | Hbl-Rh10/07 | | Hbl-Rh10/08 | | Hbl-Rh10/09 | | Hbl-Rh10/13a | | Hbl-Rh10/13b | | Hbl-Rh10/14 | |
|----|-------------|------|-------------|------|-------------|-------|-------------|------|--------------|------|--------------|-------|-------------|-------|
| | rim | core | rim | core | rim | core | rim | core | rim | core | rim | core | rim | core |
| Sc | 53.2 | 37.4 | 48.8 | 48.8 | 42.3 | 47.2 | 48.1 | 49.2 | 40.1 | 44.1 | 47.9 | 48.8 | 48.8 | 44.1 |
| V | 476 | 453 | 467 | 476 | 421 | 453 | 430 | 471 | 399 | 426 | 437 | 440 | 427 | 443 |
| Sr | 546 | 527 | 470 | 470 | 745 | 543 | 534 | 583 | 692 | 671 | 535 | 541 | 470 | 468 |
| Y | 17.2 | 20.2 | 15.0 | 14.5 | 13.2 | 14.1 | 15.8 | 17.5 | 24.7 | 25.4 | 15.5 | 15.6 | 14.3 | 14.2 |
| Zr | 62.7 | 64.4 | 51.3 | 52.5 | 47.5 | 50.6 | 66.4 | 69.4 | 88.1 | 92.8 | 58.0 | 57.3 | 51.3 | 54.7 |
| Ba | 376 | 401 | 341 | 339 | 462 | 363 | 389 | 446 | 507 | 469 | 416 | 421 | 352 | 359 |
| La | 7.36 | 7.26 | 5.26 | 5.01 | 5.54 | 5.53 | 6.54 | 7.07 | 11.2 | 10.0 | 6.08 | 6.20 | 5.65 | 5.45 |
| Ce | 22.9 | 23.7 | 17.4 | 17.3 | 17.3 | 19.7 | 22.2 | 23.7 | 37.8 | 35.3 | 20.9 | 21.1 | 17.9 | 17.9 |
| Pr | 3.92 | 4.10 | 3.07 | 3.09 | 2.87 | 3.02 | 3.90 | 4.20 | 6.63 | 5.95 | 3.76 | 3.67 | 3.21 | 3.23 |
| Nd | 20.6 | 21.6 | 17.2 | 17.0 | 15.6 | 16.2 | 20.1 | 21.8 | 33.4 | 30.6 | 19.6 | 19.7 | 16.8 | 17.3 |
| Sm | 5.21 | 5.73 | 4.63 | 4.64 | 4.12 | 4.36 | 5.27 | 5.68 | 8.53 | 7.70 | 4.99 | 5.22 | 4.52 | 4.39 |
| Eu | 1.68 | 1.66 | 1.56 | 1.37 | 1.23 | 1.47 | 1.74 | 1.77 | 2.68 | 2.39 | 1.53 | 1.58 | 1.57 | 1.47 |
| Gd | 5.04 | 5.11 | 4.86 | 4.02 | 3.92 | 4.42 | 5.81 | 5.29 | 8.21 | 7.66 | 5.06 | 4.83 | 4.61 | 4.68 |
| Dy | 3.82 | 3.71 | 3.89 | 3.54 | 2.97 | 3.22 | 3.68 | 4.09 | 5.77 | 5.72 | 3.67 | 3.72 | 3.12 | 3.30 |
| Er | 1.44 | 1.38 | 1.38 | 1.23 | 1.21 | 1.26 | 1.47 | 1.45 | 2.44 | 2.30 | 1.32 | 1.33 | 1.07 | 1.12 |
| Yb | 1.00 | 1.08 | 0.966 | 1.02 | 0.784 | 0.693 | 0.865 | 1.13 | 1.56 | 1.49 | 0.911 | 0.937 | 0.767 | 0.868 |

Table A.5: (continued)

| | Hbl-Rh10/20 | | Hbl-Rh10/21 | | Hbl-Rh10/23 | | Hbl-Rh10/25 | | Hbl-Rh10/27 | | Hbl-Rh10/32 | Hbl-Rh10/33 | | Hbl-Rh10/38 |
|----|-------------|-------|-------------|------|-------------|-------|-------------|------|-------------|-------|-------------|-------------|-------|-------------|
| | rim | core | rim | core | rim | core | rim | core | rim | core | | rim | core | |
| Sc | 51.2 | 53.4 | 40.8 | 35.6 | 78.1 | 56.0 | 39.1 | 37.8 | 49.1 | 47.2 | 73.1 | 51.7 | 51.6 | 47.8 |
| V | 405 | 423 | 342 | 321 | 528 | 576 | 394 | 381 | 460 | 462 | 203 | 454 | 441 | 568 |
| Sr | 514 | 188 | 790 | 813 | 554 | 504 | 536 | 534 | 443 | 456 | 99 | 515 | 482 | 610 |
| Y | 13.6 | 14.9 | 25.0 | 25.4 | 14.3 | 13.9 | 17.0 | 17.2 | 13.4 | 13.3 | 17.8 | 13.6 | 13.8 | 20.4 |
| Zr | 61.8 | 58.5 | 130 | 142 | 40.9 | 48.3 | 76.0 | 81.0 | 47.1 | 49.3 | 138 | 52.4 | 52.0 | 49.1 |
| Ba | 407 | 402 | 605 | 610 | 465 | 426 | 432 | 407 | 336 | 370 | n.d. | 396 | 364 | 383 |
| La | 6.04 | 6.09 | 13.6 | 14.4 | 5.10 | 4.91 | 7.20 | 7.19 | 4.87 | 5.51 | 6.88 | 5.52 | 5.53 | 4.97 |
| Ce | 20.8 | 19.0 | 44.2 | 47.5 | 15.7 | 17.0 | 24.4 | 25.0 | 15.4 | 18.1 | 25.5 | 18.2 | 18.9 | 17.0 |
| Pr | 3.54 | 3.43 | 7.50 | 7.93 | 3.13 | 2.91 | 4.26 | 4.37 | 2.85 | 3.04 | 4.93 | 3.19 | 3.30 | 3.02 |
| Nd | 18.8 | 18.0 | 37.3 | 39.8 | 16.9 | 16.6 | 22.9 | 23.9 | 15.2 | 16.5 | 26.0 | 17.4 | 17.0 | 17.2 |
| Sm | 5.07 | 4.84 | 9.43 | 9.94 | 4.84 | 4.83 | 5.88 | 5.40 | 3.91 | 4.40 | 6.73 | 4.33 | 4.73 | 5.21 |
| Eu | 1.48 | 1.46 | 3.00 | 2.88 | 1.77 | 1.26 | 1.74 | 1.79 | 1.42 | 1.20 | 2.04 | 1.44 | 1.39 | 1.73 |
| Gd | 4.04 | 4.95 | 8.99 | 8.16 | 4.44 | 4.60 | 5.78 | 5.61 | 4.59 | 4.46 | 5.54 | 4.57 | 4.43 | 4.97 |
| Dy | 3.51 | 3.32 | 5.69 | 6.39 | 2.89 | 3.44 | 3.99 | 4.03 | 2.77 | 3.10 | 5.54 | 3.42 | 3.25 | 4.40 |
| Er | 1.36 | 1.19 | 2.46 | 2.45 | 1.52 | 1.24 | 1.53 | 1.40 | 1.32 | 1.11 | 1.91 | 1.28 | 1.23 | 1.76 |
| Yb | 0.880 | 0.706 | 1.68 | 1.72 | 0.646 | 0.946 | 1.15 | 1.05 | 0.761 | 0.689 | 1.84 | 0.826 | 0.829 | 1.34 |

A Appendix

PETROGENESIS OF HORNBLLENDE-BEARING LAVAS (RHÖN, GERMANY)

Table A.6: Average trace element abundances of spot measurements in hornblende from the Rhön area using LA-ICP-MS with standard deviation (σ).

| n= | Hbl-Rh10/01 | | Hbl-Rh10/07 | | Hbl-Rh10/09 | | Hbl-Rh10/13 | | Hbl-Rh10/25 | | Hbl-Rh10/33 | | BHVO-2G | BHVO-2G | BHVO-2G | BHVO-2G |
|----|-------------|----------|-------------|----------|-------------|----------|-------------|----------|-------------|----------|-------------|----------|------------|------------|------------|-----------------------------|
| | 5 | σ | 6 | σ | 7 | σ | 9 | σ | 8 | σ | 8 | σ | this study | this study | this study | Jochum <i>et al.</i> (2006) |
| Ni | 259 | 2 | 136 | 9 | 115 | 19 | 115 | 21 | 103 | 8 | 67.9 | 17.6 | 116 | 115 | 117 | 116 |
| Cr | 1099 | 32 | 307 | 133 | 444 | 140 | 271 | 78 | 270 | 317 | 266 | 373 | 303 | 289 | 294 | 293 |
| Co | 52.5 | 0.5 | 57.1 | 1.1 | 55.5 | 1.0 | 57.0 | 1.7 | 57.0 | 2.3 | 58.1 | 1.9 | 43.0 | 42.4 | 43.4 | 44.0 |
| Cu | 4.61 | 0.29 | 0.87 | 0.19 | 3.06 | 3.29 | 0.92 | 0.17 | 1.42 | 0.36 | 0.98 | 0.49 | 109 | 106 | 107 | 127 |
| Zn | 36.9 | 1.3 | 40.5 | 1.4 | 48.3 | 2.5 | 42.8 | 1.2 | 48.2 | 3.0 | 42.7 | 2.7 | 100 | 100 | 101 | 102 |
| V | 469 | 3 | 472 | 24 | 406 | 8 | 434 | 22 | 429 | 12 | 447 | 12 | 313 | 314 | 317 | 308 |
| Rb | 8.06 | 0.26 | 9.30 | 0.58 | 9.89 | 0.97 | 10.84 | 0.51 | 10.77 | 0.98 | 9.95 | 0.53 | 8.36 | 8.11 | 8.34 | 9.2 |
| Ba | 312 | 7 | 290 | 13 | 318 | 17 | 320 | 14 | 323 | 13 | 348 | 26 | 118 | 119 | 117 | 131 |
| Th | 0.053 | 0.011 | 0.041 | 0.004 | 0.046 | 0.005 | 0.054 | 0.010 | 0.060 | 0.014 | 0.051 | 0.009 | 1.09 | 1.11 | 1.15 | 1.22 |
| U | 0.008 | 0.005 | 0.010 | 0.005 | 0.010 | 0.002 | 0.011 | 0.004 | 0.013 | 0.005 | 0.012 | 0.005 | 0.386 | 0.456 | 0.429 | 0.403 |
| Ta | 0.96 | 0.04 | 0.83 | 0.02 | 1.05 | 0.14 | 0.98 | 0.05 | 1.02 | 0.06 | 0.94 | 0.06 | 1.03 | 1.12 | 1.04 | 1.15 |
| Nb | 14.2 | 0.3 | 12.3 | 0.4 | 15.8 | 1.9 | 14.9 | 0.7 | 15.8 | 1.0 | 14.4 | 0.8 | 15.7 | 16.3 | 15.5 | 18.3 |
| La | 4.98 | 0.09 | 4.23 | 0.10 | 5.62 | 0.57 | 5.35 | 0.29 | 5.81 | 0.74 | 5.13 | 0.37 | 14.1 | 14.3 | 14.2 | 15.2 |
| Ce | 16.5 | 0.2 | 14.9 | 0.3 | 19.5 | 1.8 | 18.5 | 1.1 | 19.6 | 2.1 | 17.5 | 1.2 | 34.7 | 36.0 | 35.0 | 37.6 |
| Pb | 0.22 | 0.02 | 0.21 | 0.01 | 0.24 | 0.02 | 0.23 | 0.02 | 0.24 | 0.03 | 0.22 | 0.02 | 1.63 | 1.68 | 1.53 | 1.70 |
| Pr | 2.79 | 0.04 | 2.56 | 0.07 | 3.31 | 0.29 | 3.10 | 0.15 | 3.28 | 0.26 | 2.97 | 0.19 | 4.92 | 4.93 | 4.78 | 5.35 |
| Sr | 426 | 4 | 412 | 17 | 449 | 37 | 421 | 12 | 430 | 15 | 449 | 30 | 364 | 365 | 361 | 396 |
| Nd | 15.0 | 0.3 | 14.1 | 0.2 | 17.4 | 1.4 | 16.3 | 0.7 | 17.3 | 1.1 | 16.4 | 1.1 | 23.2 | 22.2 | 21.6 | 24.5 |
| Sm | 4.06 | 0.14 | 3.87 | 0.14 | 4.52 | 0.40 | 4.22 | 0.22 | 4.46 | 0.28 | 4.36 | 0.39 | 5.68 | 5.86 | 5.72 | 6.1 |
| Zr | 42.1 | 0.7 | 39.3 | 0.9 | 55.4 | 4.1 | 48.7 | 2.9 | 52.8 | 3.8 | 48.6 | 4.7 | 148 | 144 | 142 | 170 |
| Hf | 1.91 | 0.06 | 1.77 | 0.06 | 2.28 | 0.14 | 2.11 | 0.12 | 2.25 | 0.14 | 2.11 | 0.17 | 4.08 | 3.78 | 4.05 | 4.32 |
| Eu | 1.30 | 0.06 | 1.37 | 0.07 | 1.51 | 0.09 | 1.41 | 0.09 | 1.48 | 0.08 | 1.41 | 0.10 | 1.91 | 1.88 | 1.85 | 2.07 |
| Gd | 3.99 | 0.10 | 3.90 | 0.13 | 4.39 | 0.36 | 4.12 | 0.17 | 4.22 | 0.22 | 4.13 | 0.27 | 5.87 | 5.64 | 5.62 | 6.16 |
| Tb | 0.53 | 0.02 | 0.52 | 0.02 | 0.57 | 0.05 | 0.54 | 0.02 | 0.56 | 0.03 | 0.54 | 0.04 | 0.844 | 0.768 | 0.844 | 0.920 |
| Dy | 2.91 | 0.08 | 2.88 | 0.07 | 3.20 | 0.21 | 3.03 | 0.15 | 3.10 | 0.17 | 3.04 | 0.17 | 4.98 | 5.19 | 4.66 | 5.28 |
| Ho | 0.49 | 0.02 | 0.49 | 0.01 | 0.53 | 0.03 | 0.52 | 0.03 | 0.53 | 0.03 | 0.51 | 0.04 | 0.925 | 0.896 | 0.935 | 0.980 |
| Er | 1.17 | 0.03 | 1.14 | 0.05 | 1.24 | 0.10 | 1.18 | 0.08 | 1.19 | 0.09 | 1.17 | 0.09 | 2.36 | 2.31 | 2.44 | 2.56 |
| Tm | 0.14 | 0.01 | 0.14 | 0.01 | 0.15 | 0.00 | 0.14 | 0.01 | 0.15 | 0.01 | 0.15 | 0.01 | 0.333 | 0.342 | 0.348 | 0.340 |
| Y | 12.2 | 0.2 | 11.9 | 0.3 | 13.0 | 0.9 | 12.4 | 0.5 | 12.6 | 0.5 | 12.2 | 0.6 | 23.4 | 22.8 | 22.9 | 26.0 |
| Yb | 0.83 | 0.06 | 0.78 | 0.04 | 0.81 | 0.06 | 0.82 | 0.06 | 0.85 | 0.08 | 0.84 | 0.05 | 2.02 | 1.99 | 1.90 | 2.01 |
| Lu | 0.10 | 0.01 | 0.10 | 0.01 | 0.12 | 0.01 | 0.11 | 0.01 | 0.12 | 0.01 | 0.11 | 0.01 | 0.286 | 0.292 | 0.278 | 0.279 |

Table A.7: Sr, Nd, Pb and O isotope data for hornblende from the Rhön area. Measured Sr, Nd and Pb isotope data were recalculated using the concentrations given in Table A.6 and an age of 24 Ma. Numbers in parentheses are 2σ in-run deviations of the deviations of the measurements.

| | $\frac{87\text{Sr}/}{86\text{Sr}_{(m)}}$ | $\frac{87\text{Sr}/}{86\text{Sr}_{(i)}}$ | $\frac{143\text{Nd}/}{144\text{Nd}_{(m)}}$ | $\frac{143\text{Nd}/}{144\text{Nd}_{(i)}}$ | $\frac{206\text{Pb}/}{204\text{Pb}_{(m)}}$ | $\frac{207\text{Pb}/}{204\text{Pb}_{(m)}}$ | $\frac{208\text{Pb}/}{204\text{Pb}_{(m)}}$ | $\frac{206\text{Pb}/}{204\text{Pb}_{(i)}}$ | $\frac{207\text{Pb}/}{204\text{Pb}_{(i)}}$ | $\frac{208\text{Pb}/}{204\text{Pb}_{(i)}}$ | $\delta^{18}\text{O}$ |
|-------------|--|--|--|--|--|--|--|--|--|--|-----------------------|
| Hbl-Rh10/01 | 0.703634(4) | 0.70362 | 0.512844(8) | 0.51281 | 19.42 | 15.67 | 39.33 | 19.41 | 15.67 | 39.31 | 7.0 |
| Hbl-Rh10/07 | 0.703540(3) | 0.70352 | 0.512494(6) | 0.51245 | 18.15 | 15.62 | 38.16 | 18.14 | 15.62 | 38.15 | 6.9 |
| Hbl-Rh10/09 | 0.703527(3) | 0.70351 | 0.512439(4) | 0.51240 | 17.13 | 15.55 | 37.57 | 17.12 | 15.53 | 37.56 | 7.5 |
| Hbl-Rh10/13 | 0.703569(3) | 0.70354 | 0.512837(5) | 0.51280 | 19.26 | 15.66 | 39.20 | 19.25 | 15.66 | 39.18 | 6.4 |
| Hbl-Rh10/25 | 0.703757(3) | 0.70373 | 0.512844(3) | 0.51281 | 19.26 | 15.67 | 39.19 | 19.25 | 15.67 | 39.17 | 5.4 |
| Hbl-Rh10/33 | 0.703533(3) | 0.70351 | 0.512847(3) | 0.51281 | 19.30 | 15.63 | 39.13 | 19.28 | 15.63 | 39.11 | 6.9 |

Table A.8: Summary of results from Ar-Ar dating of hornblende from the Rhön area.

| Sample | weight | J-value | Plateau age | ^{39}Ar | MSWD | IIA all steps | $(^{40}\text{Ar}/^{36}\text{Ar})_i$ all steps | IIA selected steps | $(^{40}\text{Ar}/^{36}\text{Ar})_i$ selected steps | Steps used | Preferred age |
|-------------|--------|-----------|-------------|------------------|------|------------------|--|--------------------------|--|---------------|---------------|
| | [mg] | | [Ma] | [%] | | [Ma] | | [Ma] | | | [Ma] |
| Hbl-Rh10/01 | 25.8 | 0.0035345 | 24.0±0.2 | 95.4 | 0.15 | 23.8±1.8 | 318±10 | 24.0±0.5 | 331±50 | 12 - 17 | 24.0±0.2 |
| Hbl-Rh10/07 | 36.9 | 0.0035345 | 24.0±0.2 | 94.1 | 0.07 | 24.2±0.3 | 297.9±1.4 | 24.1±0.3 | 307±14 | 7 - 19 | 24.0±0.2 |
| Hbl-Rh10/13 | 19.2 | 0.0035345 | 24.1±0.2 | 95.2 | 0.08 | 24.1±0.3 | 295.9±1.7 | 24.1±0.4 | 297±30 | 7 - 17 | 24.1±0.2 |
| Hbl-Rh10/33 | 28.2 | 0.0035345 | 24.0±0.2 | 84.4 | 0.04 | 24.1±0.3 | 310±14 | 24.1±0.5 | 296±95 | 6 - 17 | 24.0±0.2 |

IIA = Inverse Isochron Age. Errors are 1σ . Error (1σ) in J-value is 0.57%. $\lambda^{40}\text{K} = (5.5545 \pm 0.0109) \times 10^{-10} \text{ a}^{-1}$ (Renne et al., 2010). Half life $^{37}\text{Ar} = 34.95 \pm 0.08 \text{ d}$ (Renne & Norman, 2001)

8 Acknowledgement

First of all I would like to thank Prof. Stefan Jung for supervision and guidance through the three years of my Ph.D. study. During this time I learned a great deal about the subject, experimental techniques, and scientific publishing.

Also I like to thank Prof. Dr. Rolf L. Romer (GFZ) for access to his CleanLab facility and the mass spectrometer as well as his help and advice.

For technical and experimental support during EMPA analyses I like to thank Dipl.-Min. Stefanie Heidrich. For the support during thin section and sample preparation I like to thank Peter Stutz.

E. Thun and J. Richards I thank for their support during the XRF analyses.

Further I like to thank Heidi Beier for her help during Sr and Nd isotope data acquisition and Prof. Dr. Andreas Stracke for the opportunity to work in the CleanLab at Universität Münster.

LA-ICP-MS measurements would not have been possible without the help of Dr. Andreas Klügel.

For his help during SIMS measurements I like to thank Elmar Gröner.

This work was financially supported by the Deutsche Forschungsgemeinschaft via the Grant No. DFG-Ju 326/7.